ORNL/SPR-2022/2597

Assessment of the Effect of Prototypic High-Burnup Operating Conditions of Fuel Fragmentation, Relocation, and Dispersal Susceptibility

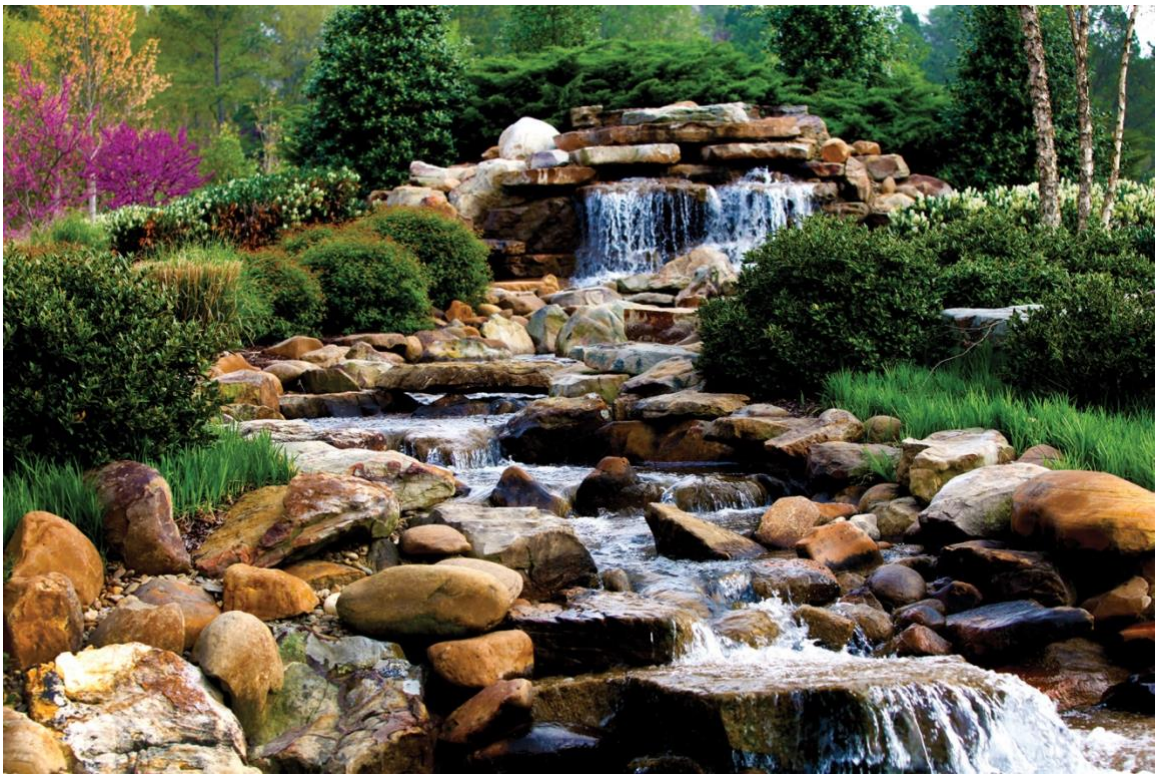

Nathan Capps
Jake Hirschhorn
Aaron Wysocki
Ian Greenquist

September 30, 2022

OAK RIDGE National Laboratory

ORNL IS MANAGED BY UT-BATTELLE LLC FOR THE US DEPARTMENT OF ENERGY

DOCUMENT AVAILABILITY

Reports produced after January 1, 1996, are generally available free via OSTI.GOV.

Website www.osti.gov

Reports produced before January 1, 1996, may be purchased by members of the public from the following source:

National Technical Information Service
5285 Port Royal Road
Springfield, VA 22161
Telephone 703-605-6000 (1-800-553-6847)
TDD 703-487-4639
Fax 703-605-6900
E-mail info@ntis.gov
Website http://classic.ntis.gov/

Reports are available to US Department of Energy (DOE) employees, DOE contractors, Energy Technology Data Exchange representatives, and International Nuclear Information System representatives from the following source:

Office of Scientific and Technical Information
PO Box 62
Oak Ridge, TN 37831
Telephone 865-576-8401
Fax 865-576-5728
E-mail reports@osti.gov
Website https://www.osti.gov/

ORNL/SPR-2022/2597

Nuclear Energy Advanced Modeling and Simulation

ASSESSMENT OF THE EFFECT OF PROTOTYPIC HIGH-BURNUP OPERATING CONDITIONS OF FUEL FRAGMENTATION, RELOCATION, AND DISPERSAL SUSCEPTIBILITY

Nathan Capps
Jake Hirschhorn
Aaron Wysocki
Ian Greenquist

September 30, 2022

Prepared by
OAK RIDGE NATIONAL LABORATORY
Oak Ridge, TN 37831
managed by
UT-BATTELLE LLC
for the
US DEPARTMENT OF ENERGY
under contract DE-AC05-00OR22725

ABSTRACT

The US nuclear energy industry is investigating strategies that further reduce the cost of energy production by using its existing fleet of nuclear generating stations. Most nuclear power plant operating costs are associated with purchasing fresh fuel assemblies or the efficiency of the reactor core design. Material costs are typically beyond the operator's control; however, the core design optimizations offer potential operational savings. The core design envelope available to operators is constrained by two primary regulatory criteria: an enrichment limit of 5% ^{235}U and a burnup limit of 62 GWD/tU. These constraints have resulted in renewed efforts by the nuclear industry to pursue extending the peak rod-average burnup beyond 62 GWd/tU. This effort will likely require additional safety analyses beyond what is currently accepted by the US Nuclear Regulatory Commission. The purpose of this work is to demonstrate a best estimate plus uncertainty pin-by-pin high-burnup loss of coolant accident analysis technique to assess full-core high-burnup fuel fragmentation, relocation, and dispersal (FFRD) and identify approaches for minimizing or potentially mitigating FFRD through core design optimizations.

1. INTRODUCTION

The first nuclear power stations licensed in the United States were approved to operate on fuel to rod average burnups of ~30 GWd/tU. This decision was based on a variety of experimental fuel performance and safety data sources that demonstrated safe operation. Extensive demonstration and testing under normal operating conditions was conducted in power generating stations to characterize relevant performance attributes in support of this limit. Simultaneous integral testing under power-cooling mismatch conditions representative of loss of coolant accident (LOCA) and reactivity insertion accident scenarios were also collected at transient test reactors to identify the dominant fuel failure modes and develop relevant fuel safety criteria. The results were essential for developing empirical fuel performance limits and validating the computer codes to demonstrate design compliance to the experimentally determined safety limits under commercial operation. The knowledge acquired during these tests is directly reflected in the fundamental structure of the US Nuclear Regulatory Commission (NRC) regulatory documents, including Title 10 of the *Code of Federal Regulations* Part 50, "Domestic Licensing of Production and Utilization Facilities," and the *Standard Review Plan for the Review of Safety Analysis Reports for Nuclear Power Plants: LWR Edition*.

Subsequent work was conducted over the following decades to extend the allowable utilization envelope for UO_2/Zr alloy (Zry)–based fuels to the current limits (i.e., 62 GWd/tU peak rod average). Burnup extension was made possible by fuel technology improvements, most notably moving cladding designs from Zircaloy-4 to Zircaloy concepts containing Nb. Additionally, fuel material responses under postulated severe accident conditions are better understood.

Historically, the design basis limits for these materials were determined by mechanically testing cladding alloys that had been irradiated under normal service condition and subsequent semi-integral LOCA testing to determine the embrittlement thresholds. Claddings were generally found to embrittle if the peak temperature exceeded ~1,200°C or if the effective cladding reacted with steam exceeded 17% of the original cladding thickness. This was further expanded upon when a limited number of integral tests were performed to identify and evaluate the dominant failure modes and remained unchanged as burnup levels increased to 62 GWD/tU. Thus, it was determined that semi-integral or separate effects test data were applicable to further extend the relevant fuel safety limits without changing the fundamental safety criteria or analysis techniques.

Integral tests using the Halden reactor in Norway—and later in semi-integral tests at Studsvik—revealed that the response of high-burnup fuel pellets to LOCA conditions could dramatically change from that historically observed. Up to ~67 GWD/tU fuel pellets were observed to fragment into pieces that were relatively large compared with the size of the cladding rupture, and large fragments relocating into the balloon region were modest. However, some Halden and Studsvik tests conducted on fuel samples irradiated to >67 GWD/tU showed that the fuel pellets could pulverize into small fragments. A significant fraction of these particles was fine enough to relocate axially within the balloon region and eject through the rupture opening into the coolant. If sufficiently significant, then this behavior could invalidate historical approaches to demonstrating safety and the effect of fuel fragmentation, relocation, and dispersal (FFRD), specifically assumptions related to core coolability and criticality.

These results led to NRC commissioners writing a letter to their staff specifically identifying a need to "…define the boundary of safe operation for key fuel design and operating parameters," stating that "the staff is challenged to evaluate the acceptability of future fuel design advancements and fuel utilization changes". The purpose of this work is to build on previously developed methodologies [1, 2, 3] to evaluate core FFRD susceptibility. This effort will assess important steady-state operational and fuel performance parameters that are known to attribute to FFRD susceptibility. The parameters will be evaluated to inform core design strategies that mitigate FFRD. Additionally, a subset of high-burnup fuel rods representing the high-burnup operation envelope will be passed to TRACE for detailed thermal-hydraulic (TH) evaluation and, subsequently, to BISON for transient fuel performance analysis. The results from this study will be used to inform semi- and fully integral LOCA tests programs, determine cladding rupture susceptibility and those parameters that increase rupture susceptibility, and FFRD susceptibility if rupture is predicted. Again, the goal of this work is to demonstrate a best estimate plus uncertainty methodology to assess core-wide FFRD susceptibility and inform high-burnup core designs approaches intended to minimize or potentially mitigate FFRD susceptibility.

1.1 REFERENCES

[1] N. Capps et al. 2021. "Full Core LOCA Safety Analysis for a PWR Containing High Burnup Fuel." *Nucl. Eng. Des.* 379: 1–22. doi: 10.1016/j.nucengdes.2021.111194.

[2] N. Capps et al. 2022. *Full Core LOCA Safety Analysis for a PWR Containing High Burnup Fuel*. ORNL/TM-2020/1700. Oak Ridge: Oak Ridge National Laboratory.

[3] N. Capps, R. Sweet, B. Wirth, A. Nelson, and K. Terrani. 2020. "Development and Demonstration of a Methodology to Evaluate High Burnup Fuel Susceptibility to Pulverization under a Loss of Coolant Transient." *Nucl. Eng. Des.* 366: 1–29. doi: 10.1016/j.nucengdes.2020.110744.

2. SUMMARY OF REACTOR AND HIGH BURNUP CYCLE DESIGN

The commercial pressurized water reactor (PWR) chosen for this analysis is a Westinghouse four-loop plant that has ambient pressure containment design with capacity of 193 nuclear fuel assemblies and a rated power of 3,626 MWth. Current fuel management strategies for the PWR employ 18 month fuel cycle designs using a typical low-leakage "ring of fire" fresh fuel layout that uses low-enriched uranium fuel. Three burnup regions are typically used with 85–92 fresh fuel assemblies in the core interior surrounded by once-burned fuel assemblies and mostly twice-burned fuel assemblies on the core periphery, as shown in Figure 1. The cycles are designed to operate continuously for approximately 500 effective full power days (EFPDs). Combinations of the burnable absorbers are used in the fresh fuel assemblies to optimize power distributions and reduce the amount of soluble B in the reactor coolant. Standard 17 × 17 fuel assembly designs were assumed for this analysis. Details of the reactor design and high-burnup core designs are provided in other works [1, 2], but a brief summary is provided here.

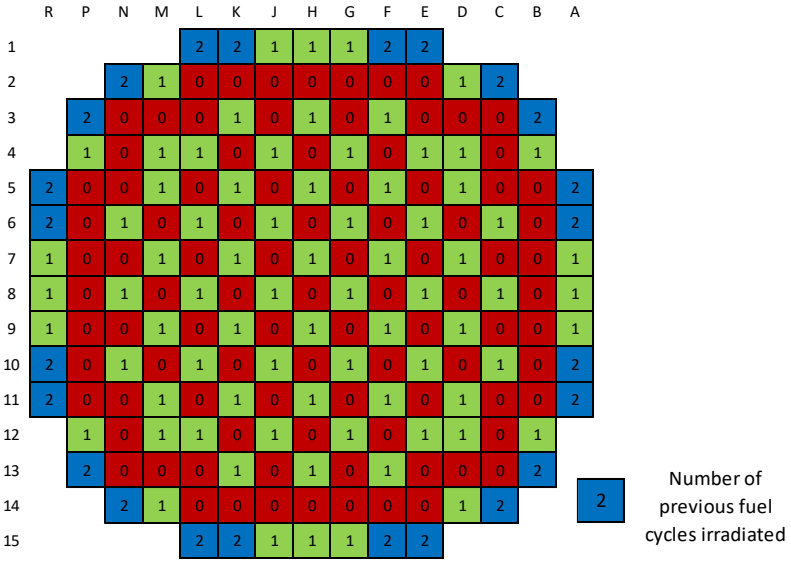

Figure 1. Standard 4-loop Westinghouse PWR core loading strategy.

The process to develop a 24 month fuel cycle design used high-enrichment and high-burnup fuel built on previous core designs and depletion results. Southern Nuclear performed the loading pattern development and optimization using in-house methods. These methods were chosen because of their computation speed and Southern Nuclear's familiarity with 4-loop PWR cores and core designs. To meet all design criteria, a transition was performed starting from a previous core design used in a 4-loop PWR. Two cycles were required to transition from 18 to 24 month designs, but in reality, utilities will likely need additional cycles to transition to 24 month core designs because additional fuel management and licensing concerns will prevent the rapid transition. Ten additional 24 month core designs were developed to reach an equilibrium pattern. Core design results that Southern Nuclear provided were compared to VERA results to ensure consistency. Southern Nuclear used the following design criteria:

- Fuel enrichments less than 6.95 wt % ^{235}U (beyond the current 4.95 wt % limit)
- Peak fuel rod exposure of ~75 GWd/tU (beyond the current 62 GWd/tU limit)
- Approximately 700 EFPD design cycle length
- Minimized number of once-burned fuel on the core periphery
- Approximately 84 fresh feed assemblies per cycle
- Typical low-leakage in/out ring-of-fire loading pattern

- FΔh limit of 1.50 (similar to existing 18 month cycle designs)
- Integral fuel burnable absorber (IFBA)/wet annular burnable absorber (WABA) only for burnable poisons (no Gadolinia)
- Fresh center assembly every other cycle

The design strategy incorporated loading one fresh assembly into the center of the reactor core and irradiating it for two cycles. This strategy is advantageous because fuel is better used and fuel rod burnups are minimized in that location as opposed to breaking up symmetric assemblies for that location. However, one drawback is that twice as many cycles are needed to reach an equilibrium design. Thus, the target 24 month cycle equilibrium design is actually a pair of cycles.

Transition and high-burnup core designs were generated by a US utility with the purpose of being realistic and feasible patterns based on current reload strategies and safety analysis constraints. The primary goal for this work was to generate power histories for high-enrichment, high-burnup fuel for detailed steady-state and transient fuel performance and thermal-hydraulic analysis. Table 1 provides some cycle design information relating to the loading pattern generation. Design strategy for the center assembly results in "pairs" of cycles that approach equilibrium, and the Table 1 core designs are not representative of the actual designs in operation.

Table 1. Transition and equilibrium 24 month cycle design information.

Cycle	Cycle length (EFPD)	Number of feed	Feed enrichments (wt % ^{235}U)	Number IFBA/WABA	Maximum fuel rod FΔh	Maximum fuel rod burnup (GWd/tU)
T1*	522.7	92	4.60/4.95/5.20	11,616/400	1.46	56.1
T2	695.1	93	5.20/5.60/5.95	16,024/784	1.48	61.6
HBu1+	700	92	5.60/5.95/6.20	16,480/848	1.47	70.2
HBu2	693	89	5.60/5.95/6.20	16,072/736	1.46	70.5
HBu3	693	84	5.95/6.20/6.60	16,096/592	1.49	73.1
HBu4	693	81	5.95/6.20/6.60	15,128/592	1.49	73.1
HBu5	693	84	5.95/6.20/6.60	16,032/624	1.50	78.1
HBu6	693	85	5.95/6.20/6.60	16,056/704	1.49	75.5
HBu7	693	84	5.95/6.20/6.60	16,032/608	1.49	73.3
HBu8	693	85	5.95/6.20/6.60	16,056/704	1.50	76.8
HBu9	693	84	5.95/6.20/6.60	16,032/608	1.49	74.3
HBu10	**693**	**85**	**5.95/6.20/6.60**	**16,056/704**	**1.50**	**76.9**
HBu11	693	84	5.95/6.20/6.60	16,032/608	1.49	74.3
HBu12	693	85	5.95/6.20/6.60	16,056/704	1.50	75.9

* *T* indicates 18–24 month transition cycles
+ *HBu* indicates 24 month cycles with increased enrichment and burnup

2.1 REFERENCES

[1] N. Capps et al. 2021. “Full Core LOCA Safety Analysis for a PWR Containing High Burnup Fuel.” *Nucl. Eng. Des.* 379: 1–22. doi: 10.1016/j.nucengdes.2021.111194.

[2] N. Capps et al. 2022. *Full Core LOCA Safety Analysis for a PWR Containing High Burnup Fuel*. ORNL/TM-2020/1700. Oak Ridge: Oak Ridge National Laboratory.

3. HIGH-BURNUP STEADY STATE OPERATING CONDITIONS AND FUEL PERFORMNACE

A methodology was developed to characterize the operating conditions and fuel performance of high-burnup fuel rods during steady-state operation. The methodology was applied to the high-burnup VERA core designs introduced in Section 2, and the operating conditions and fuel performance results are presented in this section. Specifically, high-burnup fuel rod operating conditions were extracted from VERA simulation results. The BISON [3, 4] fuel performance code was then used to simulate the steady state fuel performance of selected high-burnup fuel rods. Finally, a sensitivity study was conducted to estimate the magnitude of the effects that uncertainty in fission gas release (FGR) predictions have on fuel centerline temperature (FCT) and rod internal pressure (RIP) predictions.

The results of these studies set a baseline for high-burnup fuel performance and behavior during steady state operation. The results provide initial conditions for the follow-on thermal-hydraulic and transient analyses needed to assess the susceptibility of high-burnup fuel rods to fuel fragmentation, relocation, and dispersal (FFRD). Many of the findings of this work are specific to the fuel rod and core designs considered herein. However, the authors believe that the methodology presented in this work can be generalized and applied to assess a wide range of nuclear power plants (NPPs), core designs, and fuel rod performance.

3.1 OPERATING CONDITIONS

VERA simulation results are stored as hierarchical data format 5 (HDF5) files. Each HDF5 file contains the operating conditions needed to reconstruct fuel rod irradiation histories for one cycle. Fourteen HDF5 files were available for the high-burnup VERA core designs introduced in Section 2. These included (1) two cycles during which the core transitioned from using standard-burnup (<62 GWd/tU) fuel rods to high-burnup fuel rods, (2) nine cycles during which the core had not yet achieved equilibrium behavior, and (3) three cycles during which the core operated at equilibrium. The following sections describe operating conditions of interest, the process applied to down-select cycles for further analysis, high burnup operating conditions in the selected cycles, and the process applied to down-select fuel rods for fuel performance analysis.

3.1.1 Parameters of interest

Operating conditions of interest were selected with the ultimate goal of assessing the susceptibility of high-burnup fuel rods to FFRD. Selections were based on a high-burnup fuel fragmentation (HBFF) analysis methodology published in Reference [5]. The methodology is illustrated by the diagram in Figure 2 and considers spatial variations in burnup, temperature, and cladding ballooning. Operating conditions are compared with criteria established for each parameter to develop a composite criterion that estimates the mass of fuel susceptible to fragmentation and subsequent dispersal under LOCA conditions.

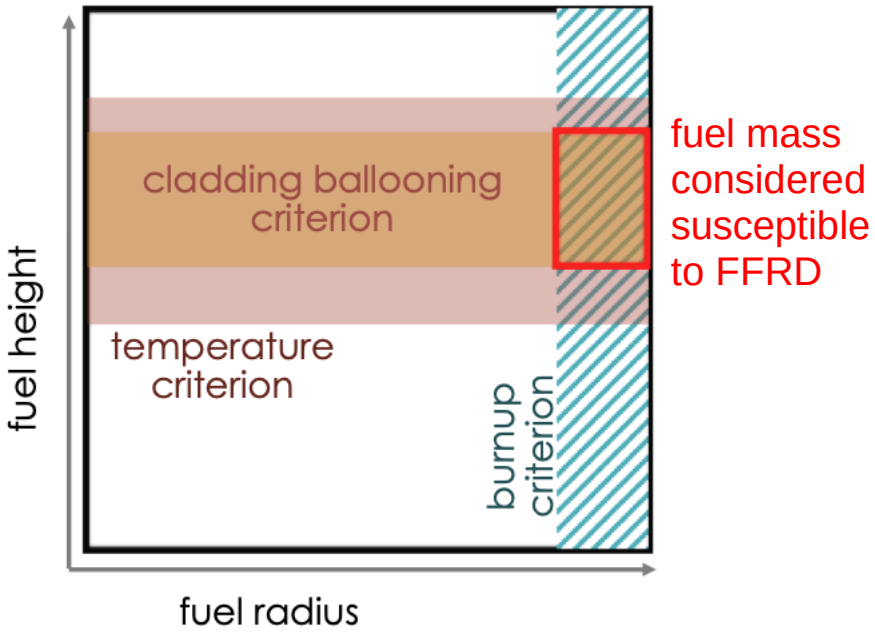

Figure 2. Diagram illustrating the cladding constraint, fuel temperature, and local burnup criteria that factor into fuel fragmentation. The fuel within the red rectangle, in which all three criteria are met, is believed to be susceptible to FFRD. Modified from Reference [5].

The methodology illustrated by Figure 2 was leveraged to identify operating conditions of interest within the VERA HDF5 files. Selections were made to characterize fuel rod temperature behaviors, burnup behaviors, and the spatial relationships between them. Nine operating conditions of interest were defined:

1. Average fuel rod burnup
2. Average fuel rod linear heat rate (LHR)
3. Average fuel rod decay heat production rate
4. Peak fuel rod burnup
5. Axial location of the peak fuel rod burnup
6. Local LHR at the axial location of the peak fuel rod burnup
7. Peak fuel rod LHR
8. Axial location of the peak fuel rod LHR
9. Local burnup at the axial location of the peak fuel rod LHR

Three aspects of these operating conditions listed above require further discussion. First, LHRs were selected as surrogates to characterize fuel rod temperature behaviors. Fuel rod temperature estimates calculated by VERA's thermal-hydraulics module, CTF [6], [7], are available in the HDF5 files. However, these results were expected to be less realistic than the LHRs calculated by VERA's neutronics module, MPACT [8], [9]. LHRs were considered suitable for the purposes of cycle and fuel rod down-selection in this work. Fuel rod temperature behaviors are analyzed directly via BISON fuel performance simulations, which are discussed in Section 3.2.

Second, decay heat production rates were assumed to be 9.5% of the LHRs according to an approximation given in El-Wakil [10]. VERA calculates irradiation history-dependent decay heat production rates using its isotope depletion, decay, and activation module, ORIGEN [11]. However, these calculations are unavailable for the high-burnup VERA core designs being examined here. Therefore, the LHR-based approximation was determined to be sufficient for the purposes of cycle and fuel rod down-selection in the current work.

Finally, several operating conditions of interest were defined to capture the spatial relationships between the burnup and temperature behaviors believed to influence HBFF. These operating conditions include the axial locations of the peak fuel rod burnup and LHR, the local LHR at the axial location of the peak fuel rod burnup, and the local burnup at the axial location of the peak fuel rod LHR. Note that VERA does not calculate radially-discretized burnups or LHRs within individual fuel rods. Examining these operating conditions helps to assess the combined effects of burnup and temperature in accordance with the HBFF analysis methodology illustrated in Figure 2. The third HBFF-relevant behavior, cladding ballooning, is analyzed via BISON fuel performance simulations, which are discussed in Section 0.

3.1.2 Cycle selection

Data were available for fourteen cycles, designated Cycles 17 through 30. The data were parsed to collect statistics on the nine operating conditions of interest and examine overall trends in the results. Box and whisker plots illustrating the end of cycle (EOC) values of those operating conditions are shown in Figure 3. For each cycle and operating condition, the boxes show the median and inter-quartile range (IQR), and the whiskers show ±1.5 IQR. Outlier values that fall outside of the ±1.5 IQR are also shown. Figure 3 illustrates how the operating conditions change as assemblies with standard-burnup fuel rods are replace by assemblies with high-burnup fuel rods in Cycles 17 and 18. The operating conditions become increasingly stable as the core approaches equilibrium behavior in Cycles 19–27, and the operating conditions remain stable while the core operates in equilibrium (Cycles 28–30).

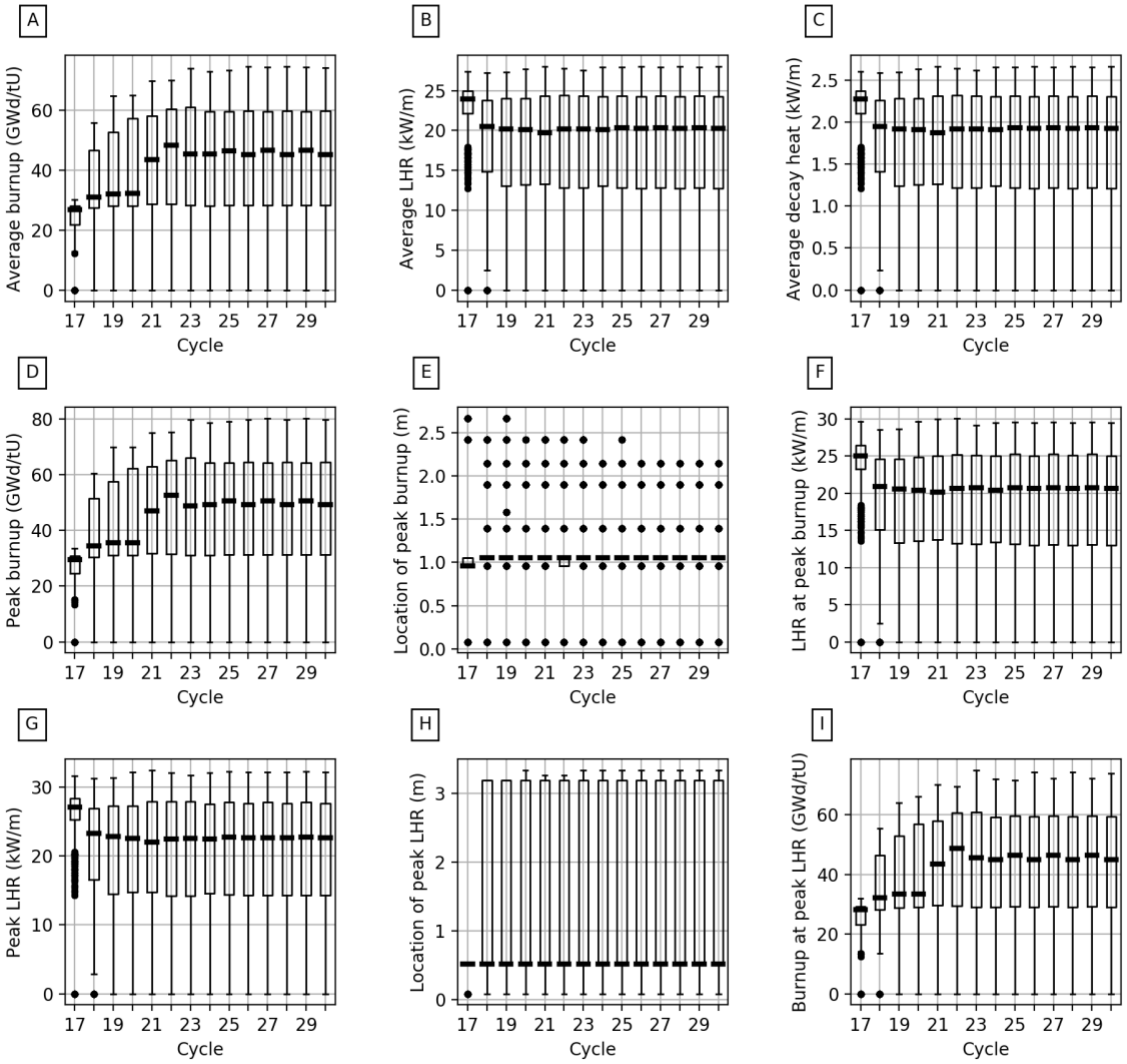

Figure 3. EOC operating conditions extracted from 351,348 fuel rods irradiated in Cycles 17–30. Fuel rods irradiated in previous cycles are not shown. For each cycle and operating condition, the boxes illustrate the median and IQR, and the whiskers illustrate ±1.5 IQR. Outliers are also shown. The transition between standard- and high-burnup fuel rod designs, which is initiated at Cycle 17, forces the distributions to evolve over time until equilibrium is reached at Cycle 28.

Cycles 28–30 were selected for further analysis in this work. Because the fuel assemblies considered in this work were shuffled a maximum of two times, analyzing three consecutive cycles enables the fuel rods with the highest core residence times to be assessed. Although operational history, core design, and fuel rod design may differ for each reactor, focusing on the equilibrium cycles in this work helps avoid uncertainties specific to the transition between standard-burnup and high-burnup fuel rod designs for this particular reactor. This should make it easier to isolate and analyze the behavior of high-burnup fuel rods and generalize the findings of this work to other reactors, cores, and fuels. This methodology could be used to assess transition cycles; however, the transition cycles considered herein are excessively aggressive and not representative of the approaches that would be used by utilities.

3.1.3 Full core results

Fuel rods in Cycles 28–30 were filtered further to eliminate those that did not achieve a rod average burnup of 62 GWd/tU by the end of Cycle 30. Existing operational and safety limits were assumed to be adequate to address undesirable fuel performance behaviors in fuel rods with average burnups of less than 62 GWd/tU. Therefore, standard-burnup fuel rods were not considered further in this work. Fuel rods inserted into the reactor before Cycle 28 were also filtered out to eliminate those that were present during nonequilibrium operation, yielding 32,944 complete high-burnup fuel rod histories.

Time-dependent operating conditions are plotted for the remaining high-burnup fuel rods in Figure 4. The plots show the threshold burnup of 62 GWd/tU, and the transparencies of the data were adjusted to display all of the data more clearly. The plots illustrate how, for this population of fuel rods, operating conditions evolve within each cycle and from one cycle to another. The results in Figure 4B, Figure 4F, and Figure 4G show that, at any given time, LHRs vary widely between fuel rods. This behavior can be attributed to the fuel rods being irradiated in different locations throughout the core. Assembly shuffling between cycles produces additional complexities. Figure 4A, Figure 4D, and Figure 4I show that these spatial variations in LHR cause fuel rods to accumulate burnup at different rates. These observations suggest that susceptibility to FFRD may vary spatially throughout the core and over time.

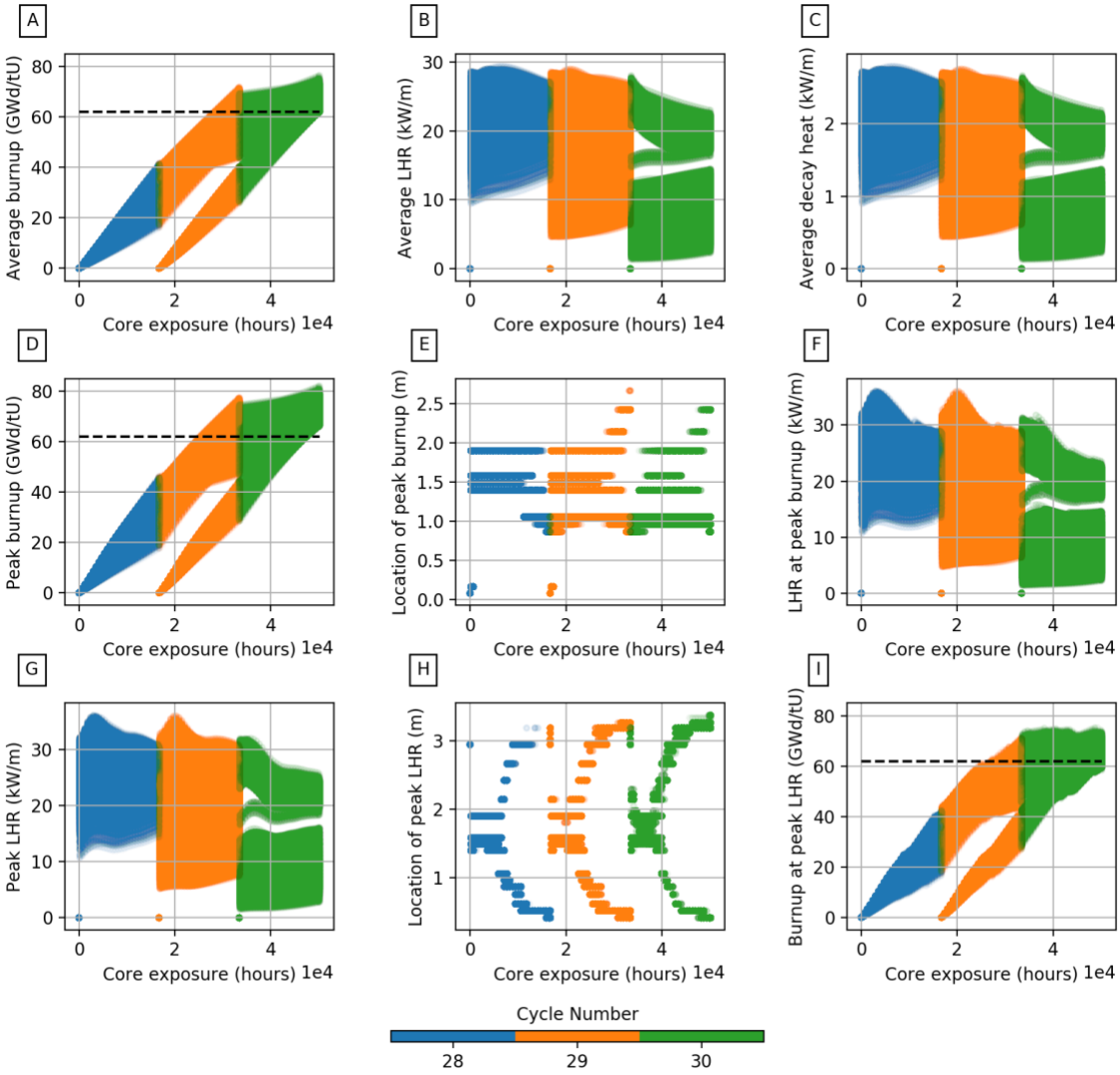

Figure 4. Time-dependent operating conditions extracted from 32,944 fuel rods irradiated in Cycles 28–30. Fuel rods irradiated in previous cycles and those that did not achieve an average burnup of at least 62 GWd/tU (marked by the dashed line) are not shown. The plots show that fuel rods experience wide ranges of operating conditions, which vary with fuel rod location and time.

The axial locations of the peak burnup and LHR shown in Figure 4E and Figure 4H, respectively, exhibit several features that warrant further discussion. Both plots reveal the axial discretization applied in the VERA simulations—49 axial regions. This level of axial discretization was considered sufficient for the purposes of characterizing steady state operating conditions in this work. Figure 4E shows that the axial location of the peak burnup lies near the midplane for most fuel rods and at values of up to about 2.5 m (~75% of the core height) for a smaller subset of fuel rods. Outlier values near the bottom of the core at the beginning of Cycles 28 and 29 correspond to fresh fuel rods being inserted into the core. The first VERA state point is initialized at low power and produces atypical burnup distributions. The burnup distributions take on the expected shapes (i.e., with a maxima near the core midplane) when power is raised to normal operating power for the second VERA state point. Note that this issue does not occur at the beginning of Cycle 30 because all fuel rods considered in Cycle 30 were previously irradiated for at

least one cycle. In general, fuel burnout is accelerated near the midplane, which depresses local LHR later in fuel life.

Figure 4H shows how the axial location of the peak LHR evolves over time. In general, the axial distribution of each fuel rod's LHR transitions from a unimodal distribution with it's maximum near the core midplane to a bimodal distribution with maxima near the top and bottom of the core. Where each fuel rod's peak LHR occurs—near the top or bottom of the core—depends on the rod's irradiation history and location in the core.

EOC operating conditions for Cycles 28–30 are shown in Figure 5. Data from fuel rods irradiated before Cycle 28 and fuel rods that did not achieve an average burnup of at least 62 GWd/tU by the end of Cycle 30 are not shown. This allows overall trends in the operating conditions of high-burnup fuel rods to be analyzed. Figure 5 shows that EOC average and peak burnup increase over time as expected. Fresh fuel assemblies are placed either on the ring of fire or inside it where more uniform irradiation conditions produce narrow burnup distributions. The distributions broaden by the end of Cycle 29 because once-burned fuel assemblies can be placed either inside or outside the ring of fire—locations with drastically different irradiation conditions. Twice-burned fuel assemblies are always shuffled into locations outside the ring of fire, producing narrow distributions by the end of Cycle 30. Some fuel rods achieve peak burnups (i.e., pellet average burnups) greater than 80 GWd/tU.

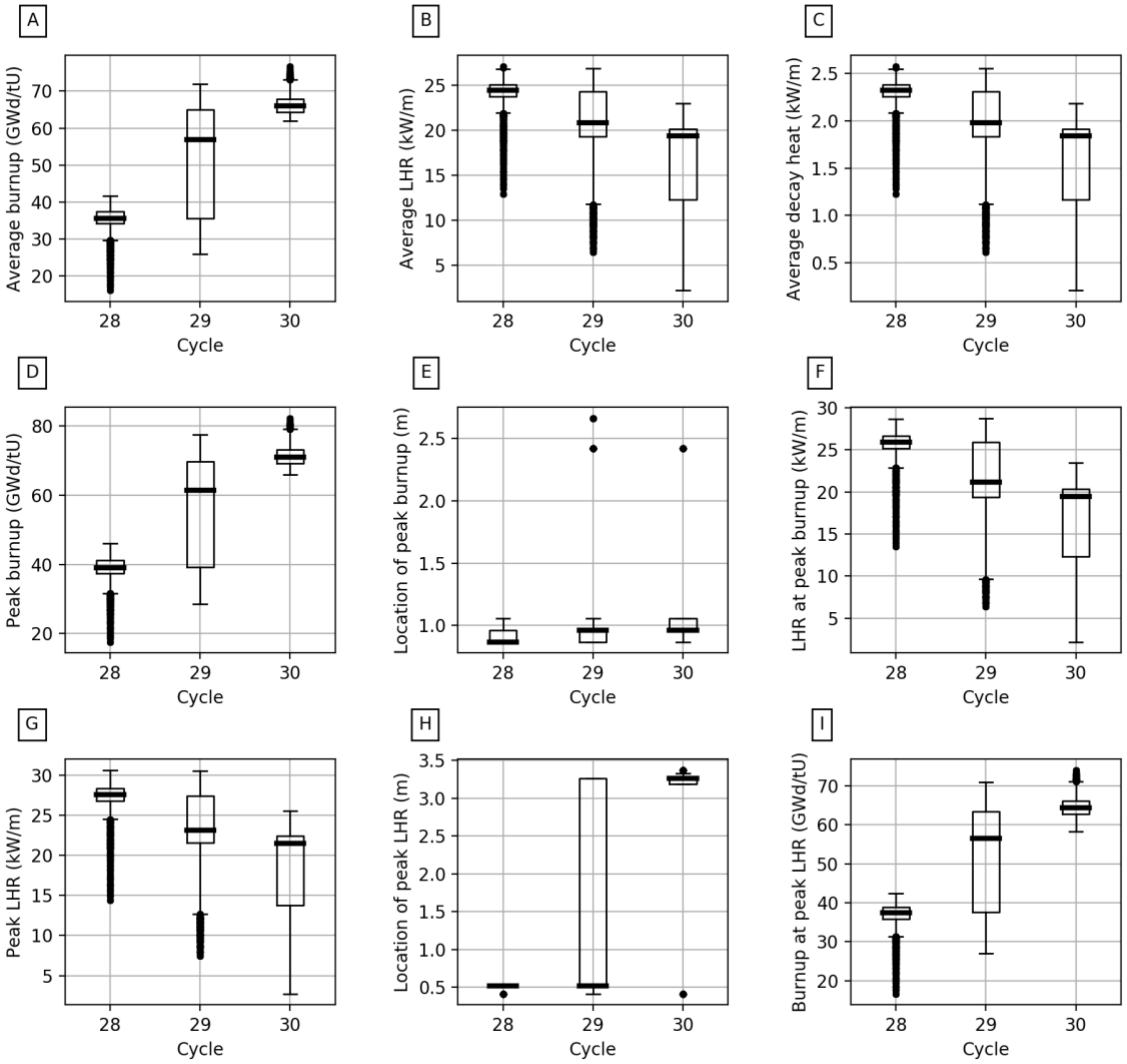

Figure 5. EOC operating conditions extracted from 32,944 fuel rods irradiated in Cycles 28–30. Fuel rods that were irradiated in previous cycles and those that did not achieve an average burnup of at least 62 GWd/tU are not shown.

Figure 5 shows that EOC LHRs generally decrease over time. Fuel rods with the highest LHRs are first placed either on the ring of fire or inside it. From there, they may be shuffled inside the ring of fire where LHRs are lower or outside the ring of fire where LHRs are lowest. Figure 5E shows that the axial location of the peak burnup lies at or above the midplane for most fuel rods. Meanwhile, Figure 5h shows that the axial location of the peak LHR generally shifts downward from the midplane at the beginning of fuel life and then back toward the top of the fuel rod over time. This suggests that the highest burnup and highest temperature regions of the fuel may align for at least a portion of fuel life as illustrated by the HBFF analysis methodology shown in Figure 2, indicating that careful consideration is required when assessing FFRD. Fortunately, the peak LHR continues to shift towards the upper regions of the rod, where the local burnup is lower. Furthermore, FFRD depends more strongly on burnup than other parameters (i.e., temperature), and a higher portion of the fuel rods exceed 62 GWd/tU at EOC, suggesting that EOC values are most limiting for FFRD susceptibility.

Comparing the time-dependent operating conditions in Figure 4 and EOC operating conditions in Figure 5 shows that the EOC values do not necessarily represent the most extreme conditions. EOC values are associated with the higher risk of FFRD from a burnup perspective because burnup increases monotonically, and more rods exceed 62 GWd/tU later in life. However, operating conditions that occur earlier in cycles may increase the risk of FFRD from a temperature/LHR perspective. Still, other times may be worse when considering spatial relationships between the two factors. Histograms showing how many of the fuel rods experienced maxima in the operating conditions of interest at a given time are included in Figure 6 to further illustrate these points. The horizontal axes show the number of VERA depletion calculation states since the beginning of Cycle 28, which can be interpreted as irradiation time.

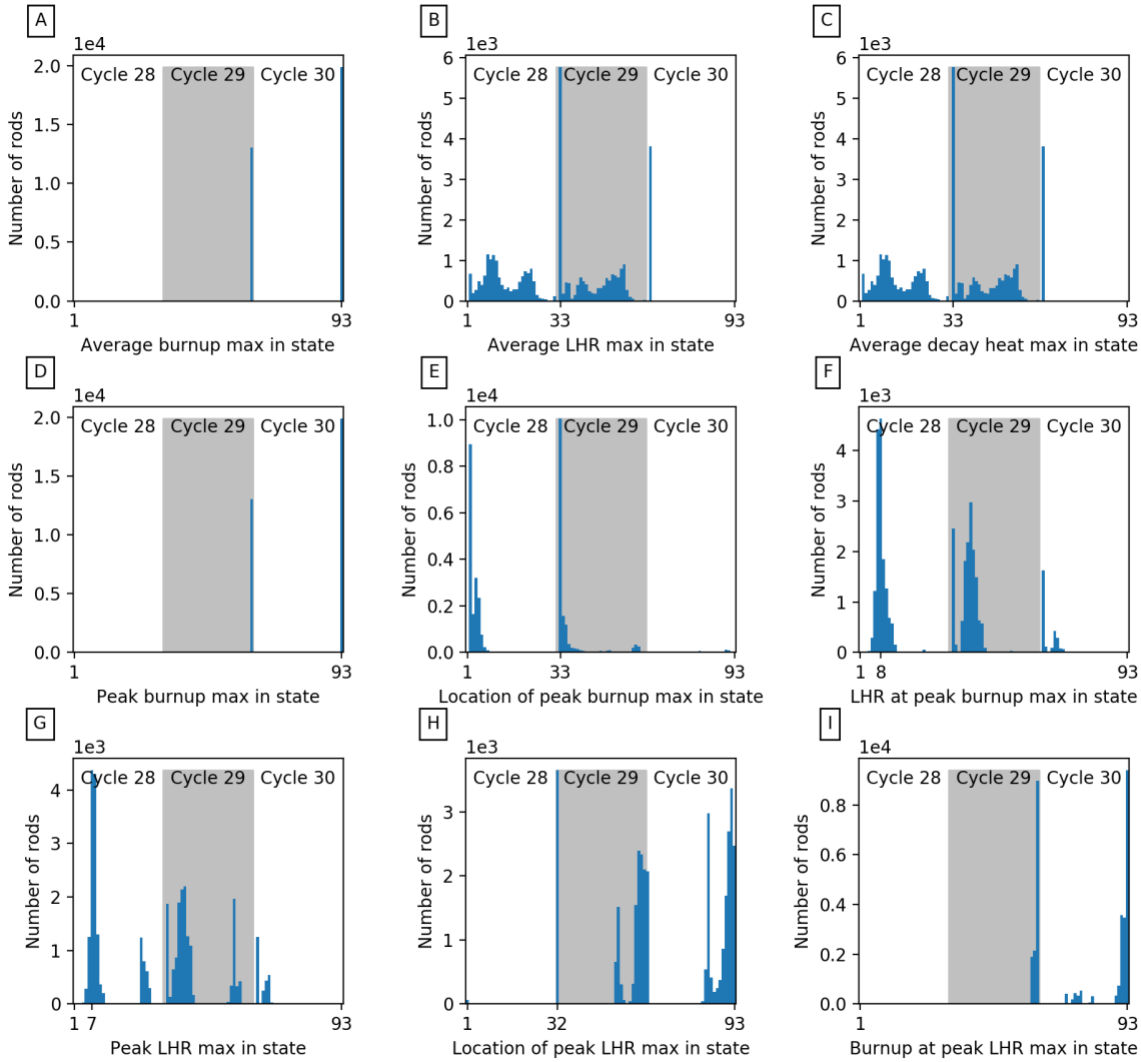

Figure 6. Histograms generated for 32,944 fuel rods irradiated in Cycles 28–30 (excluding data from fuel rods irradiated in previous cycles and those that did not achieve an average burnup of at least 62 GWd/tU). The horizontal axes show the number of states (corresponding to VERA depletion calculations) since the beginning of Cycle 28, which can be interpreted as irradiation time. For each state and operating condition, the histograms give the number of rods that experienced the maximum value of that operating condition during that state. This information illustrates how the EOC values shown in Figure 3 and Figure 5 do not necessarily capture the extremes of the operating condition distributions.

Figure 6 provides more context for several of the points raised in the preceding paragraphs. Figure 6A and Figure 6D show that burnup is always highest at the end of each cycle, as expected. Burnups are highest at the end of Cycle 29 for fuel rods that were shuffled once and highest at the end of Cycle 30 for those that were shuffled twice. Figure 6b and Figure 6g show that the highest LHRs are distributed throughout the cycles. Large groups of fuel rods experienced their highest LHRs at about one-quarter of the way into or one-quarter before the end of Cycles 28 and 29. Another large group of fuel rods experienced its highest LHRs at the beginning of Cycle 29, and all the fuel rods that experienced their highest LHRs in Cycle 30 did so near the beginning of the cycle. Finally, Figure 6h shows that the axial location of the peak LHR was highest in the last one-third of each cycle for nearly all fuel rods.

Operating condition data from the 32,944 high-burnup fuel rods in Cycles 28–30 were sampled across all cycles and VERA depletion calculation states to calculate a set of statistics that describes the overall behavior of FFRD-relevant parameters for these core and fuel rod designs. These statistics are presented in Table 2. These values provide a convenient means for selecting limiting fuel rods for BISON fuel performance analysis in this work and may be useful for comparisons with steady state operating conditions calculated for other core and fuel rod designs in the future.

Table 2. Operating condition statistics generated from 32,944 fuel rods irradiated in Cycles 28–30 (excluding data from fuel rods irradiated in previous cycles and those that did not achieve an average burnup of at least 62 GWd/tU). All cycles and states were considered in the calculations in order to capture the true extremes of the distributions.

Operating condition	Units	Minimum	Average	Standard deviation	Maximum
Average burnup	GWd/tU	0.07	36.95	20.08	76.64
Average LHR	kW/m	1.28	20.30	5.94	29.40
Average decay heat	kW/m	0.12	1.93	0.56	2.79
Peak burnup	GWd/tU	0.08	40.59	21.47	82.21
Location of peak burnup	m	0.17	1.25	0.29	2.66
LHR at peak burnup	kW/m	1.28	22.11	6.92	36.12
Peak LHR	kW/m	1.45	23.26	6.95	36.12
Location of peak LHR	m	0.41	1.73	0.97	3.37
Burnup at peak LHR	GWd/tU	0.08	38.54	20.06	75.27

3.1.4 Fuel rod down-selection

VERA simulations like those used to produce the results being examined in the current work take approximately 24 h per cycle to run on 1,000 cores. 2D axisymmetric BISON simulations for one fuel rod with a three cycle irradiation history takes approximately 3 h to run on 16 cores. The benefits of parallelization when simulating one fuel rod in BISON diminish as more cores are added, but the number of fuel rods that can be simulated in parallel is limited only by cluster availability and utilization limits. Although these values are approximate, they can be used to estimate the magnitude of the time and computational resources needed to simulate high-burnup fuel rods in BISON.

Assuming that BISON simulations are run with 16 cores each and that total cluster usage is limited to 1,000 cores total, it would take approximately 1,581 h (66 days) to run all 32,944 high-burnup fuel rods identified in Cycles 28–30. Furthermore, the BISON simulations were expected to need to run multiple times for each fuel rod to enable troubleshooting and provide support for follow-on TH and transient analyses, as needed. For these reasons, a smaller subset of fuel rods was selected for BISON fuel performance analysis.

To generalize the findings of the smaller subset to the larger population of fuel rods, it was important to ensure that the down-selected rods provided a representative sample of the whole. Ensuring that the down-selected rods adequately capture the influence of fuel rod location—both fuel rod location within an assembly and assembly location within the core—on steady-state operating conditions was also a priority. Several down-selection strategies were developed and tested. Additional context related to the process and details of the down-selection strategy ultimately selected for use in this work are described as follows.

The VERA simulations considered in this work were conducted in rotational quarter-core symmetry, meaning that only one-quarter of the core was included in each simulation. An example of quarter-core results is shown on the left-hand side of Figure 7. Within that quarter of the core, the results of both octants appeared to be very similar when reflected across the line separating the two. A symmetric geometric grid of 24 fuel rods per assembly was applied to the upper octant to select a variety of fuel rod locations with respect to both assemblies and the core. Fuel rods were selected for subsequent fuel performance analysis if (1) they were shuffled through the locations defined by the grid at any time during Cycles 28–30 or (2) they experienced an extreme (minimum or maximum) in the operating conditions of interest shown in Table 2. This process yielded 753 fuel rods. The locations of down-selected fuel rods at the end of Cycle 30 are shown on the right-hand side of Figure 7.

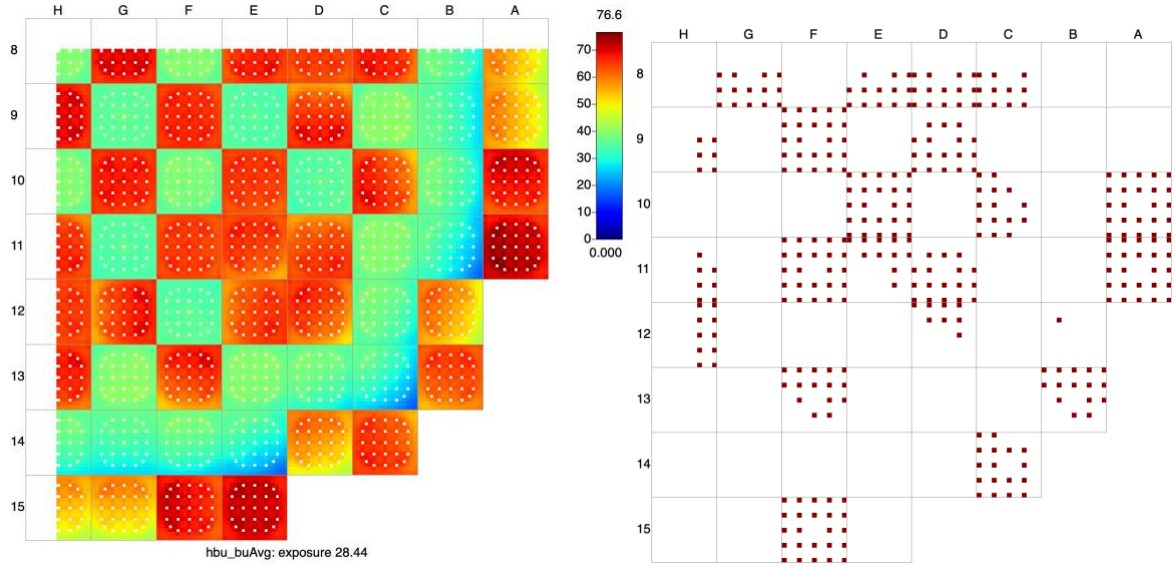

Figure 7. VERAView plots illustrating average burnup at the end of Cycle 30 in GWd/tU (left), and the locations of the fuel rods selected for fuel performance analysis in BISON (right).

Operating condition data from the 753 down-selected fuel rods were sampled across all cycles and states to calculate statistics as was done for all 32,944 high-burnup fuel rods in Section 0. Averages and standard deviations from the two sets of statistics are compared in Table 3. Minimum and maximum values were not compared because the fuel rods that experienced extremes in the operating conditions of interest were explicitly included in the down-selections. Relative differences were calculated for the averages and standard deviations, and all were found to be less than 2%. This suggests that the down-selections provide a representative sample of the larger set.

Table 3. Operating condition statistics generated from all 32,944 fuel rods shown in Table 2 compared with statistics generated from the 753 fuel rods selected for fuel performance analysis in BISON. The small relative differences between the two sets' statistics improve confidence that the smaller set provides a representative sample of the larger set.

Operating condition	Units	Average			Standard deviation		
		All rods	Selected rods	Rel. diff.	All rods	Selected rods	Rel. diff.
Average burnup	GWd/tU	36.95	36.93	-0.05%	20.08	19.90	-0.90%
Average LHR	kW/m	20.30	20.12	-0.89%	5.94	6.02	1.35%
Average decay heat	kW/m	1.93	1.91	-1.04%	0.56	0.57	1.79%
Peak burnup	GWd/tU	40.59	40.47	-0.30%	21.47	21.25	-1.02%
Location of peak burnup	m	1.25	1.26	0.80%	0.29	0.29	0.00%
LHR at peak burnup	kW/m	22.11	21.95	-0.72%	6.92	7.01	1.30%
Peak LHR	kW/m	23.26	23.10	-0.69%	6.95	7.05	1.44%
Location of peak LHR	m	1.73	1.73	0.00%	0.97	0.97	0.00%
Burnup at peak LHR	GWd/tU	38.54	38.45	-0.23%	20.06	19.86	-1.00%

Histograms showing how many of the 753 fuel rods experienced maxima in the operating conditions of interest at a given time were then created and compared with those plotted for the larger set in Figure 6. Overall trends in the two sets of plots were inspected manually and found to compare favorably. This further improved confidence that the down-selections provide a representative sample of the larger set. The down-selections were therefore determined to be satisfactory for the current work. Other sampling techniques and down-selection methods may be considered in future work.

3.2 FUEL PERFORMNACE ANALYSIS IN BISON

The VERA–BISON coupling module, VERAOneWay [12], was applied to generate BISON input files for the selected fuel rods using the geometry and irradiation histories described by the VERA input files and simulation results. The following sections describe fuel performance parameters of interest, the modeling approach applied to simulate fuel rods in BISON, BISON simulation results, and results derived by combining BISON predictions with VERA predictions presented in Section 3.1. The BISON input files and results produced in this portion of the work provide the complete set of inputs needed to conduct follow-on thermal-hydraulic and transient simulations.

3.2.1 Parameters of interest

Fuel performance parameters of interest were selected to help assess the susceptibility of high-burnup fuel rods to FFRD. Like the VERA-derived operating conditions of interest introduced in Section 3.1.1, the fuel performance parameters of interest were selected according to the HBFF analysis methodology shown in Figure 2 [5]. Specifically, selections were made to characterize fuel rod temperature behaviors, cladding ballooning behaviors, and the spatial relationships between them. Six fuel performance parameters of interest were defined:

1. RIP
2. Fuel rod FGR
3. Peak FCT
4. Axial location of the peak FCT
5. Local burnup at the location of the peak FCT
6. Local LHR at the axial location of the peak FCT

Several aspects of these fuel performance parameters listed above require further discussion. First, the fuel performance parameters listed above complement the LHR-based operating conditions of interest by providing direct fuel temperature estimates. Second, these parameters offer additional insights into the cladding ballooning behaviors relevant to FFRD. Key parameters that affect fuel rod ballooning behaviors include (1) RIP, which impacts the stress state in the cladding by opposing external coolant pressure, (2) FGR, which can contribute to rapid increases in RIP and degrade heat conduction across the fuel–cladding gap, and (3) fuel rod temperatures, which directly affect RIP and influence cladding thermal creep.

3.2.2 Modeling approach

VERAOneWay uses template files to generate BISON input files from the geometry and irradiation histories described by the VERA inputs and simulation results. The default VERAOneWay template file was modified to construct a BISON modeling approach suitable for the current work. Noteworthy modifications included making minor updates to allow for use of the most recent version of BISON, selecting particular behavioral models and material properties, and adding FFRD-related output objects. Default models and parameter values were used wherever possible. Key models and settings associated with the modeling approach are listed in Table 4. Complete descriptions of the models listed in Table 4 are beyond the scope of this text. Readers are encouraged to refer to the complete BISON syntax manual for a complete description of the theory behind each model, instructions for its use, and references to the literature from which it was derived [4].

Table 4. Physical behaviors and material properties included in the fuel performance simulations and the names of the BISON object(s) used to model each [4].

Physical behavior or material property	BISON object(s)
Conservation of energy	HeatConductionTimeDerivative, HeatConduction, NeutronHeatSource
Conservation of momentum	TensorMechanicsMasterAction, Gravity
Fast neutron flux	FastNeutronFluxAux
Fast neutron fluence	FastNeutronFluenceAux
Fuel grain growth	GrainRadiusAux
Fuel-cladding mechanical contact	ContactAction (frictionless)
Fuel-cladding thermal contact	GapHeatTransferLWR
Fuel burnup	BurnupAction
Fuel and cladding density	Density
Fuel thermal conductivity, heat capacity	ThermalFuel
Fuel thermal expansion	ComputeThermalExpansionEigenstrain (10^{-6} 1/K)
Fuel elasticity tensor	UO2ElasticityTensor
Fuel creep	UO2CreepUpdate
Fuel swelling	UO2VolumetricSwellingEigenstrain
Fuel relocation	UO2RelocationEigenstrain
Fuel FGR	Sifgrs
Cladding thermal conductivity, heat capacity	ZryThermal
Cladding thermal expansion	ZryThermalExpansionMATPROEigenstrain
Cladding elasticity tensor	ZryElasticityTensor
Cladding creep	ZryCreepLOCAErbacherLimbackHoppeUpdate
Cladding swelling	ZryIrradiationGrowthEigenstrain

VERAOneWay uses VERA input files and the results of MPACT neutronic and CTF TH calculations to define fuel rod geometry, fuel density, cladding density, initial fuel porosity, fuel enrichment, average LHR, axial LHR distribution, cladding surface temperature, and coolant pressure. BISON simulations were conducted using an adaptive time-stepping scheme and 2D axisymmetric smeared pellet meshes. The meshes contained four radial fuel elements, 300 axial fuel elements, three radial cladding elements, and 300 axial cladding elements.

3.2.3 Results

Fuel performance parameters of interest are plotted against average burnup and average LHR in Figure 8. Note that the cycles (and therefore colors) in the plots overlap because the fuel performance parameters are plotted against average burnup and average LHR rather than time. The opacities of the data have been adjusted to show the overlapping cycles more clearly and to better illustrate the overall trends. The RIP and FGR predictions in Figure 8A and Figure 8B, respectively, correlate well with average burnup and exhibit the expected behaviors. The peak FCT predictions in Figure 8C and Figure 8I show that peak FCT is correlated more strongly with average LHR than with average burnup. These relationships suggest that FFRD-relevant parameters depend not only on the fuel rod burnup, but also on the way that fuel rods with various burnups are operated (i.e., their LHRs and temperatures).

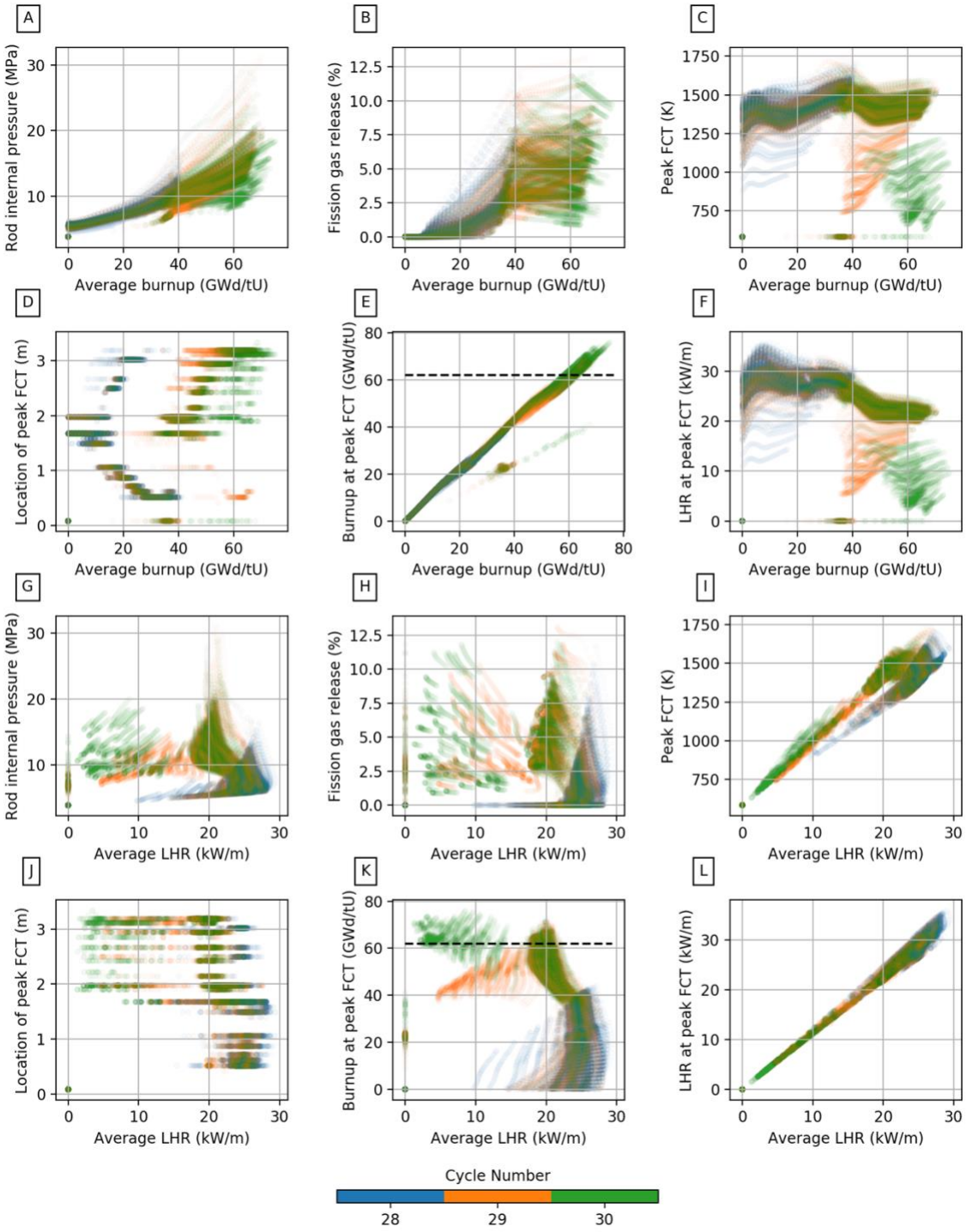

Figure 8. Average burnup- and average LHR-dependent fuel performance results extracted from the 753 fuel rods selected for analysis in BISON. Opacity is adjusted to show data that overlap in burnup- and LHR-space more clearly. Subplots A–C Plots show that the fuel rods exhibit a wide range of responses to irradiation. Subplots D–L Plots begin to illustrate correlations among the fuel performance results and the operating conditions examined in Section 3.1.

EOC fuel performance predictions for Cycles 28–30 are shown in Figure 9. Figure 9B shows that EOC FGR predictions generally increase with irradiation time, as expected. Figure 9C shows that peak FCTs generally decrease over the course of the three cycles, which is consistent with the cycle-by-cycle decreases in average fuel rod LHR due to their being shuffled into lower-power assembly positions. Figure 9C shows that RIP, which is a function of both FGR and fuel rod temperature, generally increases with irradiation time. When interpreting these results, it is important to remember that a portion of the 753 fuel rods were irradiated for only two cycles. As such, the size of the fuel rod population varies from cycle to cycle.

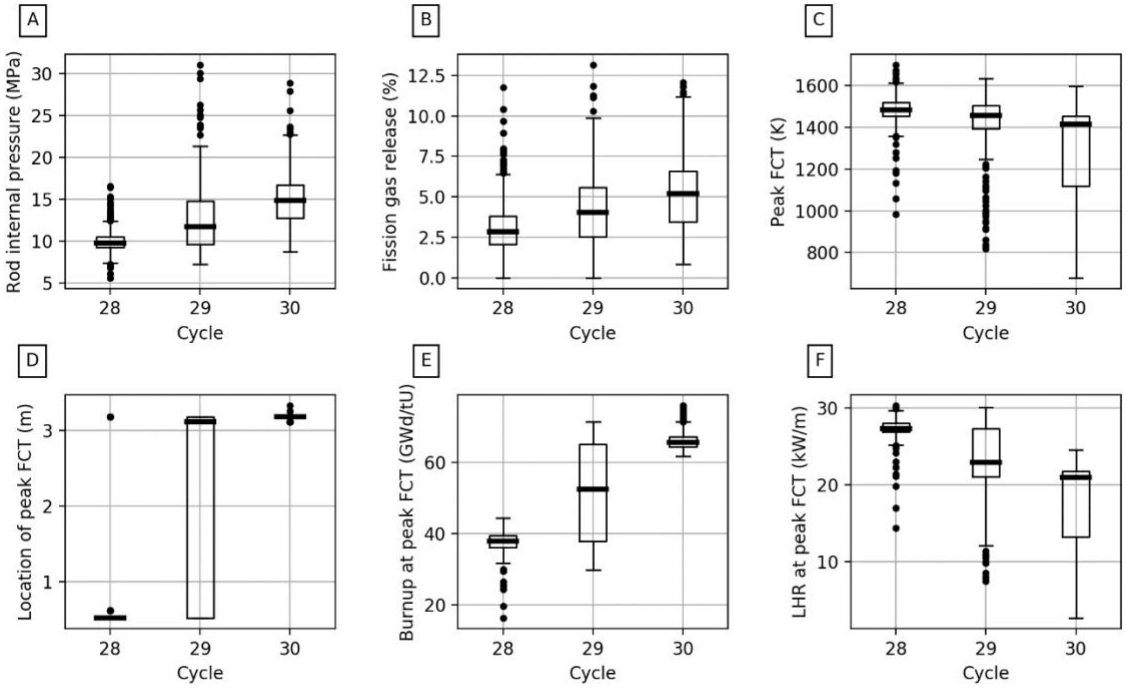

Figure 9. EOC fuel performance results extracted from the 753 fuel rods selected for analysis in BISON.

Figure 9D shows that the location of the peak FCT tends to increase with irradiation time. This is consistent with changes in the location of the peak LHR, as shown in Figure 5H. The general trends in the burnup and LHR behaviors shown in Figure 9E and Figure 9F, respectively, are also consistent with those shown in Figure 5I and Figure 5F. These observations help to confirm that using LHR data to down-select fuel rods with particular temperature behaviors was a reasonable approach. BISON predictions were then sampled across all cycles and VERA depletion states to (1) characterize the full ranges of fuel performance parameters experienced by the fuel rods and (2) determine when in the life-cycle of the fuel rods those conditions were experienced. The results are presented in Figure 10 as functions of average fuel rod burnup.

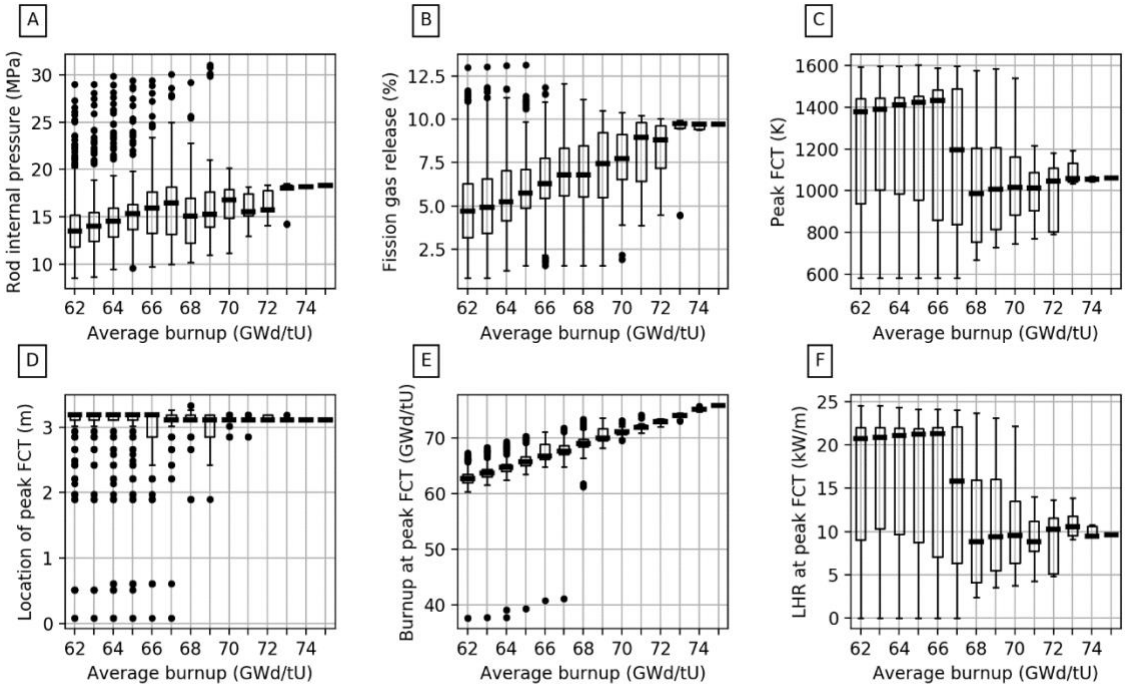

Figure 10. Fuel performance results extracted from the 753 fuel rods selected for analysis in BISON. All cycles and states were considered in the calculations in order to illustrate the ranges of fuel performance parameters that BISON predicts for fuel rods with different average burnups.

Several points should be noted before interpreting the data shown in Figure 10. As with the previous set of results, it is important to remember that the size of the fuel rod population changes over time due to variations in core residence time associated with assembly shuffles. Furthermore, not all fuel rods achieve the highest burnups. This is due to fuel assembly shuffling. These factors tend to make the distributions shown in Figure 10 narrow as burnup increases. The widths of the distributions at each burnup increment are not necessarily related to the levels of uncertainty associated with those predictions; instead, it is likely that uncertainties increase with burnup. With these limitations in mind, the data shown in Figure 10A–Figure 10C are generally consistent with and reinforce the observations made for Figure 9A–Figure 9C above.

Histograms showing how many of the fuel rods experienced maxima in the fuel performance parameters of interest at a given VERA depletion state are shown in Figure 11. As before, the horizontal axes can be interpreted as irradiation time. Figure 11B shows that most fuel rods experience their highest FGRs at the EOCs. Figure 11C shows that large groups of fuel rods also experience their highest peak FCTs at the ends of cycles or within the first quarter of Cycles 29 and 30. Figure 11A also shows that most fuel rods experience their highest RIPs at the ends of cycles.

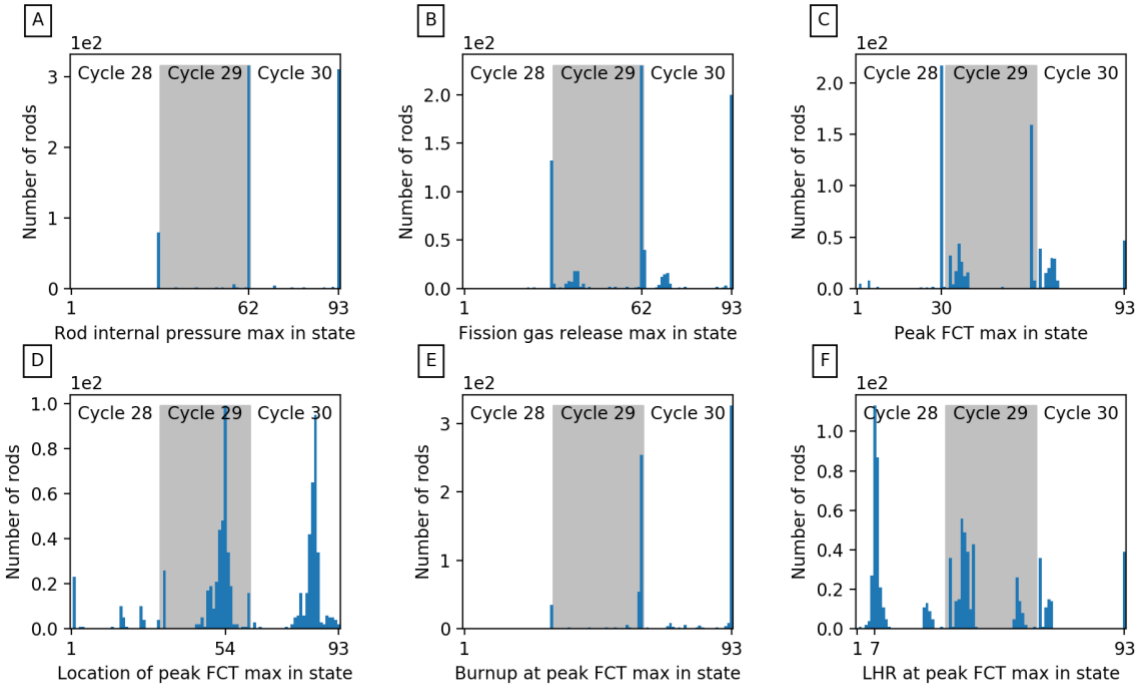

Figure 11. Histograms generated for the 753 fuel rods selected for analysis in BISON. The horizontal axes show the number of VERA depletion states since the beginning of Cycle 28, which can be interpreted as irradiation time. For each state and fuel performance result, the histograms give the number of rods that experienced the maximum value of that fuel performance result during that state. As was the case in Section 3.1, this information illustrates how the EOC values shown in Figure 9 do not necessarily capture the extremes of the fuel performance distributions.

These observed FCT behaviors are partially consistent with the cycle-by-cycle decreases in LHR for particular fuel rods. However, the absence of fuel rods with maxima in their peak FCTs early in Cycle 28 (i.e., when LHRs are the highest) suggests that another factor is involved. Fresh fuel rods conduct heat away from the fuel more efficiently than irradiated fuel rods. Lack of fuel thermal conductivity degradation and FGR early in the fuel rod life cycle likely mitigate the effects of the highest LHRs. Therefore, the observed burnup, peak FCT, and RIP behaviors suggest that FFRD susceptibility may be highest near the end of a fuel rod's second and/or third cycles. Thus, safety analyses may address FFRD concerns at EOC and use those results as bounding for the entire cycle.

Fuel performance data from the 753 high-burnup fuel rods in Cycles 28–30 were sampled across all cycles and states to calculate a set of statistics similar to those presented in Section 3.1. The statistics are presented in Table 5. These values may be useful for comparison with future steady state operating conditions calculated for other core and fuel rod designs in the future.

Table 5. Fuel performance statistics generated from 753 fuel rods selected for analysis in BISON. All cycles and states were then considered in the calculations in order to capture the true extremes of the distributions.

Operating condition	Units	Minimum	Average	Standard deviation	Maximum
Rod internal pressure	MPa	4.49	9.88	3.39	31.04
Fission gas release	%	0.00	3.04	2.64	13.14
Peak FCT	K	627.02	1352.44	192.17	1737.98
Location of peak FCT	m	0.41	1.99	0.91	3.33
Burnup at peak FCT	GWd/tU	0.08	37.73	19.97	75.94
LHR at peak FCT	kW/m	1.41	23.47	6.57	35.86

It is worth noting that 47 (6%) of the 753 BISON simulations did not run to completion. There are no clear similarities or trends in the failed simulations with regards to assembly location, pin location, operating conditions, or fuel performance behaviors. The cause of the simulation failures is still under investigation, but the failures do not appear to meaningfully affect the aforementioned fuel performance distributions above, so the results were considered acceptable for follow-on thermal-hydraulic and transient analyses.

3.3 SENSITIVITY OF FUEL PERFORMANCE PARAMETERS TO FISSION GAS RLEASE

FGR is a multiphysics phenomenon involving thermomechanics, diffusion, grain growth, high-burnup structure, and more. The process contaminates the fuel rod's gap with fission gases, which contribute to increases in RIP and degrade heat transfer out of the fuel, increasing FCTs. FGR is regarded as a significant source of uncertainty in fuel performance modeling. Uncertainties in BISON's FGR predictions and their sensitivities to various inputs have been characterized [13]. FGR predictions are generally considered reasonable when within a factor of two of the measured value. Uncertainties are even higher when attempting to predict FGR values less than 10%.

Although uncertainties associated with FGR and its sensitivities to model inputs have been studied previously, little work has been done to characterize the effect of these uncertainties on parameters such as FCT and RIP for commercial applications. Furthermore, these uncertainties may effect FFRD susceptibility predictions. A preliminary study was conducted to estimate the magnitude of these effects and to begin to understand their role in assessing susceptibility to FFRD. These findings are expected to aid in understanding how fuel performance uncertainties may propagate through follow-on TH and transient analyses.

A simple approach was devised to estimate the magnitude of these effects directly from BISON calculations. Given $y = f(x)$, the estimates take the form $\Delta y/\Delta x$, where y is the predicted FGR, and x is either the FCT or RIP. This approach allows the results to be interpreted quickly and easily; changes in FCT and RIP can be related directly to unit changes in FGR. Numerous other factors, such as LHR and coolant temperature, also affect FCT and RIP calculations, but these effects are considered to be beyond the scope of this work.

Variations in BISON's FGR predictions were induced by artificially manipulating scalar multipliers associated with the intragranular, grain boundary, and effective fission gas diffusion coefficients used by the Sifgrs FGR model: igdiffcoeff_scalef, gbdiffcoeff_scalef, and effdiffcoef_scalef, respectively. Manipulating only these parameters, upon which FCT and RIP have no direct dependence, allows changes in FCT and RIP to be attributed to changes in FGR. Fifteen fuel rods, which defined extremes in the operating conditions and fuel performance parameters examined in Sections 3.1 and 3.2, were

considered in the analysis. Each fuel rod was simulated three times using scalar multipliers of 0.5, 1.0, and 1.5 to produce low, nominal, and high FGR predictions, respectively.

FGR predictions from the 45 BISON simulations are shown in Figure 12. The results demonstrate how manipulating the fission gas diffusion coefficients while maintaining all of the other input parameters the same produced the desired changes in FGR. The subplot titles denote the VERA-defined names of individual fuel rods. Note that some fuel rods were irradiated longer than others.

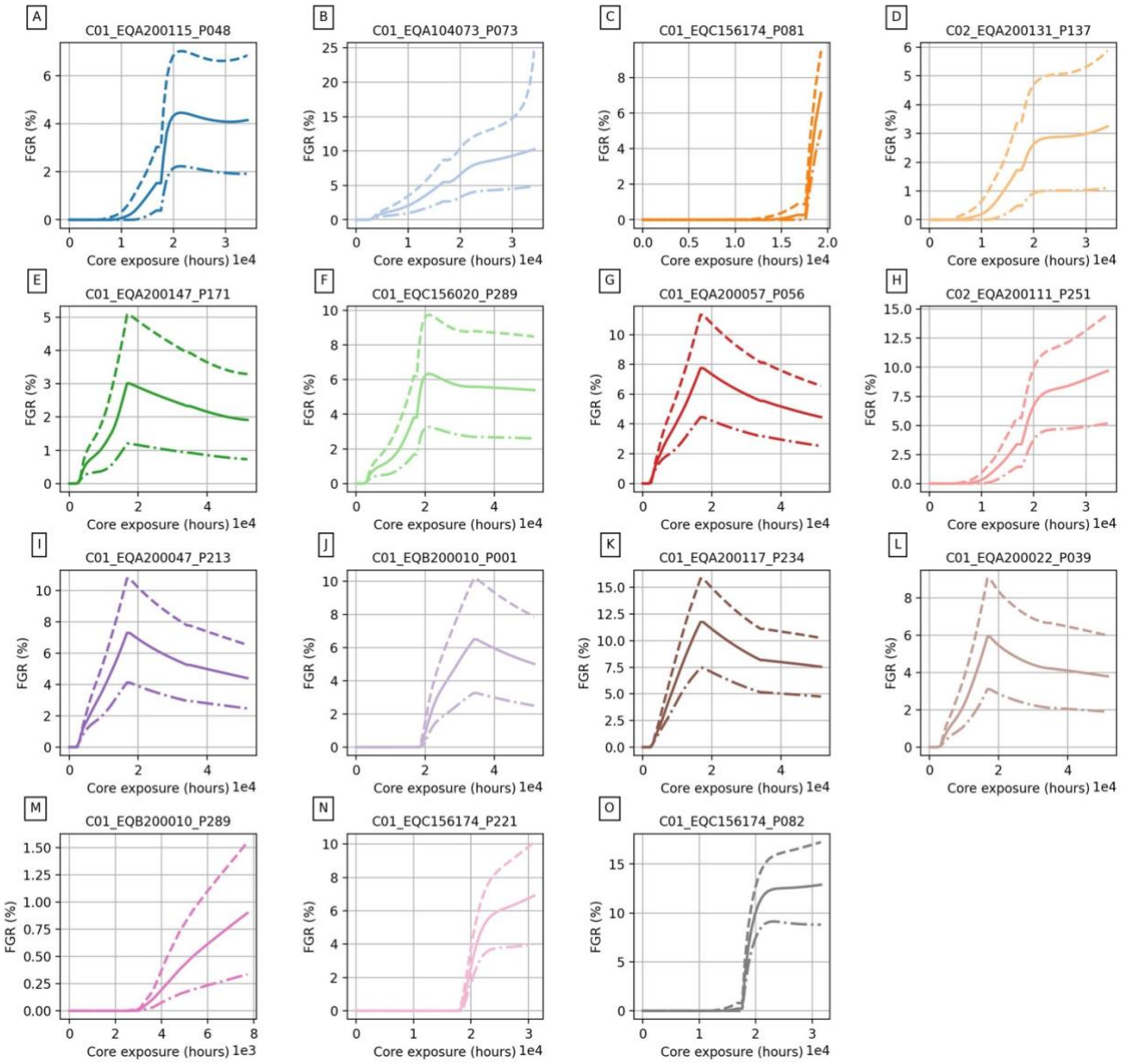

Figure 12. BISON FGR predictions for the 15 fuel rods that lie at the extremes of the operating condition and fuel performance distributions. The FGR model was manipulated to obtain results for high, nominal, and low FGR cases (shown with dashed, solid, and dot-dashed lines, respectively).

FCT predictions from the 45 BISON simulations are shown in Figure 13. The results show that FCT increases slightly with FGR, as expected. Initial, inter-cycle, and final startups and shutdowns are clearly visible in the form of vertical discontinuities in the results. These discontinuities clearly illustrate the number of cycles during which each rod was irradiated during. At least one simulation did not run to

completion for the four fuel rods shown in Figure 13C and Figure 13M–Figure 13O. Although the cause of these simulation failures is still under investigation, the available data were determined to be acceptable for the purposes of this study because the fuel rods had undergone sufficient amounts of FGR. Figure 13b is an outlier in the fuel temperature start rapidly increasing towards the end of cycle. This shows the inherent relationship between FGR and fuel temperatures. FGR is strongly dependent on burnup (FG buildup) and temperature. What is observed in Figure 13b is associated with the amount of FG being released has a significant impact on fuel temperatures, and as fuel temperatures increase, more FG is released to further decrease in thermal transport from the fuel to the coolant.

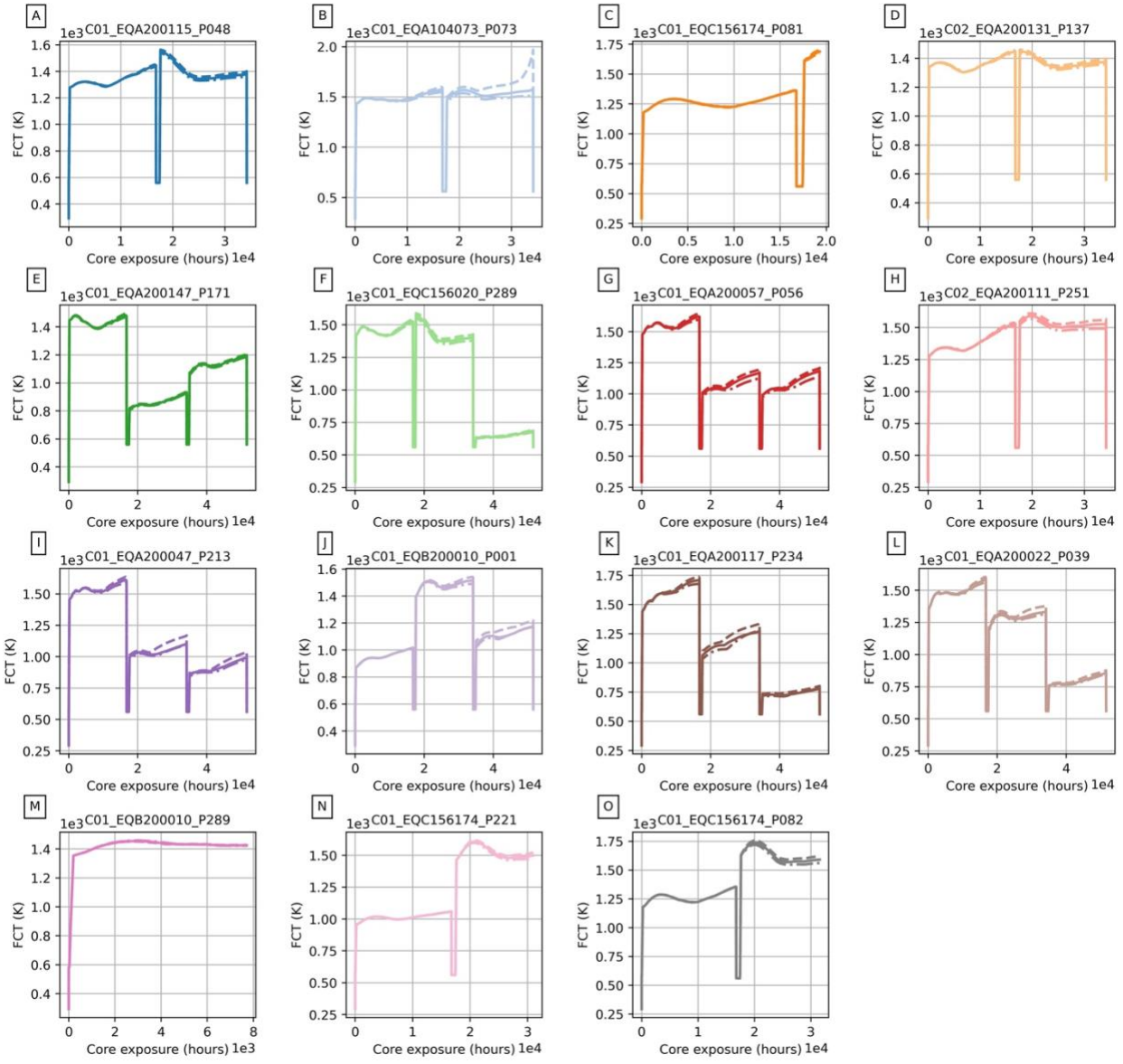

Figure 13. BISON FCT predictions for the 15 fuel rods that lie at the extremes of the operating condition and fuel performance distributions. The FGR model was manipulated to obtain results for high, nominal, and low FGR cases (shown with dashed, solid, and dot-dashed lines, respectively).

Finally, RIP predictions from the 45 BISON simulations are shown in Figure 14. The results show that RIP increases significantly with FGR, as expected. Startups and shutdowns are again visible in the form of vertical discontinuities in the results. The data demonstrate how uncertainties in FGR can substantially

affect other fuel performance predictions relevant to FFRD. The predictions in Figure 14b illustrate this point particularly well. This fuel rod exhibited unusually large RIPs with the high, nominal, and low FGR cases yielding peak RIPs of approximately 53, 31, and 8 MPa, respectively. Figure 12B shows that these RIPs correspond to FGR values of approximately 5, 11, and 24%, respectively. These FGR values vary from each other by factors of approximately two, which is consistent with the magnitude of the variations that are expected to arise from uncertainties inherent to the BISON FGR model [13]. Given the strong influence of FGR on RIP and the large uncertainties in FGR predictions, all of the variations in RIP shown in Figure 14 may be considered reasonable.

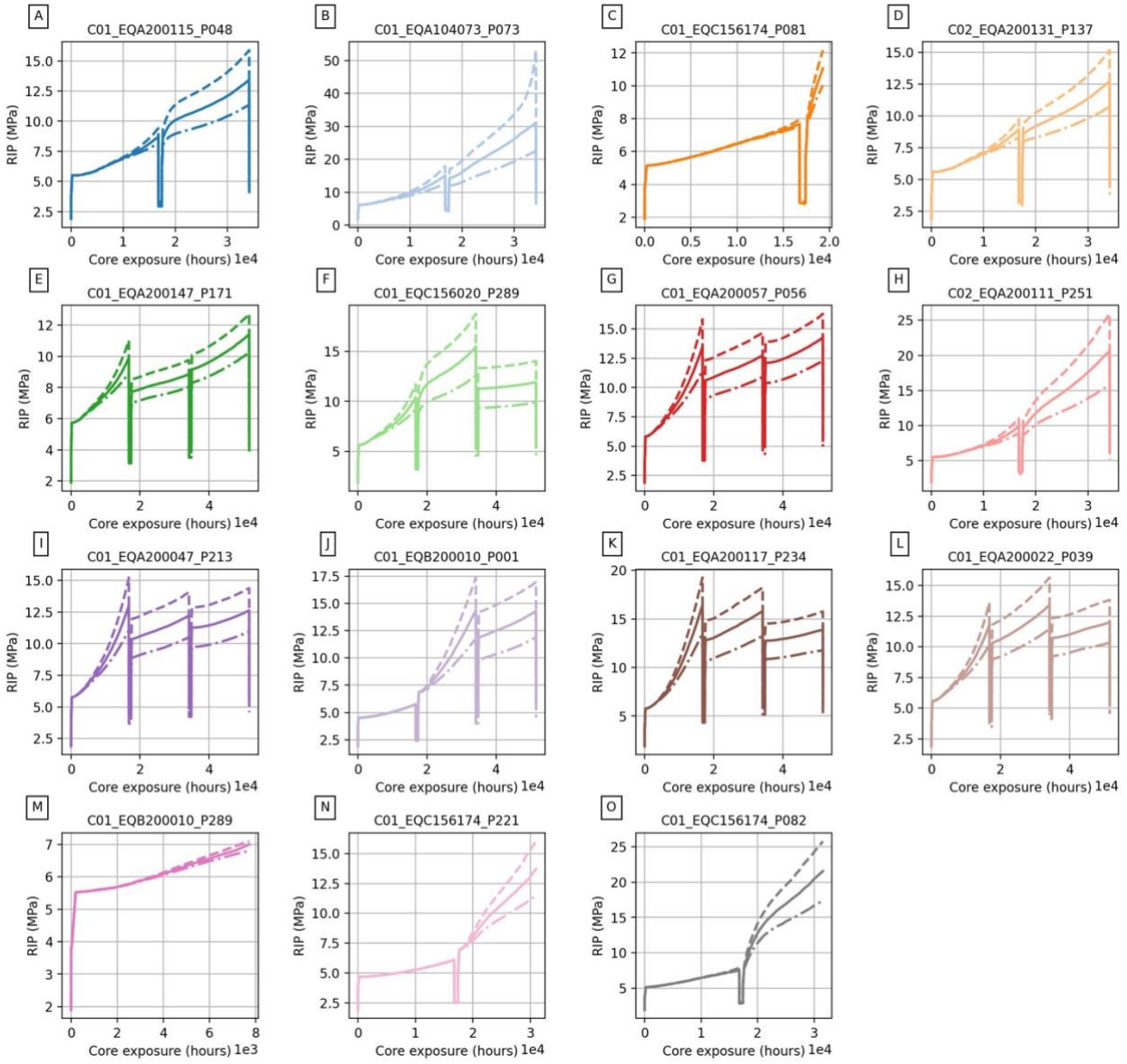

Figure 14. BISON RIP predictions for the 15 fuel rods that lie at the extremes of the operating condition and fuel performance distributions. The FGR model was manipulated to obtain results for high, nominal, and low FGR cases (shown with dashed, solid, and dot-dashed lines, respectively).

Accounting for additional uncertainties in operating conditions such as power and coolant flow and irradiation behaviors such as fuel cracking and thermal conductivity degradation is expected to further compound uncertainties. These observations have important implications with regards to predicting even

more sophisticated multiphysics behaviors, such as quantifying susceptibility to FFRD. FGR predictions, and therefore FCT predictions, RIP predictions, and FFRD susceptibility estimates, may need to be interpreted as best estimate plus uncertainty rather as deterministic.

Calculated $\Delta FCT/\Delta FGR$ and $\Delta RIP/\Delta FGR$ values are plotted in Figure 15. Colored solid lines denote time-averaged values for each fuel rod, and the overall rod-averaged value is denoted with dashed black lines. The values with the 0.5 subscripts (e.g., $\Delta FCT_{0.5}/\Delta FGR_{0.5}$) were calculated by comparing predictions for the nominal and low FGR cases. Similarly, the values with the 1.5 subscripts were calculated by comparing the high and nominal FGR cases. The results provide estimates for how much FCT and RIP can be expected to change with FGR and how much those values can be expected to vary between fuel rods.

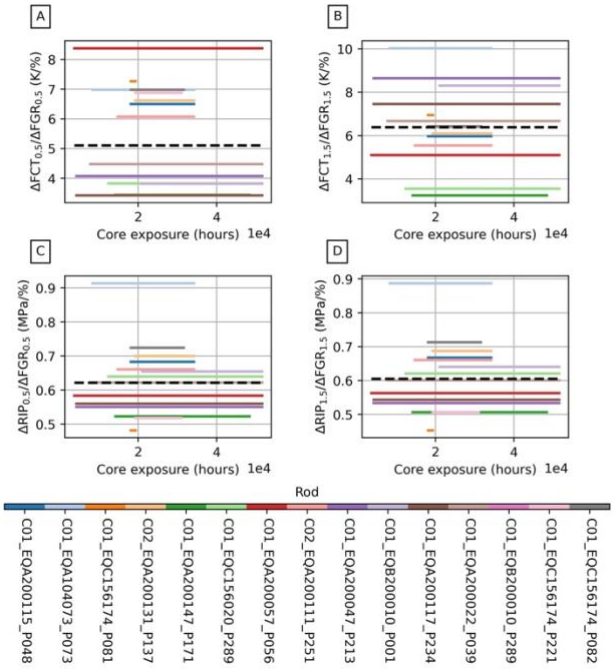

Figure 15. Time-averaged changes in FCT (A and B) and RIP (C and D) per change in FGR for fuel rods that lie at the extremes of the operating condition and fuel performance distributions. Results obtained from the nominal versus low FGR cases (A and C) and high versus nominal FGR cases (B and D) are shown. Results from BISON simulations that failed are not included. Rod-averaged values are shown with dashed black lines in each subplot. The results provide an estimate of how uncertainties in FGR modeling may affect predictions for other key figures of merit.

Time- and rod-averaged numerical results from Figure 15 are summarized in Table 6. The results indicate that FCT and RIP can be expected to change by about 6 K and by about 0.6 MPa per percent FGR, respectively. Consistency between the $\Delta\text{RIP}_{0.5}/\Delta FGR_{0.5}$ and $\Delta\text{RIP}_{1.5}/\Delta FGR_{1.5}$ values suggests that these estimates should be applicable regardless of whether BISON is underpredicting or overpredicting FGR. The $\Delta\text{FCT}_{0.5}/\Delta FGR_{0.5}$ and $\Delta FCT_{1.5}/\Delta FGR_{1.5}$ values are slightly less consistent, but their magnitudes are both significantly smaller than typical differences between fuel operating and melting temperatures.

Table 6. Time- and rod-averaged responses based on the data shown in Figure 15.

Parameter	Units	Value
$\Delta FCT/\Delta FGR_{0.5}$	K/%	5.11
$\Delta FCT/\Delta FGR_{1.5}$	K/%	6.39
$\Delta RIP/\Delta FGR_{0.5}$	MPa/%	0.62
$\Delta RIP/\Delta FGR_{1.5}$	MPa/%	0.61

As an example of how these values could be used, consider a fuel rod with a BISON-predicted FGR of 10%. According to Giovanni et al. [13], this prediction could be considered reasonable if the measured FGR were 5–20%. Assuming that were the case, BISON-predicted FCT and RIP values could be expected to include errors of up to 30–60 K and 3–6 MPa, but only because of uncertainties in the FGR model. These points should be considered when interpreting fuel performance predictions against temperature and cladding ballooning criteria to estimate susceptibility to FFRD. The authors expect that more robust uncertainty quantification would need to be performed for specific fuel rod and core designs to refine these methods further.

3.4 EFFECTS OF ROD AND ASSEMBLY LOCATIONS ON FUEL PERFORMANCE

Several times in Sections 3.1 and 3.2, FFRD-relevant operating conditions and fuel performance behaviors were observed to correlate to fuel rod and assembly locations. These correlations indicate that core design and shuffling patterns may influence the character and/or magnitude of FFRD susceptibility. Limiting behaviors and scenarios are more likely to differ for various fuel rod and core designs, but overall trends may be more generally applicable. This section briefly introduces these concepts, and the influence of core design with regards to FFRD is discussed in more detail in the following section.

As noted in Section 0, fresh fuel assemblies are placed either on the ring of fire or inside of it. Fresh fuel assemblies placed within the ring of fire are interspersed with once-burned fuel assemblies. Once-burned fuel assemblies are also placed outside of the ring of fire on the core periphery. Twice-burned fuel assemblies are always placed on the core periphery. Among other benefits, this approach helps to reduce pressure vessel dose and neutron leakage from the core. This core loading pattern is shown in Figure 16 (top left).

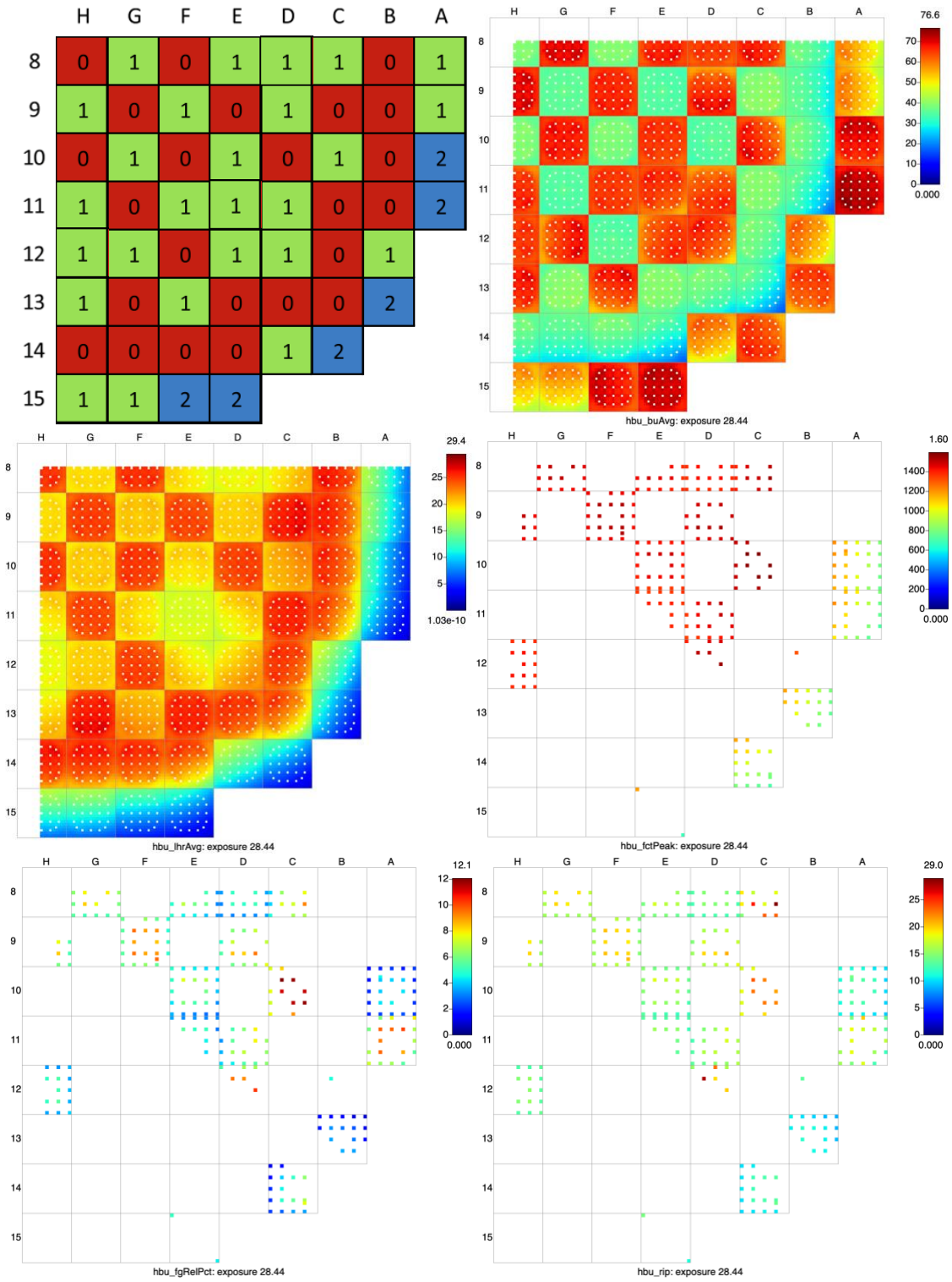

Figure 16. VERAView plots illustrating the core loading pattern, which denotes the number of previous irradiation cycles for each fuel assembly (top left, modified from Reference [5]), average burnup in GWd/tU (top right), average LHR in kW/m (mid left), FCT in K (mid right), FGR in % (bottom left), and RIP in MPa (bottom right) at the end of Cycle 30. These results begin to illustrate how spatial variations in operating conditions and fuel performance throughout the core may affect the susceptibility of high-burnup fuel to fragmentation.

Average fuel rod burnup and LHR at the end of Cycle 30 are shown in Figure 16 (top right and mid left, respectively). The burnup results correspond to the shuffling patterns described in the preceding paragraph—fresh fuel assemblies are placed on or inside the ring of fire, once-burned fuel assemblies are placed inside or outside the ring of fire, and twice-burned fuel assemblies are always placed on the core periphery. The LHR results illustrate how the power levels of these locations vary significantly from one another. These variations affect the temperatures of fuel rods in those locations and the rates at which they accumulate burnup.

These spatial variations in operating conditions and irradiation histories affect on fuel performance. The peak FCT, FGR, and RIP predictions shown in Figure 16 (mid right, bottom left, and bottom right, respectively) illustrate this point. Although, the BISON results exhibit several recognizable spatial trends, which are discussed further below. When interpreting these results, it is important to remember that BISON simulations were run only for high-burnup fuel rods (i.e., fuel rods that achieved average burnups of at least 62 GWd/tU). Existing operational and safety limits were assumed to be adequate to address undesirable fuel performance behaviors in standard-burnup fuel rods.

The peak FCT predictions shown in Figure 16 (mid right) correspond well with the LHR results (mid left). The peak FCTs are generally higher and flatter within the ring of fire and decrease significantly near the core periphery. Peak FCTs are highest in once-burned fuel assemblies immediately inside of the ring of fire (e.g., in fuel assembly positions C-10 and D-12). Peak FCTs are lowest in once- and twice-burned fuel assemblies on the core periphery (e.g., in fuel assembly positions A-10, A-11, B-13, and C-14).

The spatial variations in the FGR predictions shown in Figure 16 (bottom left) are less intuitive. FGR is a function of burnup, which is analogous to the amount of fission gas produced, and temperature, which largely determines the rate of fission gas diffusion through the fuel. Both once- and twice-burned fuel assemblies inside and outside of the ring of fire exhibit a range of FGR values. However, the highest FGR values again occur in once-burned assemblies immediately inside of the ring of fire (e.g., in fuel assembly position C-10).

The spatial variations in the RIP predictions shown in Figure 16 (bottom right) are also less intuitive. RIP, which is the primary contributor to cladding ballooning, is a function of temperature and FGR. The results show that fuel rods tend to have intermediate to high RIPs inside of the ring of fire and low to intermediate RIPs outside of it. Again, the highest RIP values were found in once-burned fuel assemblies just inside the ring of fire (e.g., in fuel assembly positions C-8, C-10, and D-12). This would suggest that once-burned fuel assemblies near the ring of fire will be more likely to rupture than those elsewhere.

The fuel rods with the highest burnups (approximately 77 GWd/tU in fuel assembly position A-11) consistently exhibit lower temperatures and pressures than certain other fuel rods with intermediate burnups (e.g., 71 and 70 GWd/tU in fuel assembly positions C-10 and D-12, respectively). These observations suggest that (1) using high-burnup fuel rods may increase the total mass of fuel susceptible to FFRD and (2) core design may offset a portion of that increase by shuffling fuel rods with the highest burnups into lower-power assembly positions, which reduces fuel rod temperatures and RIPs.

LHR gradients also occur within individual fuel assemblies, as illustrated for fuel assembly position E-10 in Figure 17. The fuel assembly shown was surrounded by fresh fuel assemblies on three sides (top, left, and right) and a once-burned fuel assembly (bottom). The LHR, burnup, and fuel performance results exhibit two notable trends. First, the values are more limiting for fuel rods near the center of the fuel assembly than those near its periphery. This behavior may be influenced by spatial variations in coolant flow and/or moderation. Second, the values are more limiting for fuel rods that were closer to the fresh fuel assemblies than those near the once-burned fuel assembly. These observations suggesting that cladding rupture and susceptibility to FFRD may vary from rod to rod within individual fuel assemblies.

The assembly shown below utilizes a uniform enrichment across the assembly, however, the results do suggest opportunities may exist to optimize fuel assemblies' enrichment zones. Additionally, there may be opportunities to use axially varying burnable absorbers and replacing the blanket pellets with enriched pellets to push the peaking factors to more axial locations (i.e., lower burnup) that may reduce FFRD in the event of a rupture.

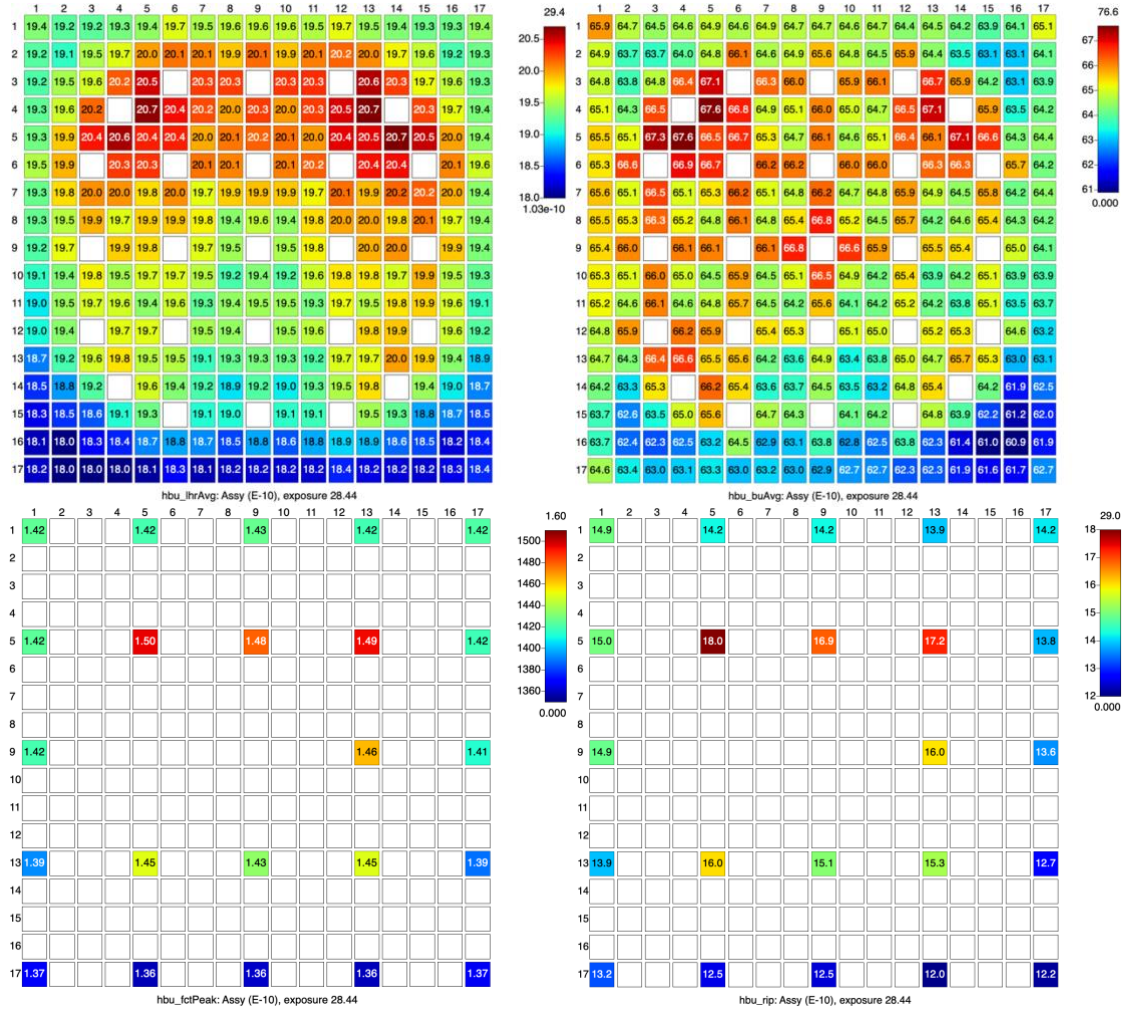

Figure 17. VERAView plots illustrating average burnup in GWd/tU (top right), average LHR in kW/m (top left), FCT in K (bottom left), and RIP in MPa (bottom right) for fuel assembly position E-10 at the end of Cycle 30. These results show how FFRD susceptibility may vary spatially within individual fuel assemblies. Fuel performance results are not shown for fuel rod position 5-9 because the BISON did not run to completion.

Overall, these results demonstrate that fuel performance characteristics important to FFRD (i.e., burnup, powers, temperatures, RIP) vary throughout the core and even within fuel assemblies. Within the context of the HBFF analysis methodology referenced in Section 3.1.1, this suggests that FFRD susceptibility would also vary spatially throughout the core and within fuel assemblies. Therefore, it may be critical for any methodology that assesses FFRD to consider FFRD on a pin-by-pin basis because the operating and fuel performance conditions may have a significant effect on cladding ballooning and rupture behavior and subsequent FFRD susceptibility.

This preliminary analysis examined overall fuel performance trends and identified specific areas of concern, but aforementioned discussions above are based only on steady state operating conditions. Thermal-hydraulic and transient analyses are needed to capture the unique effects that LOCAs transients have on fuel performance, and ultimately, estimate susceptibility to FFRD. The influence of core design on FFRD susceptibility is discussed further in the following section.

3.5 DISCUSSION

A methodology was developed and applied to existing high-burnup VERA core designs to characterize the operating conditions and fuel performance of high-burnup fuel rods during steady-state operation. The ultimate goal was to assess the susceptibility of high-burnup fuel rods to FFRD and identify mitigation strategies (i.e., core design optimizations). Nine operating conditions of interest were selected to characterize fuel rod temperature behaviors, burnup behaviors, and the spatial relationships between them. Equilibrium Cycles 28–30 was selected for detailed analysis. Analyzing three consecutive cycles allows fuel rods with the highest core residence times to be assessed. Focusing on equilibrium cycles helps avoid uncertainties specific to the transition between standard-burnup and high-burnup fuel rod designs for this particular reactor, making make it easier to isolate and analyze the behavior of high-burnup fuel rods and generalize the findings of this work for other reactors, cores, and fuels.

The steady-state operating conditions of 32,944 fuel rods with average burnups greater than 62 GWd/tU were characterized in detail with respect to their behaviors over time, overall trends, and possible correlations between them. A geometric sampling technique was developed and applied to down-select 753 fuel rods for fuel performance analysis in BISON, significantly reducing computational cost. The spatial distribution of the sampling technique and statistical comparisons between the two sets of rods helped ensure that the smaller set provided a representative sample of the larger set.

VERAOneWay was applied to generate BISON input files for the selected fuel rods. Six fuel performance parameters of interest related to temperature, cladding ballooning, and the spatial relationships between them, were selected to help assess the susceptibility of high-burnup fuel rods to FFRD. As before, steady state fuel performance predictions were characterized in detail with respect to their behaviors over time, overall trends, and possible correlations between them. These operating conditions and fuel performance predictions set a baseline for how high-burnup fuel rods are expected to behave during steady state operation and provide initial conditions for the follow-on TH and transient analyses needed to assess the susceptibility to FFRD.

A preliminary study was then conducted to estimate the magnitudes of the effects that uncertainties in FGR predictions have on FFRD-relevant parameters such as FCT and RIP. Variations in BISON's FGR predictions were induced by artificially manipulating scalar fission gas diffusion multipliers in its FGR model for 15 fuel rods, which defined extremes in the operating conditions and fuel performance parameters. FGR predictions from high, nominal, and low FGR cases varied from one another by factors of up to approximately two, which is consistent with the variations that are expected to arise from uncertainties inherent to the BISON FGR model. This analysis showed that the range of FGR predictions that are generally considered reasonable correspond to a wide range of RIP predictions. Specifically, time- and rod-averaged results indicate that FCT and RIP can be expected to change by approximately 6 K and approximately 0.6 MPa per percent FGR, respectively. These findings suggest that FGR predictions—and, therefore, FCT predictions, RIP predictions, and FFRD susceptibility estimates—may need to be interpreted as best estimate plus uncertainty rather than as deterministic.

Throughout these analyses, several FFRD-relevant operating conditions and fuel performance behaviors were observed to correlate to fuel rod and assembly locations, indicating that core design and shuffling patterns may influence the character and/or magnitude of FFRD susceptibility. Twice-burned fuel rods on

the core periphery accumulated the highest burnups (up to approximately 77 GWd/tU). However, they consistently exhibited lower temperatures and pressures than once-burned fuel rods with intermediate burnups (71 and 70 GWd/tU), which were located immediately inside the ring of fire. These observations suggest that core design may offset a portion of any increase in FFRD susceptibility by shuffling fuel rods with the highest burnups into lower-power assembly positions, reducing their temperatures and RIPs. Similarly, fuel rod location within the high burnup assemblies, their locations in the core, and their adjacency to fresh fuel assemblies are important considerations for limiting FFRD susceptibility.

These preliminary analyses examined overall fuel performance trends and identified specific areas of concern, but these analyses focused only on steady-state operating conditions. TH and transient fuel performance analyses are needed to capture the unique effects that LOCAs have on fuel performance and, ultimately, estimate susceptibility to FFRD. Many of the findings from this work are specific to the fuel rod and core designs considered herein. However, the authors believe that the methodology presented in this work can be generalized and applied to assess a wide range of fuel rod and core designs.

3.6 REFERENCES

[1] N. Capps *et al.*, "Full core LOCA safety analysis for a PWR containing high burnup fuel," *Nucl. Eng. Des.*, vol. 379, pp. 1–22, 2021, doi: 10.1016/j.nucengdes.2021.111194.

[2] N. Capps *et al.*, "Full Core LOCA Safety Analysis for a PWR Containing High Burnup Fuel - ORNL/TM-2020/1700," Oak Ridge, Tennessee, 2022.

[3] J. D. Hales *et al.*, "BISON Theory Manual: The Equations Behind Nuclear Fuel Analysis - BISON Release 1.3 - INL/EXT-13-29930," Idaho Falls, Idaho, 2016.

[4] "Complete BISON Input Syntax and Reference Manual," 2020. https://mooseframework.inl.gov/bison/syntax/index.html (accessed Oct. 27, 2020).

[5] N. Capps, R. Sweet, B. Wirth, A. Nelson, and K. Terrani, "Development and demonstration of a methodology to evaluate high burnup fuel susceptibility to pulverization under a loss of coolant transient," *Nucl. Eng. Des.*, vol. 366, pp. 1–29, 2020, doi: 10.1016/j.nucengdes.2020.110744.

[6] R. Salko *et al.*, "CTF Theory Manual Version 4.2 - CASL-U-2019-1886-002," Oak Ridge, Tennessee, 2019. doi: 10.2172/1817571.

[7] R. Salko *et al.*, "CTF User's Manual Verson 4.2 - CASL-U-2019-1885-002," Oak Ridge, Tennessee, 2019. doi: 10.2172/1737480.

[8] B. Collins *et al.*, "MPACT Theory Manual Version 2.2.0 - CASL-U-2016-1107-000," Oak Ridge, Tennessee, 2016. doi: 10.2172/1340449.

[9] B. Collins *et al.*, "MPACT Standard Input User's Manual Version 2.2.0 - CASL-U-2016-1108-000," Oak Ridge, Tennessee, 2016. doi: 10.2172/1342674.

[10] M. El-Wakil, *Nuclear heat transport*. La Grange Park, IL: American Nuclear Society, 1978.

[11] B. T. Rearden and M. A. Jessee, "SCALE Code System Version 6.2.3 - ORNL/TM-2005/39," Oak Ridge, Tennessee, 2018. doi: 10.2172/1426571.

[12] L. Cornejo, S. Stimpson, A. Graham, and B. Collins, "Coupling MOOSE-Wrapped MPACT to BISON - ORNL/TM-2020/1804," Oak Ridge, Tennessee, 2020. doi: 10.2172/1797669.

[13] G. Pastore *et al.*, “Uncertainty and sensitivity analysis of fission gas behavior in engineering-scale fuel modeling,” *J. Nucl. Mater.*, vol. 456, pp. 398–408, 2015, doi: 10.1016/j.jnucmat.2014.09.077.

4. HIGH BURNUP TRANSIENT THERMAL HYDRAULIC EVALUATION

4.1 TRACE COMPARISON TO INTERNATIONAL LBLOCA BENCHMARK

The starting point for the TRACE analysis was a preexisting TRACE model based on the Zion NPP, a Westinghouse 4-loop PWR. The model was provided to users as part of the TRACE code distribution and it was chosen as a starting point for the BEMUSE OECD International Benchmark conducted in the late 2000s to simulate a realistic large break LOCA (LBLOCA) event in PWRs [1]. The benchmark specifications prescribed a set of enhancements and alterations to this model in order to improve its fidelity and representativeness for PWR LBLOCA. Each of the 13 international benchmark participants applied the changes to their own models using the analysis code of their choice, and the transient LOCA results were compared between participants.

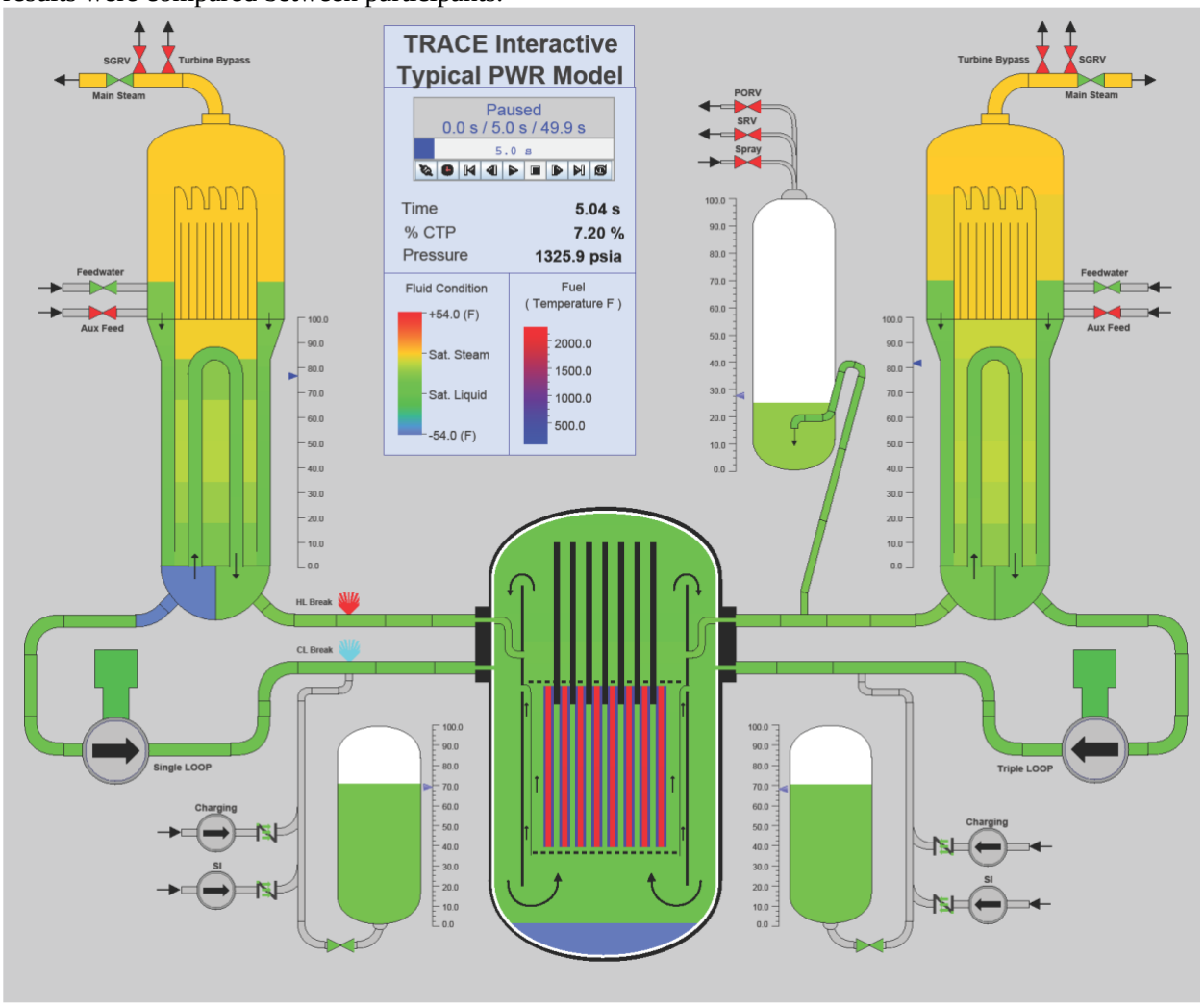

Figure 18. Primary system diagram for the Zion NPP TRACE model.

Extension to high-burnup operating cycles primarily affects the core fuel behavior, and for the present work, high-burnup operation was assumed to not affect plant system configuration or operating conditions. Therefore, for this work, the same modifications were made to the Zion NPP model as were prescribed in the BEMUSE benchmark specifications. Results were then compared with the benchmark participants' results and found to be in good agreement. This formed a realistic and well-vetted baseline

LBLOCA model, which was subsequently applied to the high burnup analysis as described in the following section. At this time, only a best-estimate analysis has been performed based on nominal parameters provided by BEMUSE; future work will investigate the effect of uncertainties provided within the BEMUSE benchmark specifications or in other references.

BEMUSE-recommended improvements to the original Zion NPP model that which were applied in the present work include the following [1]:

- Increased the number of core axial nodes from 6 to 18
- Separated the core into multiple regions to explicitly model specific rods and assemblies of interest, including cross-flow between regions
- Improved the geometric representation of the core downcomer and bypass
- Rearranged the safety injection system to include explicit modeling of low-pressure injection
- Replaced the constant containment conditions with a prescribed containment pressure versus time
- Implemented realistic specifications and setpoints for the safety injection, accumulators, steam generators, pressurizer heaters, core decay power, and reactor coolant pump transient behavior

An additional improvement was to implement automated steady state system controllers to achieve the desired steady state operating conditions. These conditions include the following:

- Primary coolant outlet temperature control by adjusting the secondary loop pressure
- Steam generator level control by adjusting the feedwater flow rate
- Primary system pressure control by adjusting of the pressurizer heater power
- Primary flow rate control by adjusting of the reactor coolant pump rotational speed

The core channel and rod grouping approach recommended by the BEMUSE specifications is shown in Figure 19. In this grouping scheme, the core is divided into three coarse concentric regions. The hottest rod in the core and its surrounding subchannel are modeled separately, along with an additional separate channel for the containing assembly. This results in five solved channels and rods. Channels physically adjacent to each other are connected by cross-flow connections. Each of the five solved rods is provided a power level corresponding to the average radial power peaking factor among the physical rods in that channel.

The current work employs a similar approach for discretizing the core, except a single average channel and rod are used in place of the three coarse core regions. This simplification was made because the hot channel location will vary on a case-by-case basis for the high-burnup cycle analysis, and employing a single core average region ,avoids the undesirable complexity of connecting the hot assembly to different coarse core regions depending on the case. The resulting three channel and three rod model remained capable of calculating reasonable core-average LBLOCA behavior while also predicting the hot rod

behavior accounting for local subchannel and assembly effects. The same discretization approach was used in the BEMUSE benchmark comparisons as well as the high-burnup cycle analysis.

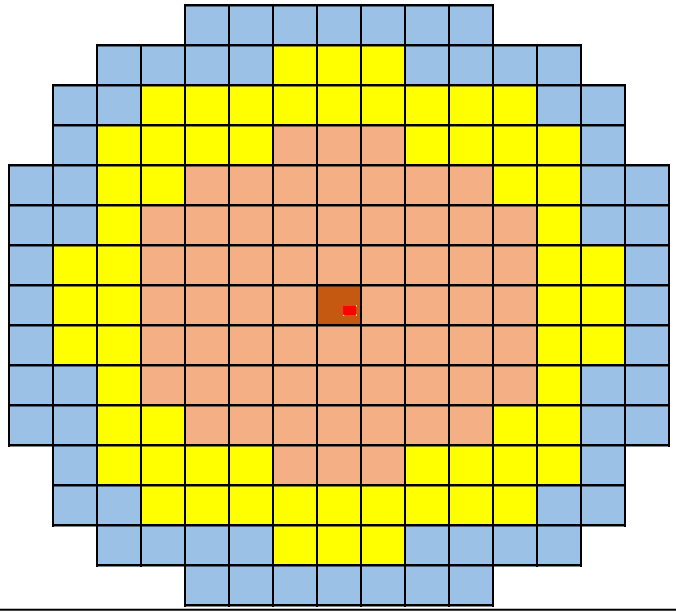

Number of Fuel Assemblies	Name	Number of Fuel Rods
64	Peripheral Channel	13056
64	Average Channel	13056
64	Hot Channel	13056
1	Hot Fuel Assembly in Hot Channel	203
1 rod	Hot Rod in Hot Fuel Assembly	1
193	TOTAL	39372

Figure 19. TRACE core channel and rod grouping recommended in the BEMUSE benchmark specifications [1].

The BEMUSE benchmark specified 18 uniform axial nodes in the core, which was selected based on engineering judgment to provide reasonable LOCA results. This 18 coarse node axial discretization was adopted in the present study for both the benchmark comparisons as well as the high burnup cycle analyses. Note, however, that the fine-mesh renodalization option was enabled in the TRACE model in the present study, which subdivides each fuel rod coarse node into 3 permanent fine mesh nodes (plus an additional zero-length node at the top and bottom of the active fuel region) for the transient radial and axial heat conduction analysis. TRACE automatically subdivides these nodes further during the transient, where appropriate, to accurately capture the quench front propagation along the cladding surface. TRACE results were ultimately passed to BISON on the 56-node axial mesh corresponding to the permanent fine mesh nodes. This nodalization results in a uniform 6.8 cm node spacing along the length of the fuel. By comparison, the nonuniform 49-node BISON mesh consists of longer nodes (~7-11 cm) between grid spacers interspersed with shorter nodes (~2-4 cm) representing the heights of the grid spacers themselves. As can be seen in Figure 19, this nodalization scheme allows BISON to explicitly model the reduced fission power generation at the spacer locations, whereas the uniform TRACE nodalization smears out this effect. The impact of the TRACE axial nodalization on the LBLOCA results will be investigated in FY23 in conjunction with other sensitivity and uncertainty analyses.

4.1.1 TRACE BENCHMARK RESULTS

The steady state conditions predicted by the TRACE model are compared against the BEMUSE-specified values in Table 7. Many of these parameters were applied directly as input values to the TRACE model, whereas others such as core outlet temperature and hot leg pressure were achieved via controllers. The parameters show close agreement with the BEMUSE specifications, except for secondary pressure which was computed to be 0.7 MPa higher in order to achieve the desired core outlet temperature. The secondary pressure value is not expected to significantly affect the LBLOCA transient results.

Table 7. TRACE reference model steady state conditions compared with BEMUSE

Operating Condition	Units	TRACE	BEMUSE
Power	MW	3250	3250
Hot Leg Pressure	MPa	15.53	15.5
Pressurizer Level	m	8.8	8.8
Core Outlet Temperature	K	603	603
Core Flow Rate	kg/s	17357	17357
Secondary Pressure	MPa	7.44	6.7
Feedwater Flow Per Loop	kg/s	436	439
Accumulator Gas Volume	m^3	15.1	15.1
Accumulator Liquid Volume	m^3	23.8	23.8
RCP Speed	rad/s	118.26	120.06

The TRACE LBLOCA and BEMUSE benchmark system TH results are compared in Figure 20 through Figure 25. Note that transient results are available from all 12 BEMUSE benchmark participants; the "BEMUSE (typical)" values shown in the figures merely represent typical behavior among the 13 participants' results and are provided here for general comparison. All system thermal hydraulic (TH) system responses exhibit good agreement with the typical BEMUSE results. The break flow rate and system depressurization behavior follow similar trends in both sets of results, leading to similar emergency core cooling system (ECCS) safety injection and accumulator injection timings. The result is a comparable primary system fluid mass as a function of time, which is expected to lead to similar predictions for the core fluid response and quench front propagation behavior.

Figure 20 compares the time-dependent peak cladding temperature (PCT) from TRACE against results from selected BEMUSE participants. The three selected participants represent the earliest (EDO) and latest (CEA) quench time as well as a roughly average quench time (AEKI) among the 13 benchmark participants. EDO also predicted the highest PCT (1326 K) among the 13 participants. The PCT value in the current TRACE analysis (1343 K) exceeds that of the participants by 17 K to 184 K. The current TRACE model predicts a later quench time (shortly after 500 sec) than the benchmark participants as well, which is likely related to the higher PCT because the two phenomena are linked. The cause for the higher PCT and later quench is unknown, due to the broad consistency in core and system modeling parameters enforced between these models. However, importantly, the expected qualitative LBLOCA behavior is observed in the present TRACE results. Namely, a rapid PCT increase is seen during the first ~5 seconds of the transient due to the flashing to steam within the core and sudden impairment of core cooling at the onset of LOCA. This causes the cladding temperature to rise based on the amount of stored energy within the fuel rod during steady state. Subsequently, a more gradual heatup of the cladding is observed out to nearly 200 seconds, due to continual decay heat generation and impaired heat transfer until the PCT location is finally quenched with liquid and the PCT decreases. The timing and qualitative

behavior of both of these LBLOCA phases is well captured in the current TRACE model, indicating the model is establishing realistic TH boundary conditions for BISON. The elevated PCT values relative to the BEMUSE participants indicates an apparent conservatism in the model which is likely to carry forward into the high burnup analyses as well.

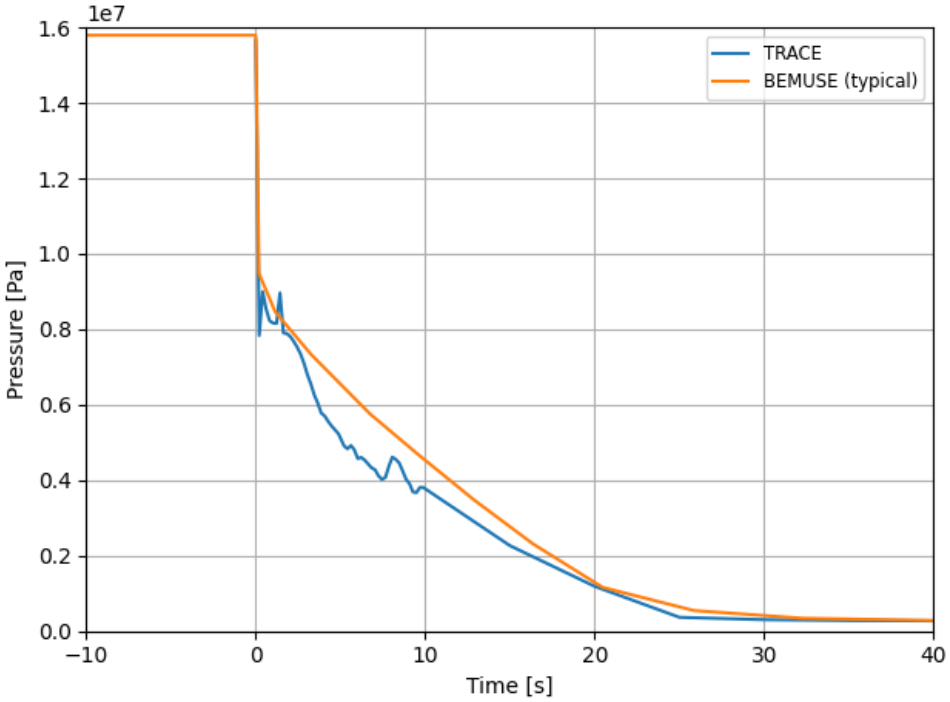

Figure 20. LBLOCA break pressure.

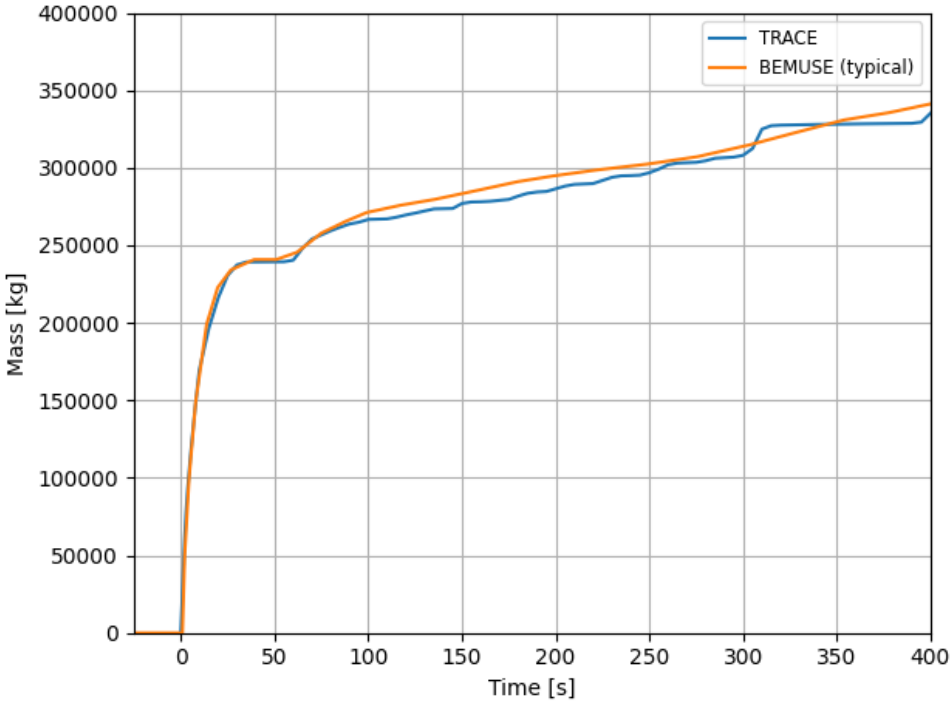

Figure 21. LBLOCA integral break flow rate.

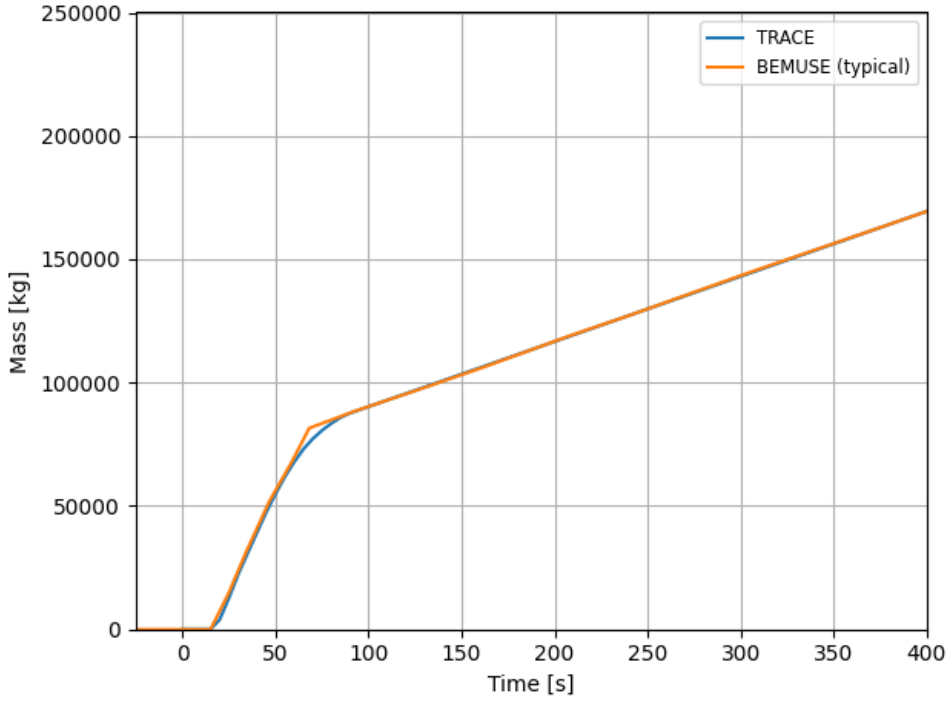

Figure 22. LBLOCA total ECCS flow rate.

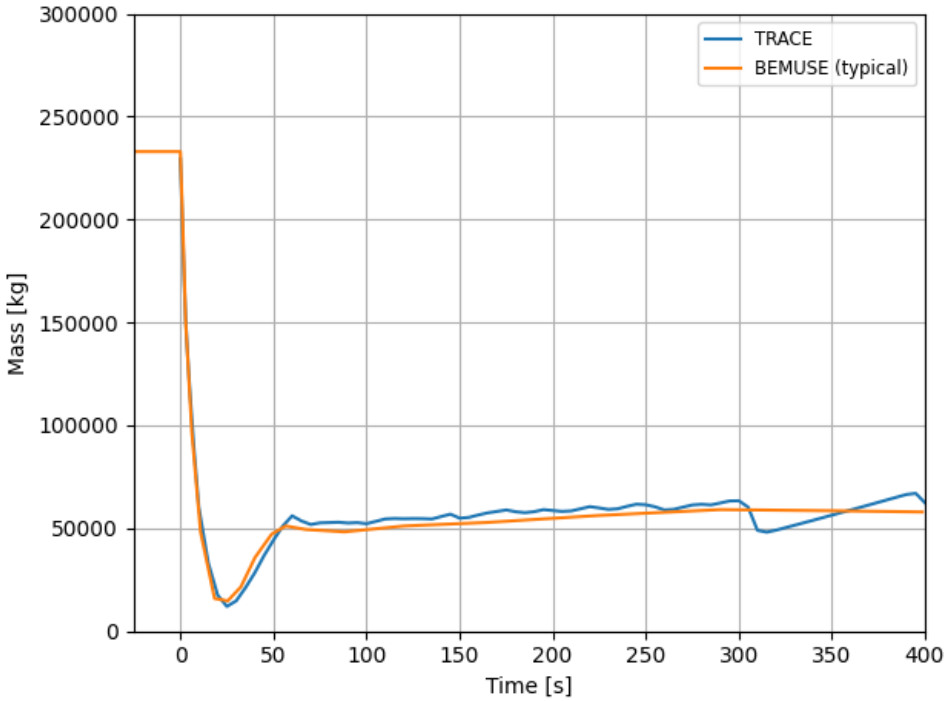

Figure 23. LBLOCA primary system fluid mass.

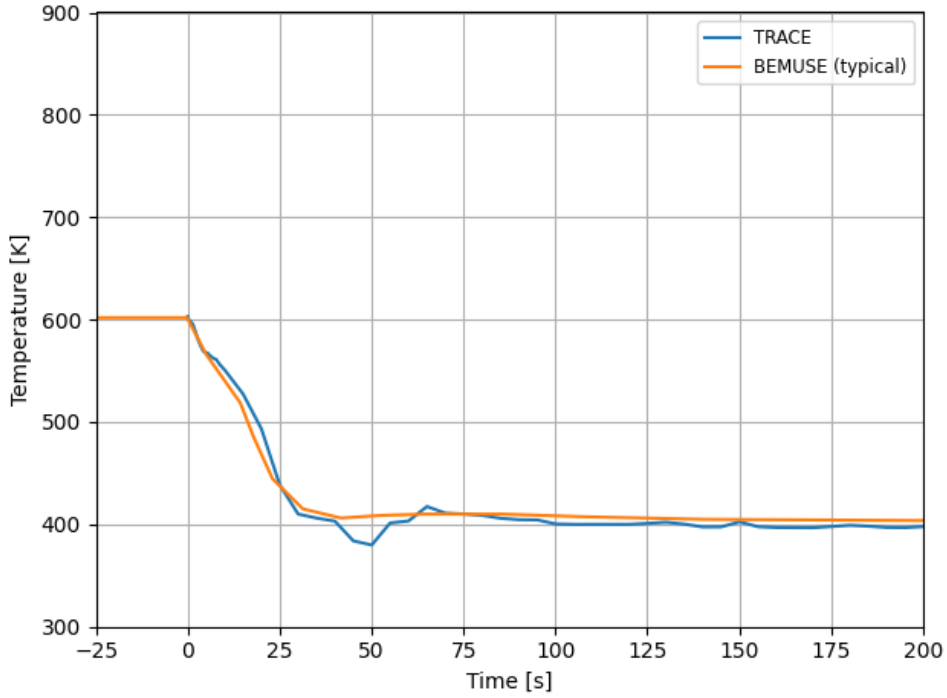

Figure 24. LBLOCA intact loop hot leg temperature.

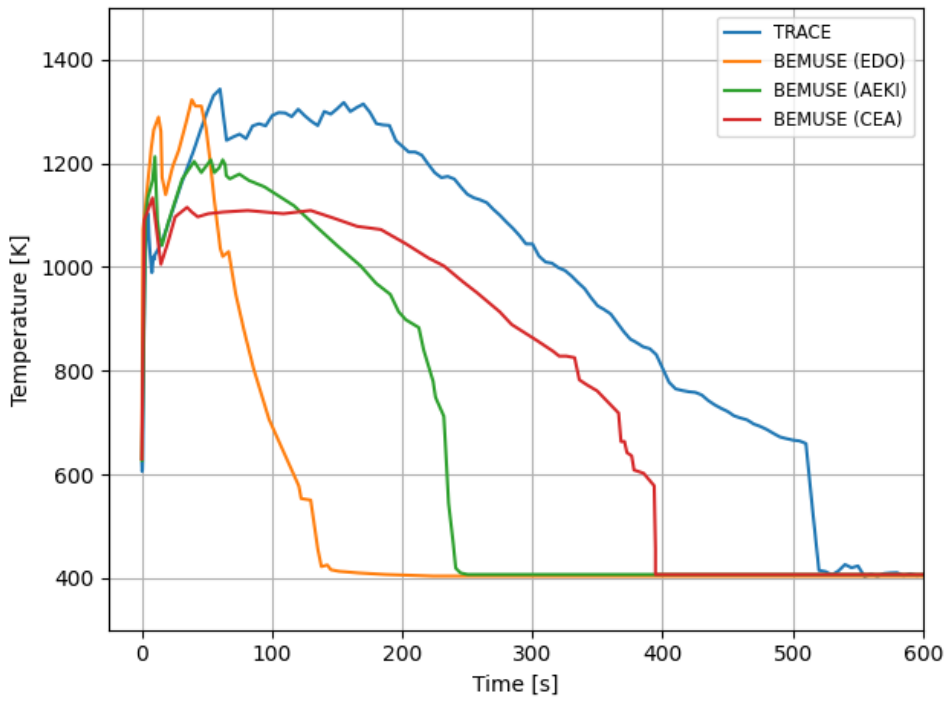

Figure 25. Time-dependent PCT during the LBLOCA for the current TRACE model (left) and BEMUSE benchmark participants (right).

4.2 TRACE HIGH BURNUP CYCLE METHODOLOGY

The high burnup cycle analyses used the same system assumptions and modeling options as the benchmarked TRACE model, except for the following differences:

- The core inlet temperature, flow rate, pressure, and power level were set consistently with the VERA high burnup cycle operating conditions
- The VERA 3D pin power and burnup distributions for the high burnup cycle were applied to the TRACE fuel rods

Once again, three TRACE grouped rods were solved in each TRACE calculation: the rod of interest, the assembly containing that rod, and the remainder of the core. The VERA 3D power and burnup distributions were averaged onto these TRACE grouped rods to produce an axial-dependent power and burnup profile for each grouped rod. Python scripts were used to read the 3D values from the VERA HDF5 output file and write appropriate values to the TRACE text input file.

The final statepoint of Cycle 30 was chosen for the TRACE analysis because it provided the highest rod burnups and likely the most limiting FFRD consequences per the conclusions of the previous section. The BISON steady-state analyses in the previous section included a total of 771 high-burnup rods across cycles 28-30. 281 of these rods were present in cycle 30 and had BISON results available at the end of the cycle. All 281 of these rods were analyzed in TRACE by performing a separate TRACE run for each rod, resulting in 281 separate TRACE calculations. In each calculation, the power and burnup distributions were applied consistent with the given rod of interest and its containing assembly.

The calculations were performed using Idaho National Laboratory's (INL's) Sawtooth high-performance computing platform. Each calculation required approximately 6 h to complete. Although TRACE includes robust time advancement logic, which automatically adjusts the time step size and rewinds the calculation as needed to avoid numerical errors, a minority of cases failed to reach the requested problem end time (t = 600 s), including some that failed within the first few seconds of the transient. Additional logic was added via Python scripting to rerun repeatedly any failed cases with a smaller maximum time step size until the problem end time reached at least t = 500 s (i.e., more than sufficient time to reach the peak PCT and rewet). This was successfully achieved for all 281 cases. To accommodate these automatic reruns, the actual wall time required to complete all 281 cases was approximately 20 h.

4.2.1 TRACE MODELING ASSUMPTIONS

TRACE includes a dynamic fuel rod modeling capability based largely on FRAPTRAN. Because TRACE is being used to calculate TH boundary conditions for BISON, it is important that the TRACE model must accurately predict the initial stored energy (i.e., initial average rod temperature) in the fuel rods of interest. This initial stored energy will directly lead to cladding heatup in the first several seconds of the LBLOCA transient. It is less important for TRACE to capture the detailed behavior within the pellet and gap regions after the stored energy heatup (SEH) phase of the event, as the fuel temperatures will remain essentially in equilibrium with the cladding temperature for the remainder of the event and both will be driven by the cladding-to-coolant heat transfer dynamics at that point.

Therefore, sufficient physics models were activated in TRACE to ensure reasonable agreement with BISON steady-state fuel temperature predictions, but some physics models were deactivated to avoid unneeded complexity. Namely, the following models or phenomena were used by the TRACE analyses:

- Dynamic gap width calculation
- Fuel thermal expansion
- Fuel relocation
- Cladding thermal expansion
- Cladding elastic strain
- Burnup-dependent fuel conductivity
- Fuel porosity
- Fully-implicit 2D (r,z) conduction, using the second-order finite element solver

These phenomena were modeled using only the axial pin power and burnup values taken from VERA. The following were not included in the TRACE analyses:

- Fuel swelling and densification
- Cladding inelastic strain
- Cladding creep down
- Cladding rupture

These excluded phenomena would have required additional information to be read and/or post-processed from the BISON outputs, using various assumptions. However, omitting these was found to still provided reasonable agreement with the BISON steady state fuel temperature predictions, as shown in the next section.

All TH modeling parameters and options were chosen based on the recommendations provided in the TRACE user guide for LOCA analyses, including the following:

- CHF based on the 2006 look-up table
- Critical quality based on Biasi
- Minimum film boiling temperature based on Groeneveld-Stewart

- Default CCFL parameters
- Quench front tracking including fine-mesh renoding and axial conduction

4.3 TRACE HIGH BURNUP CYCLE RESULTS

4.3.1 Steady State Fuel Temperature

To ensure that the TRACE steady state fuel temperatures reasonably matched the BISON steady state predictions, six potentially bounding rods were selected from among the 281 available BISON rods at the end of cycle 30. In addition to these high burnup rods, a lower burnup rod was selected which had the highest power peaking factor in the core. The steady state fuel temperature distribution was then compared between TRACE and BISON for these seven rods.

Table 8. Potentially Bounding Rods Used for the Fuel Temperature Study

Description	Assembly	Pin Column	Pin Row	Value
Max. power rod	C-10	13	9	1.137
Min. power rod	E-15	17	17	0.115
Max. burnup rod	A-11	5	13	74.7 GWd/tU
Min. burnup rod	F-11	16	16	61.7 GWd/tU
Max. internal pressure rod	C-8	13	13	28.9 MPa
Min. internal pressure rod	B-13	17	1	8.7 MPa
Max. power rod (global)	G-13	13	14	1.393

The same axial power distribution was applied to TRACE and BISON for each rod; however, the 18 coarse axial nodes in the TRACE model did not resolve the grid effects that were seen in the BISON power distribution provided from VERA. For example, in Figure 26, local dips in LHR are observed due to the reduced neutron flux at each of the spacer grid locations. The TRACE axial nodalization averages out these dips so that this local grid information is lost.

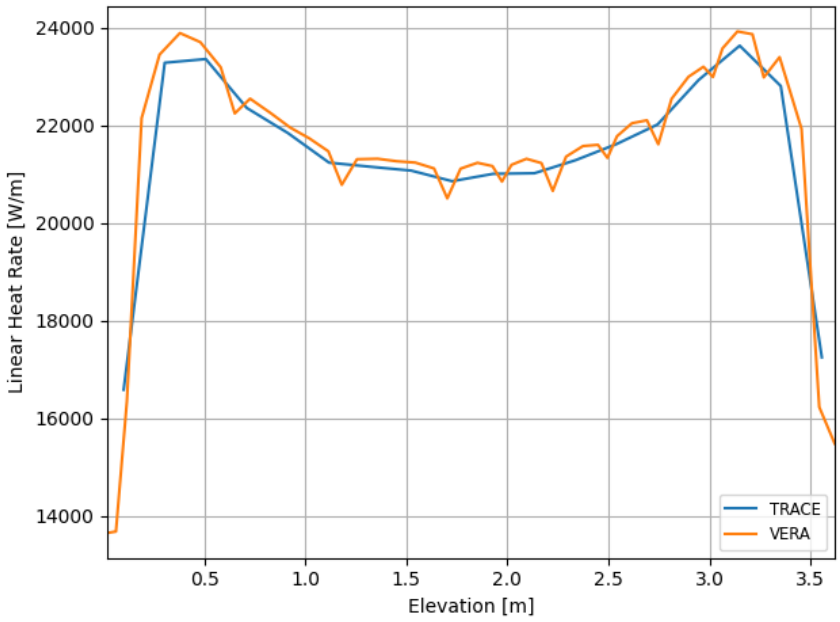

Figure 26. TRACE and BISON LHR distribution for the maximum power high burnup rod

Despite the local power differences and the less detailed rod physics models employed in TRACE, the fuel temperatures showed reasonable agreement between the two codes. An example of the temperature profile comparisons is shown in Figure 27, which illustrates the overall very similar behavior despite the local dips seen in the BISON profiles. Table 9 compares the axially-averaged centerline temperatures between TRACE and BISON. The less than 86 K difference in each case is acceptable considering the uncertainties associated with centerline fuel temperature calculations and the differences in modeling approaches between the two codes. These differences are small enough that the impact on the cladding heatup behavior during the LBLOCA is expected to be minor. Note, however, that the centerline temperatures in TRACE were generally higher than in BISON (i.e., in 5 of the 6 rods in this study), which will lead to slightly more conservative TRACE results.

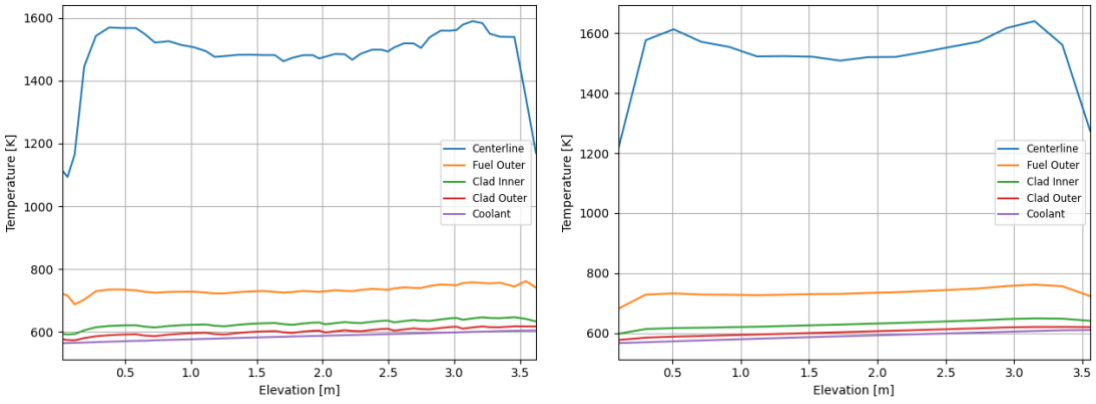

Figure 27. 2D steady state rod temperature profile in BISON (left) and TRACE (right) for the maximum power high burnup rod

Table 9. TRACE/BISON Average Centerline Temperature Comparisons

Rod	Power Factor	Rod-Avg. Burnup (GWd/tU)	Axial-Average Centerline Temperature (K)		
			TRACE	BISON	Diff.
Max. power rod	1.137	62.8	1640.4	1589.3	51.1
Min. power rod	0.115	68.3	678.4	677.8	0.6
Max. burnup rod	0.439	74.7	993.7	1059.8	-66.1
Min. burnup rod	0.931	62	1435.3	1349.4	85.9
Max. internal pressure rod	1.087	66.2	1601.8	1555.7	46.1
Min. internal pressure rod	0.275	65.3	822.4	799.9	22.5

4.3.2 LBLOCA Results

Figure 28 shows the distribution of rod-averaged burnup and LHR among the 281 high burnup rods. In this and later figures, "Reload Number" indicates the number of previous irradiation cycles for a given fuel rod and its assembly, consistent with the numbering in Figure 16. The twice-irradiated high burnup rods, all of which are located at the core periphery (Figure 16), have lower rod-averaged LHR values than the once-irradiated high burnup rods that are located in the core interior. However, as expected, higher burnup values are present among many of the twice-irradiated rods. Therefore, both sets of rods must be included in the transient FFRD analysis.

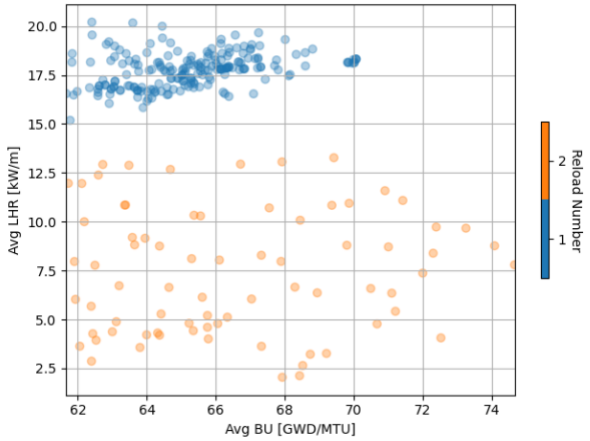

Figure 28. Rod-averaged burnup and LHR for the 281 high burnup rods.

The time-dependent PCT results for all 281 high burnup rods are shown in Figure 29 and Figure 30. As with the BEMUSE benchmark results, the predicted PCT shows the expected trend of a rapid cladding

heatup during the “stored energy heatup” (SEH) phase followed by a more gradual cladding heatup during the “decay energy heatup” (DEH) phase.

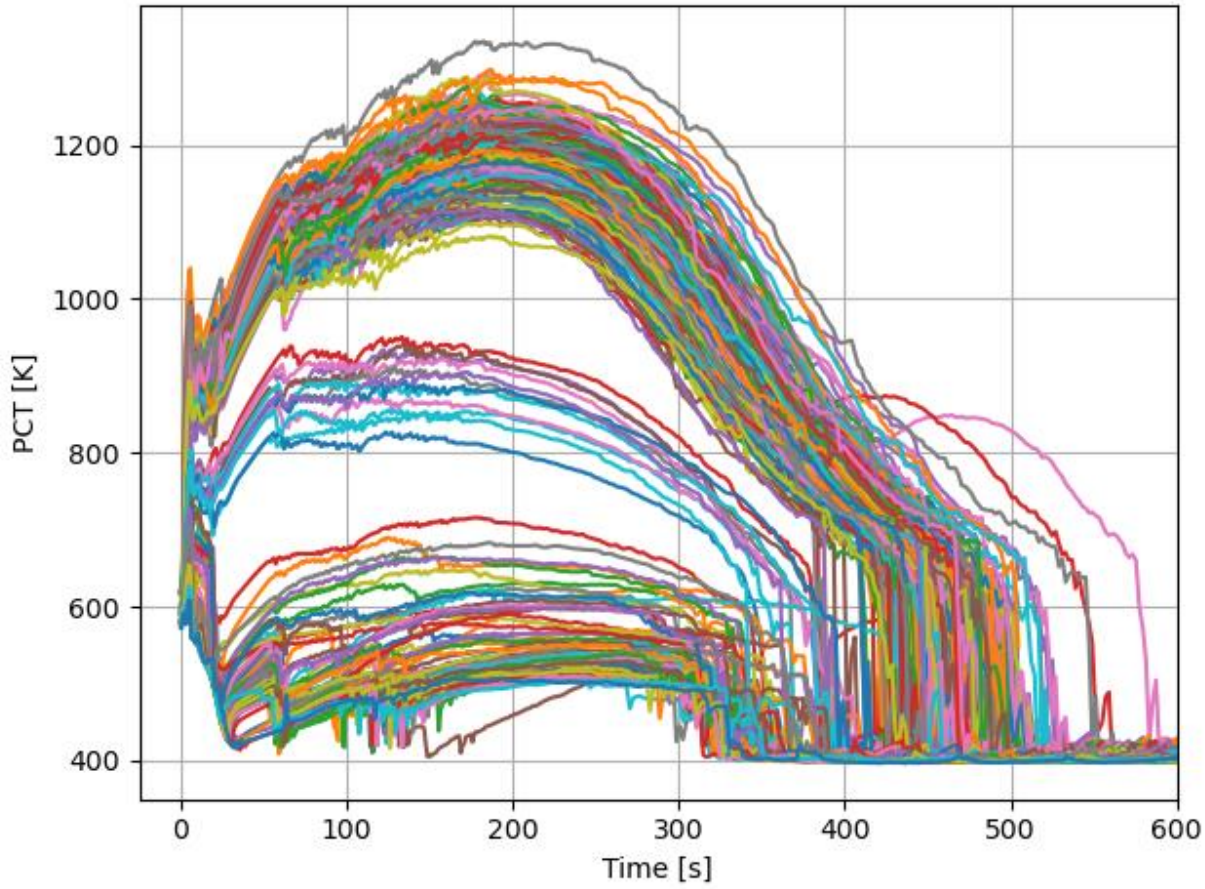

Figure 29. LBLOCA PCT versus time for the 281 high burnup rods.

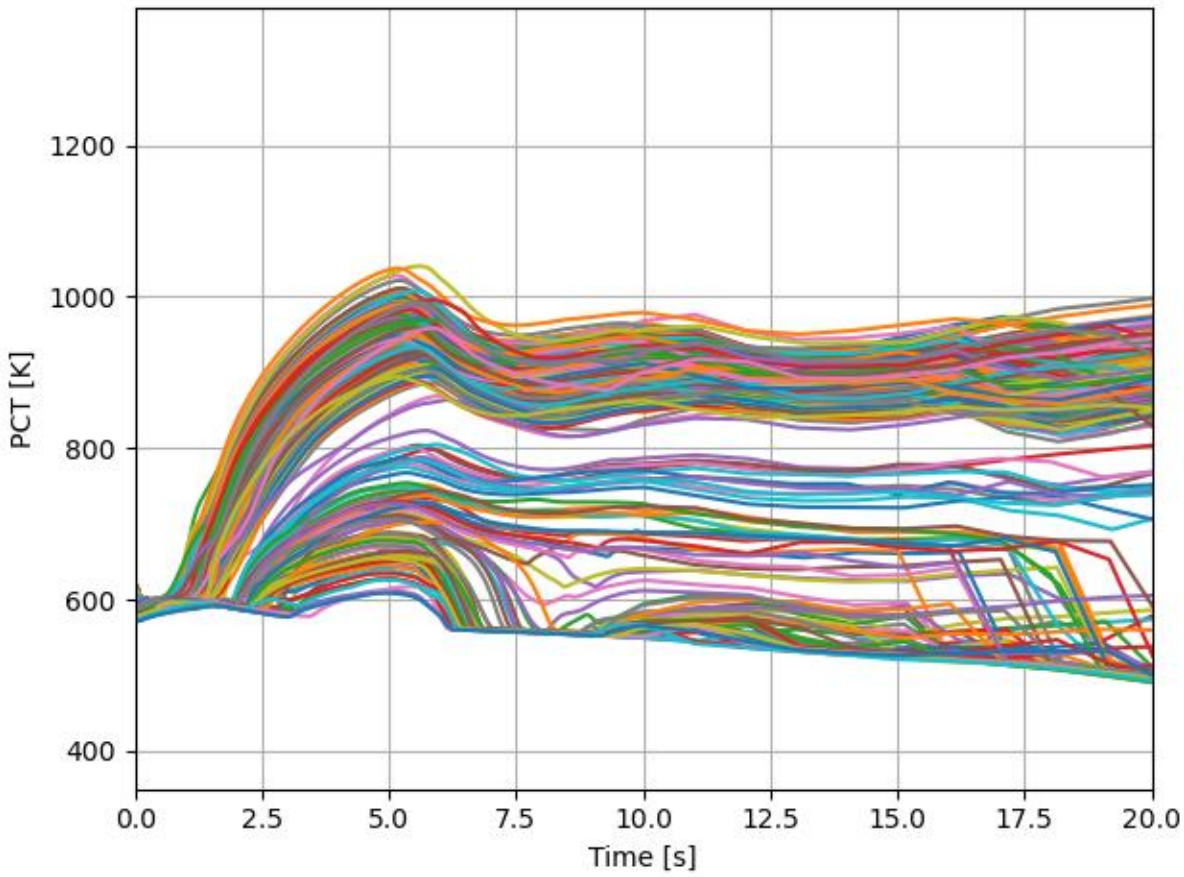

Figure 30. LBLOCA PCT versus time for the 281 high burnup rods (t = 0 to 20 sec).

Beyond the 281 high burnup cases, an additional TRACE run was performed for the overall highest LHR rod in the core, corresponding to the last row in Table 8. The peak PCT for this case was 1413 K, whereas the peak PCT for the high burnup rods ranged from 609 K to 1335 K. LOCA analyses performed under existing NRC safety guidelines would compare the peak PCT for the single hottest rod in the core against the 1478 K cladding temperature limit defined by 10 CFR 50.46 [2]. Although the high burnup rods exhibited lower PCT values than the peak power rod, the combination of elevated PCT and high burnup levels necessitates detailed fuel performance evaluation of these high burnup rods to assess their FFRD susceptibility.

Results for the remainder of this section are presented separately for the SEH and DEH phases. For these purposes, the SEH peak PCT is defined as the peak PCT occurring between t = 1 sec (the approximate start of cladding heatup) and t = 10 sec (sufficient to capture the initial peak due to stored energy heatup in all cases). The DEH peak PCT will be defined as the peak PCT occurring between t = 20 sec (which provides sufficient time for the cladding temperature to recover following the initial peak) and t = 600 sec.

Figure 31 shows the time and axial location at which the SEH peak PCT occurs among the 281 high burnup rods. All of these rods exhibited a peak between 4.7 sec and 6.2 sec, at an elevation between 2.8 m and 3.4 m from the bottom of the active fuel. This top-peaking of the PCT location is expected because the initial coolant temperature is highest near the top of the fuel (therefore the initial cladding temperature is highest here and the coolant flashes to steam earliest here) and the “double peaked” axial power

distribution gives high peaking factors (and therefore high initial fuel temperatures) near the top of the fuel as well.

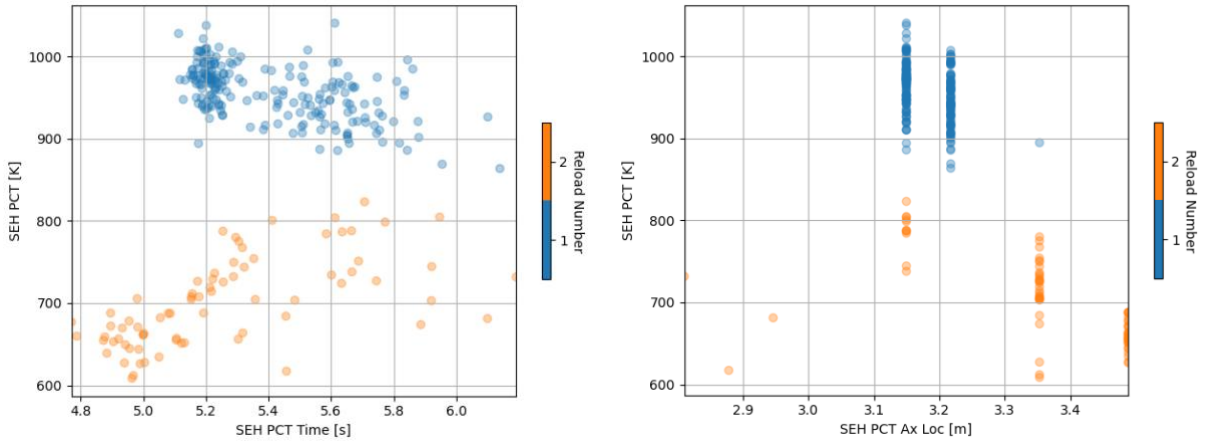

Figure 31. SEH peak PCT time (left) and axial location (right) distributions.

The SEH peak PCT as a function of rod-average LHR and burnup is shown in Figure 32. A clear trend of increasing SEH peak PCT with LHR is observed, which is expected because higher LHR means higher initial stored energy (i.e., higher initial average fuel temperatures) in the fuel rod. The SEH peak PCT versus rod-averaged burnup follows a similar behavior as the rod-averaged LHR versus burnup (Figure 32). This indicates that rod LHR is the primary predictor of transient PCT, while burnup effects (gap conductance, fuel conductivity, etc.) have only a secondary effect on the PCT.

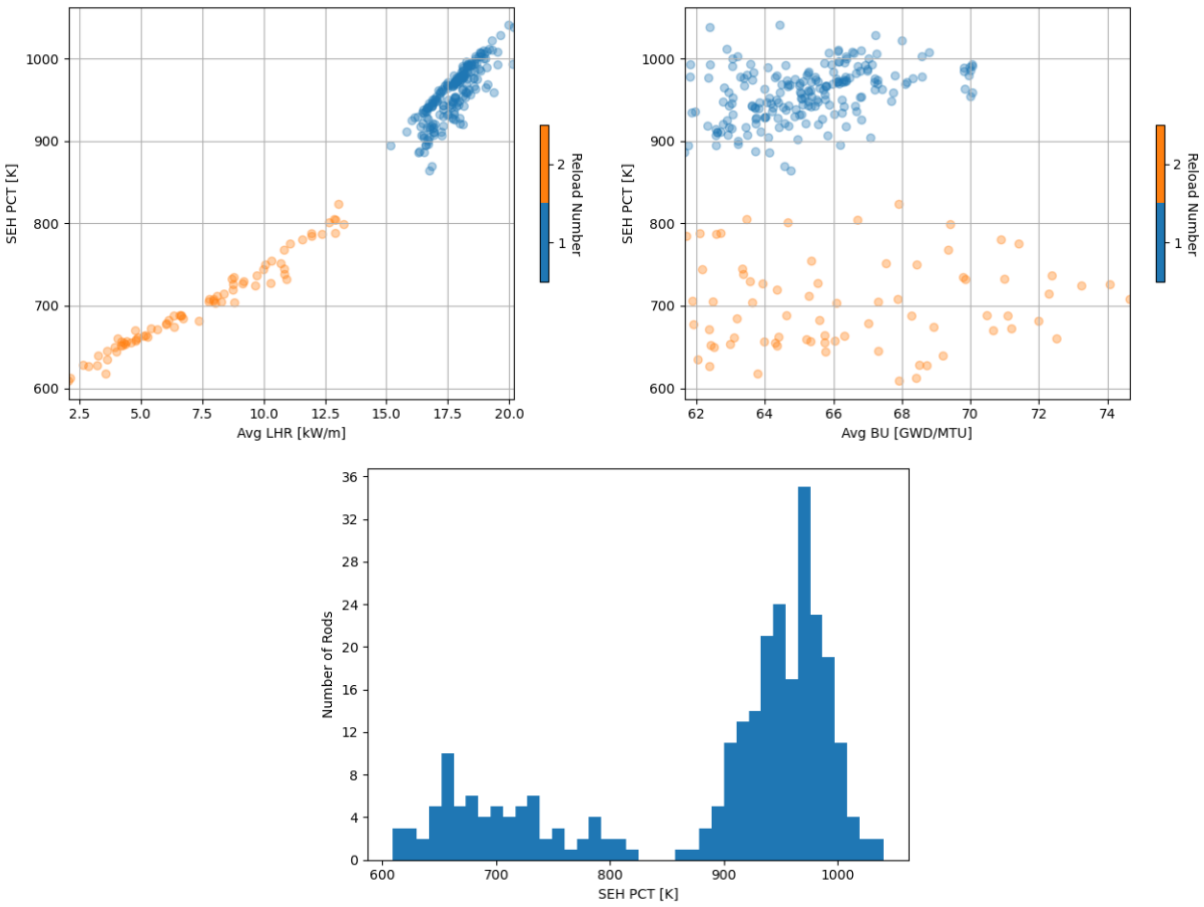

Figure 32. SEH peak PCT versus rod-average LHR (left), versus rod-average burnup (right), and as a histogram (bottom).

The SEH clad heatup rate, shown in Figure 33, was calculated as the change in PCT from t = 1 sec to the peak PCT time, divided by that time interval. Because all 281 rods exhibited fairly similar peak PCT times, the SEH cladding heatup rate follows similar trends similar to SEH peak PCT with respect to both LHR and burnup. For all high burnup rods, the cladding heatup rate was below 100 K/s.

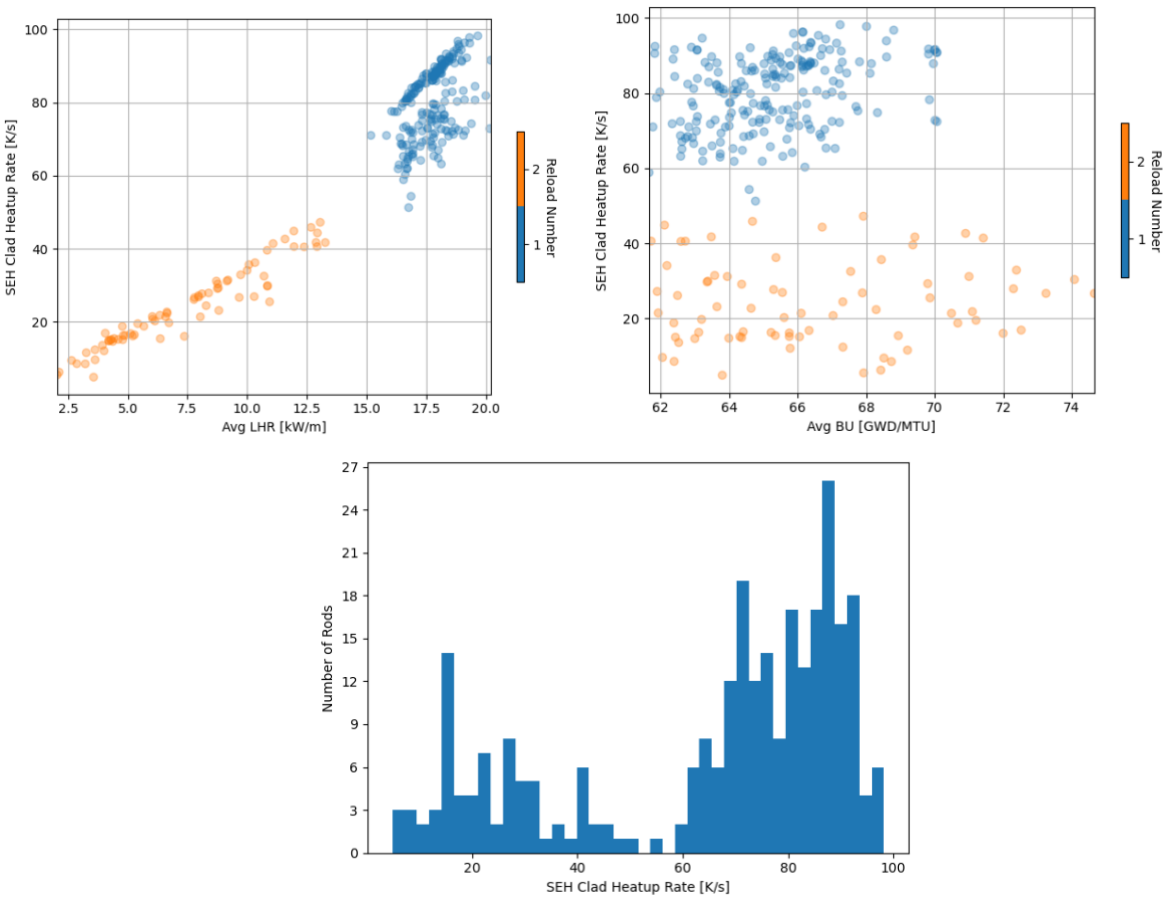

Figure 33. SEH clad heatup rate versus rod-average LHR (left), versus rod-average burnup (right), and as a histogram (bottom).

Figure 34 shows the SEH peak PCT relative to local LHR and local burnup, as opposed to the rod-average values. The trend compared with local LHR was similar to the trends compared wtih average LHR. However, the local burnups at which PCT occurred spanned a fairly wide range, from 46 GWd/tU to 75 GWd/tU. Much of this spread occurred for twice-irradiated rods. Among the once-irradiated rods, the spread was smaller (58 GWd/tU to 71 GWd/tU). Correspondingly, Figure 35 shows that the once-irradiated rods tend to have PCT occur at a local burnup within roughly 3 GWd/tU below to 2 GWd/tU above the rod-average burnup, whereas most twice-irradiated rods have PCT occur well below the rod-average burnup (roughly 5 GWd/tU to 17 GWd/tU below).

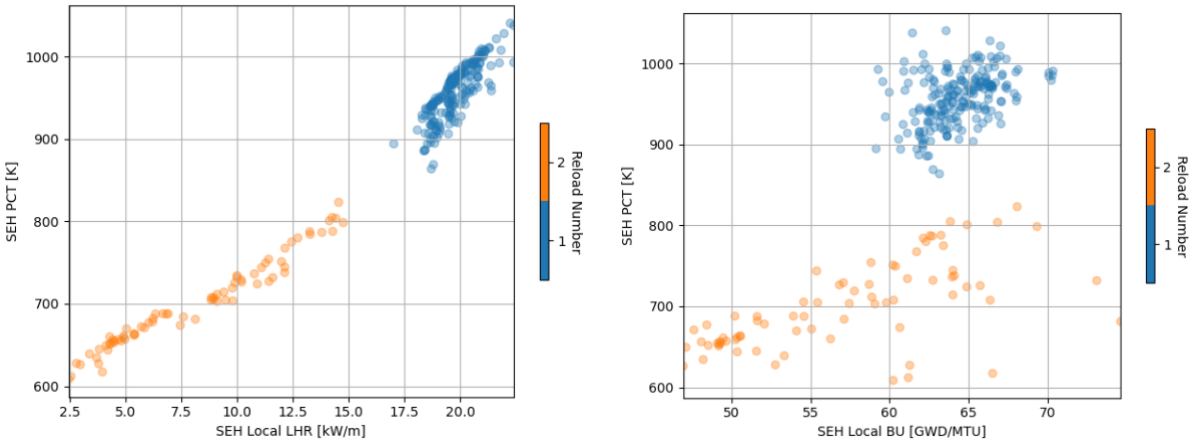

Figure 34. SEH peak PCT versus local LHR (left) and local burnup (right).

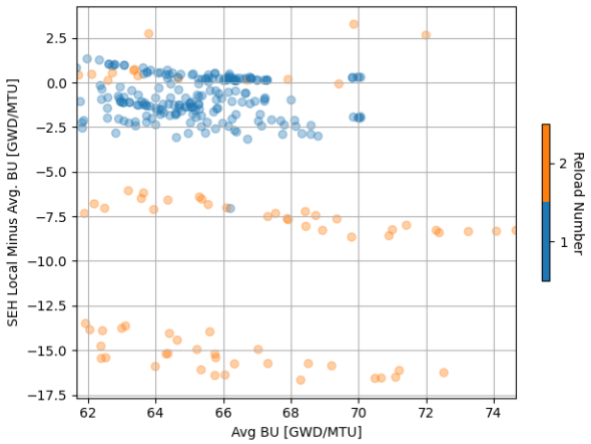

Figure 35. Difference between the local burnup where the SEH peak PCT occurred and the rod average burnup.

Figure 36 presents the same data, except with all axial locations at less than 62 GWd/tU are filtered out. This may be more relevant for a FFRD analysis because only local locations greater or equal than 62 GWd/tU are considered. Interestingly, the PCT values among high burnup locations were only slightly less than (or the same as) the PCT when considering all locations.

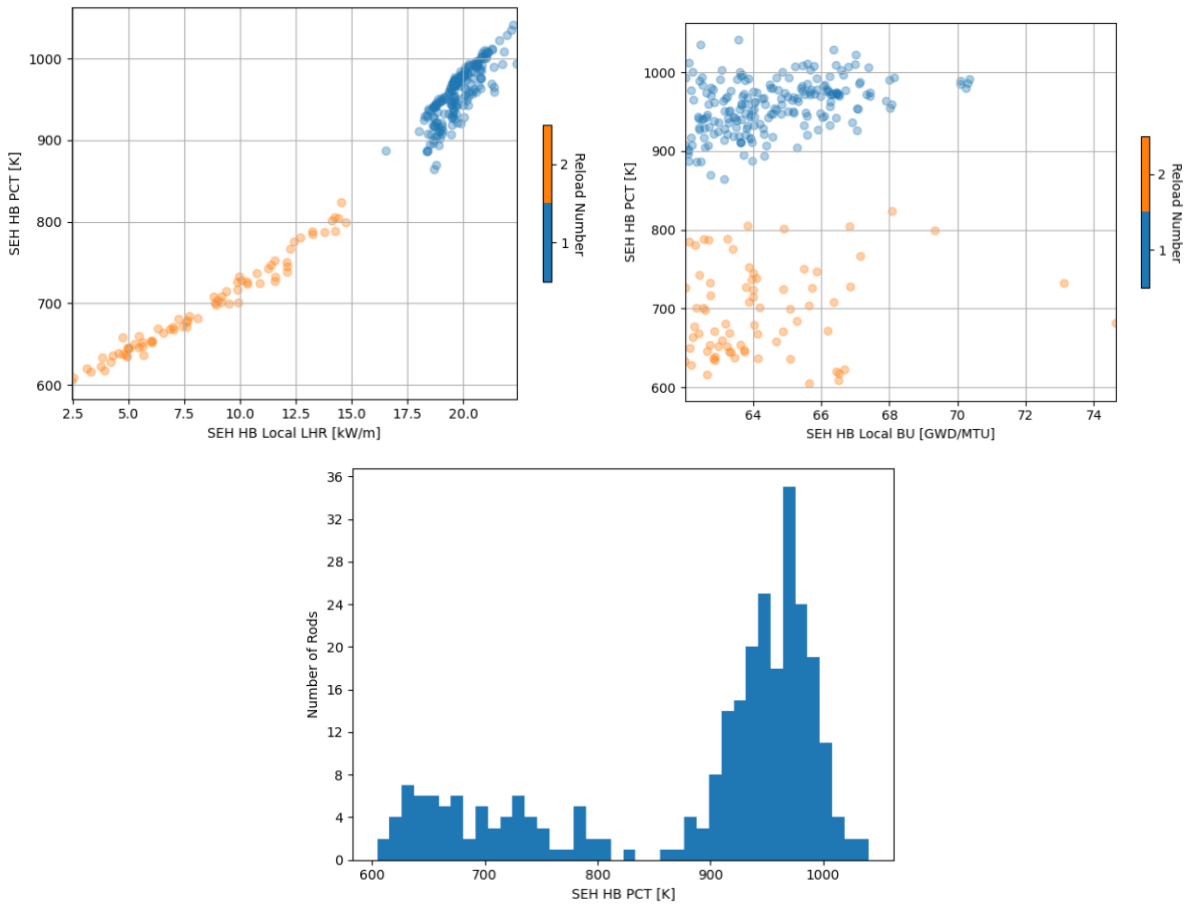

Figure 36. SEH peak PCT versus local LHR (left), versus local burnup (right), and as a histogram (bottom), considering only high-burnup locations.

Figure 37 through Figure 41 show the same quantities for the DEH phase as were shown previously for the SEH phase. The DEH peak PCT time showed a large spread for lower-LHR rods (50 sec to 300 sec) but a smaller spread for higher-LHR rods (mostly occurring between 160 sec to 200 sec). The peak PCT location was once again near the top of the active fuel, with the exception of a single rod. All but a few rods exhibited a local burnup at the PCT location that was lower (typically 5 GWd/tU to 18 GWd/tU lower) than the rod-average burnup. This trend was more pronounced for DEH than it was for SEH, and both once- and twice-irradiated rods exhibited this trend. As with the SEH peak PCT, the DEH peak PCT increased with increasing rod-average and local LHR but showed no clear trend with rod-average or local burnup. When the lower-burnup locations were filtered out, the peak PCT occurred at a noticeably lower local LHR in some cases, although the peak PCT itself did not greatly decrease.

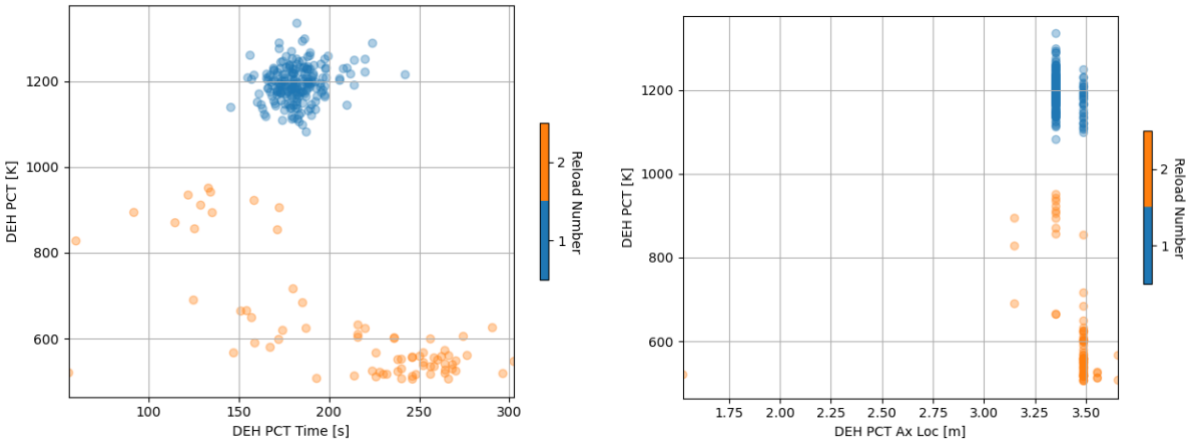

Figure 37. DEH peak PCT time (left) and axial location (right) distributions.

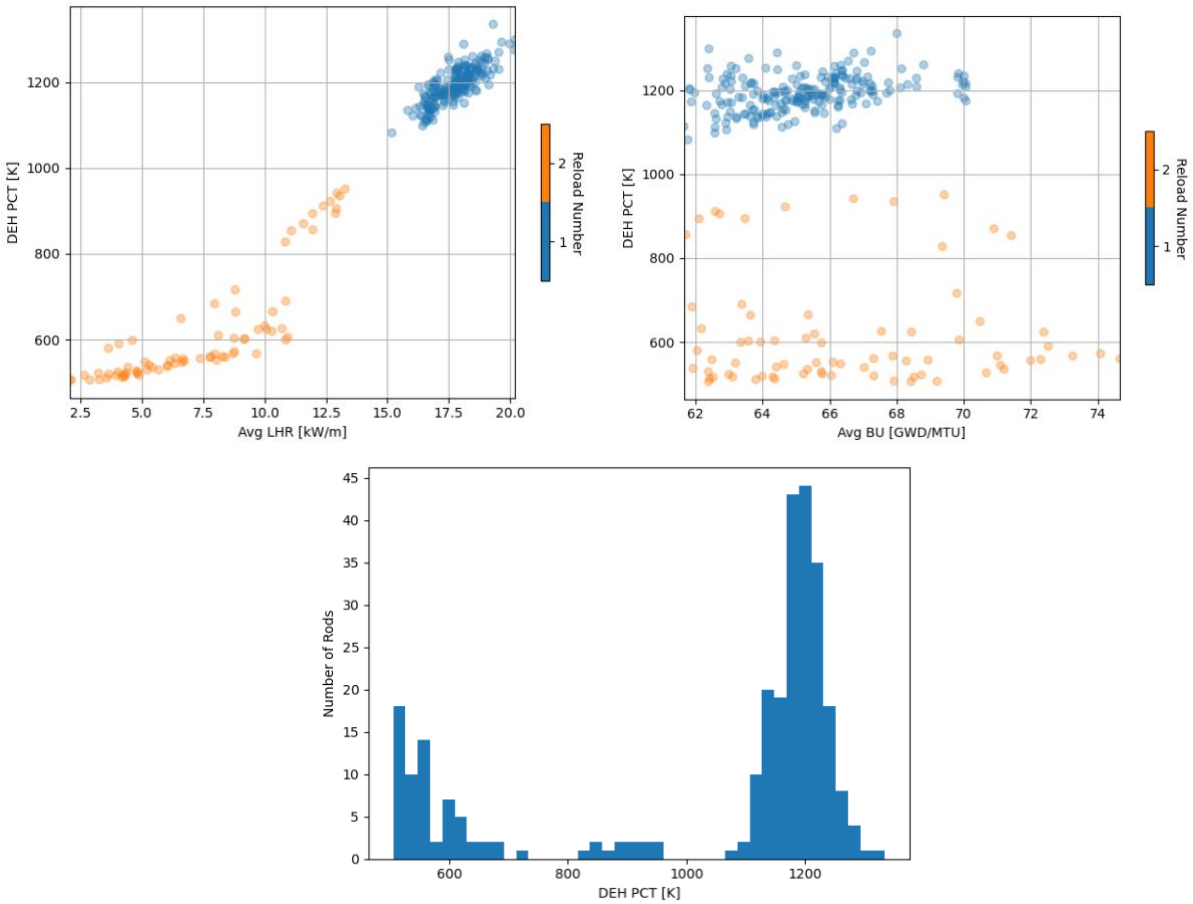

Figure 38. DEH peak PCT versus rod-average LHR (left), versus rod-average burnup (right), and as a histogram (bottom).

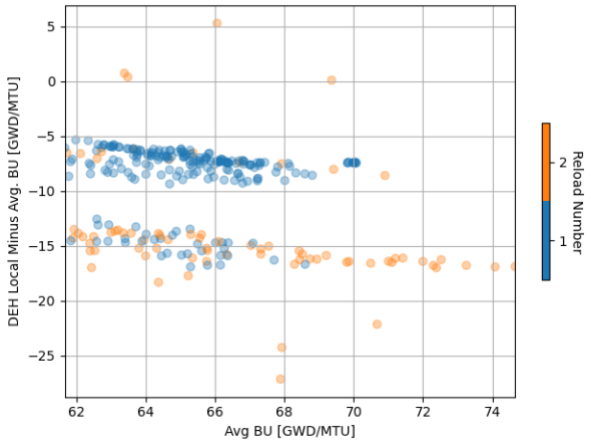

Figure 39. Difference between the local burnup where the DEH peak PCT occurred and the rod average burnup.

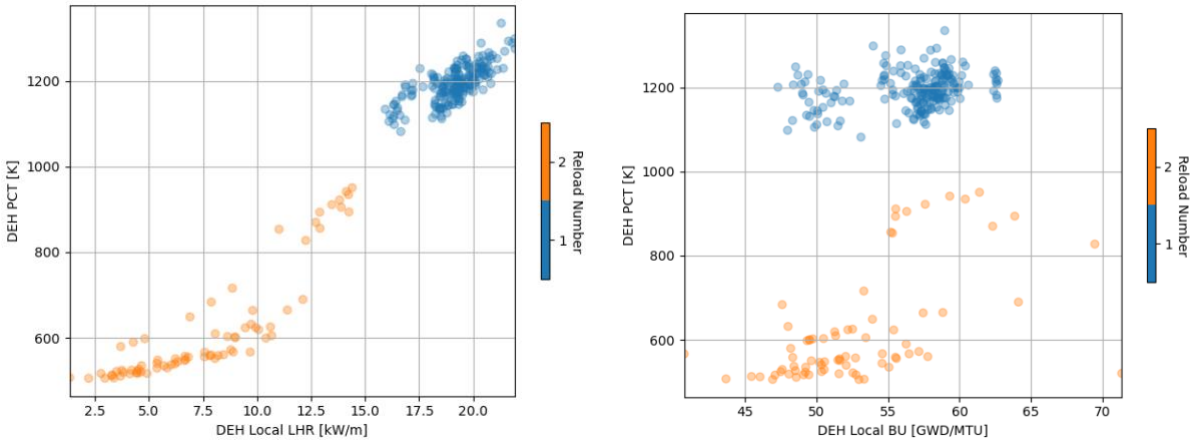

Figure 40. DEH peak PCT versus local LHR (left) and local burnup (right).

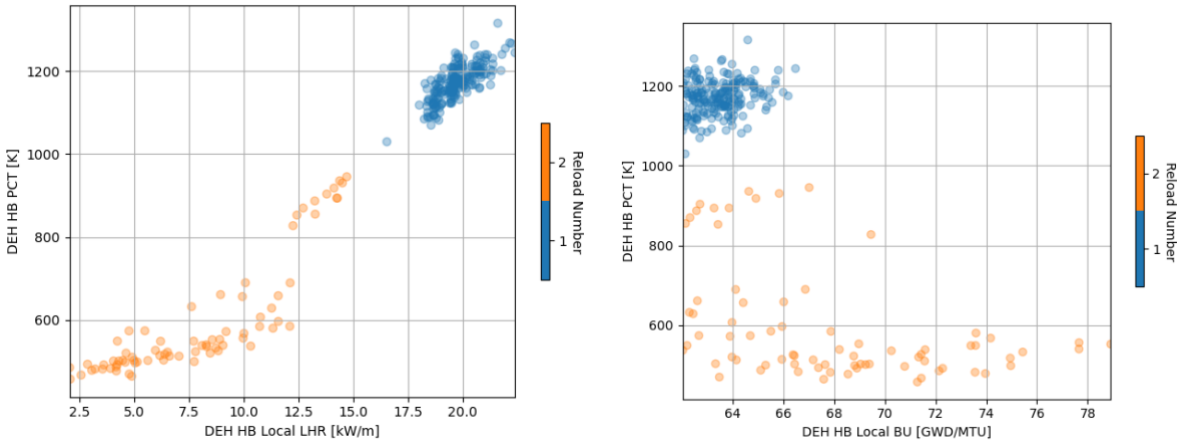

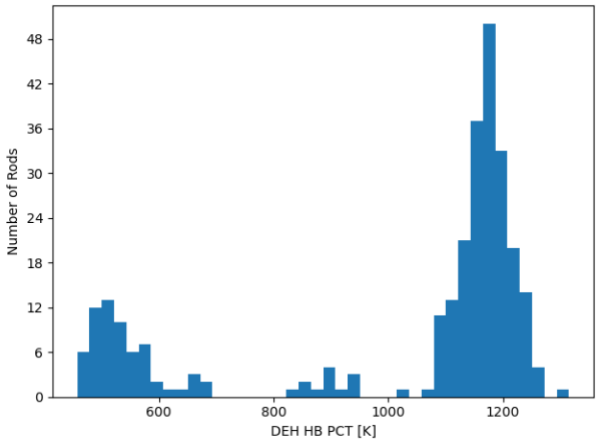

Figure 41. DEH peak PCT versus local LHR (left), versus local burnup (right), and as a histogram (bottom), considering only high-burnup locations.

The cladding temperature and coolant pressure as a function of time and axial location were taken from theses 281 TRACE runs and used to prescribed TH boundary conditions in the subsequent BISON transient fuel rod analyses.

4.4 REFERENCES

1. Reventos, F., et al. 2008. *BEMUSE Phase IV Report: Simulation of a LB-LOCA in ZION Nuclear Power Plant*. NEA/CSNI/R(2008)6/VOL1. Organisation for Economic Co-operation and Development (OECD).
2. *Acceptance criteria for emergency core cooling systems for light-water nuclear power reactors*. 10 CFR 50.46 [accessed 2022 August 29]. Available from: https://www.nrc.gov/reading-rm/doc-collections/cfr/part050/part050-0046.html.

5. BISON LBLOCA FUEL PERFORMANCE PREDICTIONS

5.1 BISON SIMULATION SETUP

BISON was used to predict the thermomechanical fuel and cladding performance of the 281 high burnup rods simulated in TRACE under LBLOCA conditions. The steady state BISON input files for the 281 rods were used as a starting point, however, additional data related to system response provided from TRACE was added to evaluate fuel performance under LBLOCA conditions. Therefore, each BISON transient simulation included the steady state and LOCA fuel performance. The rod-average LHRs, axial peaking factors, cladding surface temperatures, and system pressure were input received from the TRACE results and applied to the final full power time step as boundary conditions using a custom Python script. The script also added additional materials, postprocessors, vector-postprocessors, and cladding failure models.

The finite element method (FEM) utilized by BISON does not allow the mesh to break apart as it would if the cladding ruptured. Rather, BISON implements several failure criteria that are available from the literature. Three such failure criteria are available [1,2,3]. Two were used to evaluate the rods for this case: the strain rate criterion, in which the rod has failed if the rate of change of the cladding hoop strain exceeds 100 h^{-1} [3]; and the Chapman correlation, in which the rod has failed if the cladding temperature exceeds a burst temperature based on an empirical correlation of hoop stress and cladding heating rate [1,2]. The way the Chapman correlation was implemented in BISON requires the cladding heating rate to be a constant value. Therefore, the Chapman correlation was implemented twice, once with a heating rate of 28 °C s^{-1} (the highest heating rate used to make the correlation), which is most appropriate for the initial blowdown phase, and again at 1 °C s^{-1}, which is more appropriate for the refill phase. These values where selected based on the TRACE results, however, it would be more appropriate if the model could calculate the rate of change to provide a more accurate and consistent value. The burst temperature has a positive correlation with heating rate, so the 1°C s^{-1} rate is the most limiting (i.e., lower burst temperature) scenario for the model.

The simulations were performed on INL's Sawtooth cluster using one CPU per rod and a maximum walltime of 7 days.

5.2 BISON RESULTS

Of the 281 rods simulated, five crashed before reaching the transient, resulting in 276 rods: 73 twice-burned rods and 203 once-burned rods. The fuel rods transient results are shown in Figure 42. Plots a and b show the decay heat in terms of LHR and PCT for each rod, respectively. These values were boundary conditions based on TRACE results. Plots c and d show the peak fuel surface and centerline temperatures, respectively. Plot e shows the plenum pressure, and Plot f shows the peak cladding hoop strain. In every case, the behaviors of the once-burned rods are drastically different compared to the twice-burned rods. In addition, none of the once-burned rods' simulations completed. They tended to reach a time of approximately 60–100 seconds (before reaching the peak temperature) and stalled due to cladding plastic instability-induced deformations in their meshes. The simulations did not crash in the sense that they encountered an error and stopped. Rather, the necessary time step size to achieve convergence would become so small that no significant progress could be made in the allotted wall time. Several options exist to increase the simulation times beyond 60 seconds, including preventing cladding deformation after predicting failure, increasing the simulation wall time, and trying to optimize simulation preconditioning for rapidly deforming meshes. Another important feature to highlight is the convergence of the fuel centerline and fuel periphery temperatures. Fuel centerline temperatures for all simulations (once and twice burned) decreased from the initial steady state full power conditions at the onset of the transient.

Surface temperatures for the once burned fuel rods increased at a similar rate as the fuel centerline decreased, and eventually, the two-temperature converged, resulting in a near flat temperature profile. The twice burned fuel rods show an initial decrease of both the fuel centerline and periphery temperatures before increasing again. There are a few exceptions, and those exceptions performed similar to the once burned fuel rods.

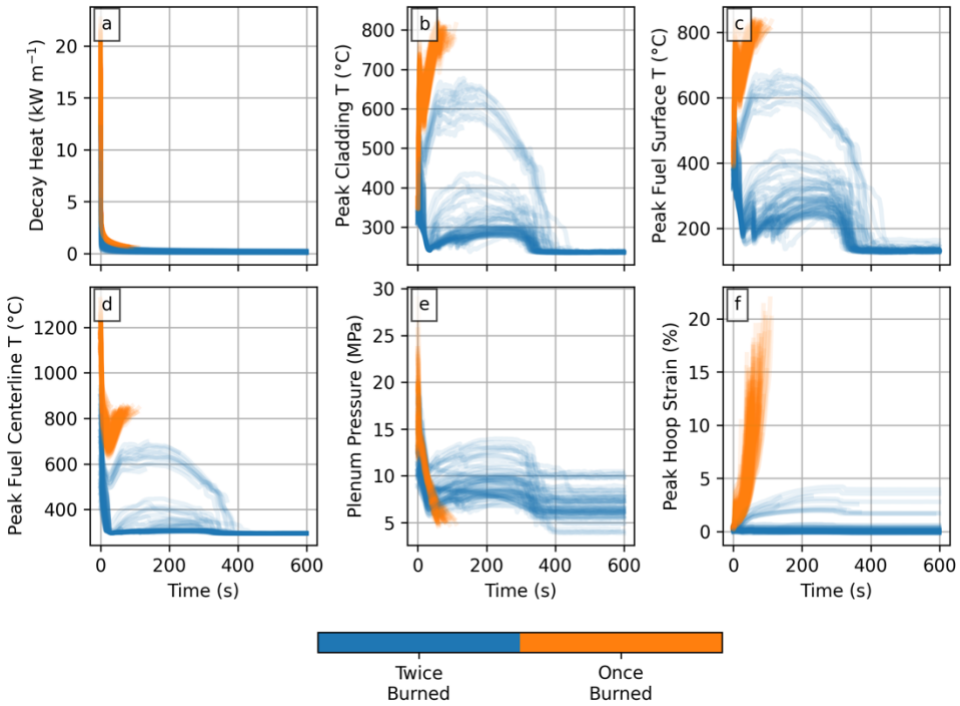

Figure 42. BISON predictions of fuel and cladding performance of 276 high burnup rods during the LBLOCA transient. Lines are colored according to the number of cycles each rod had been in the core. Plot a shows the average LHR and b shows the peak cladding temperature, both of which were set boundary conditions in the simulation. Plots c and d show the peak fuel surface and centerline temperatures, respectively. Plot e shows the plenum pressure, and plot f shows the peak cladding hoop strain.

Figure 42.b shows three groups of rods: orange once-burned rods, twice burned rods reach a peak cladding temperature greater than 500°C, and twice burned rods with peak temperatures below 500°C. One rod was selected from each of these groups for a comparison of their radial temperature profile evolutions. These are shown in Figure 43 for a number of different times during the transient. The axial position of each rod was chosen at the location where the peak hoop strain occurred, but for the sake of a more direct comparison, the dimensions shown reflect the fresh-fuel dimensions. Plot a shows the twice burned rod with a low peak temperature, b shows the twice burned rod with a high peak temperature, and c shows the once-burned rod. All three show the radial temperature profile flattening in approximately 10 seconds, which corroborates the general behaviors observed in Figure 42.

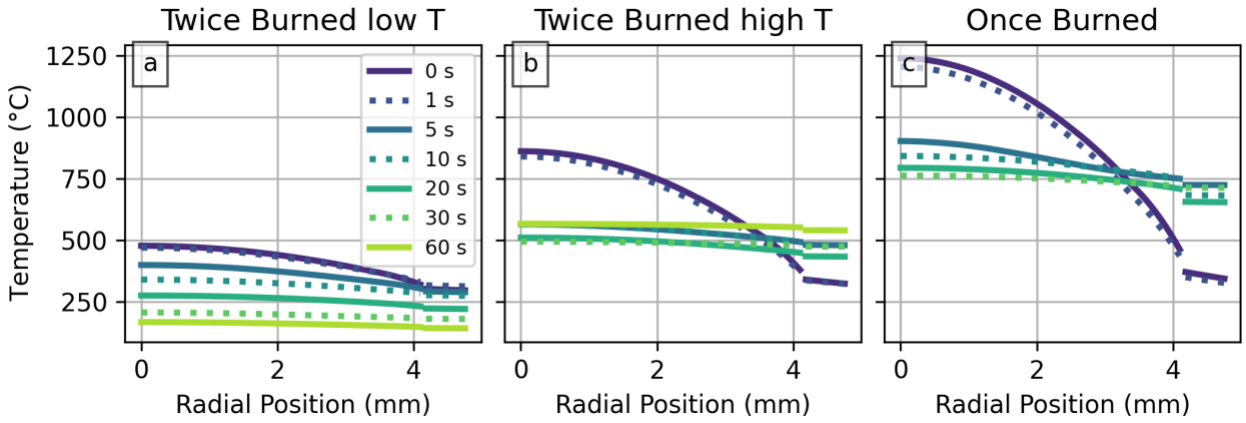

Figure 43. Radial temperature profiles at the point of peak hoop strain for three representative fuel rods

Three different failure models were implemented into the BISON simulations to determine if, when, and where cladding failure occurred: the Chapman correlation with a heating rate of 28 °C s^{-1}, the Chapman correlation with a heating rate of 1 °C s^{-1}, and the strain rate criterion [1]. The Chapman correlation predicted zero rod failures at a heating rate of 28°C s^{-1}, but 152 rod failures (out of 276) at a heating rate of 1 °C s^{-1}. The strain rate criterion predicted a single failure of the 276 rods. Every rod predicted to fail was among the once-burned rods, and BISON did not predict failure of any twice-burned rods using any correlation. However, this may change if the simulations were able to reach the PCT and complete the transient.

The predictions of once-burned rods in Figure 42 were plotted again to determine if there are any colorations between the failed (red) and non-failed rods (black) with the coloration changed to reflect whether a given rod failed or not. Figure 44 presents the failed vs. non-failed rods when considering the Chapman correlation of a heating rate of 1 °C s^{-1}, while Figure 45 presents the failed vs. non-failed rods according to the strain rate criterion.

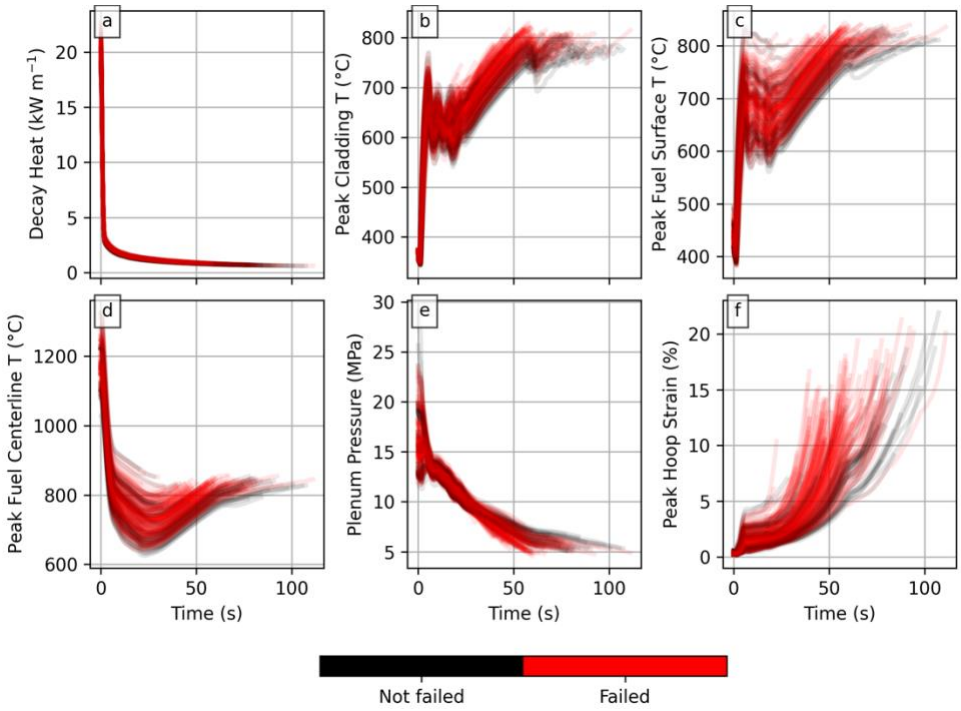

Figure 44. BISON predictions of fuel and cladding behavior of 203 high burnup, once-burned rods. Lines are colored based on whether the Chapman correlation predicted rod failure.

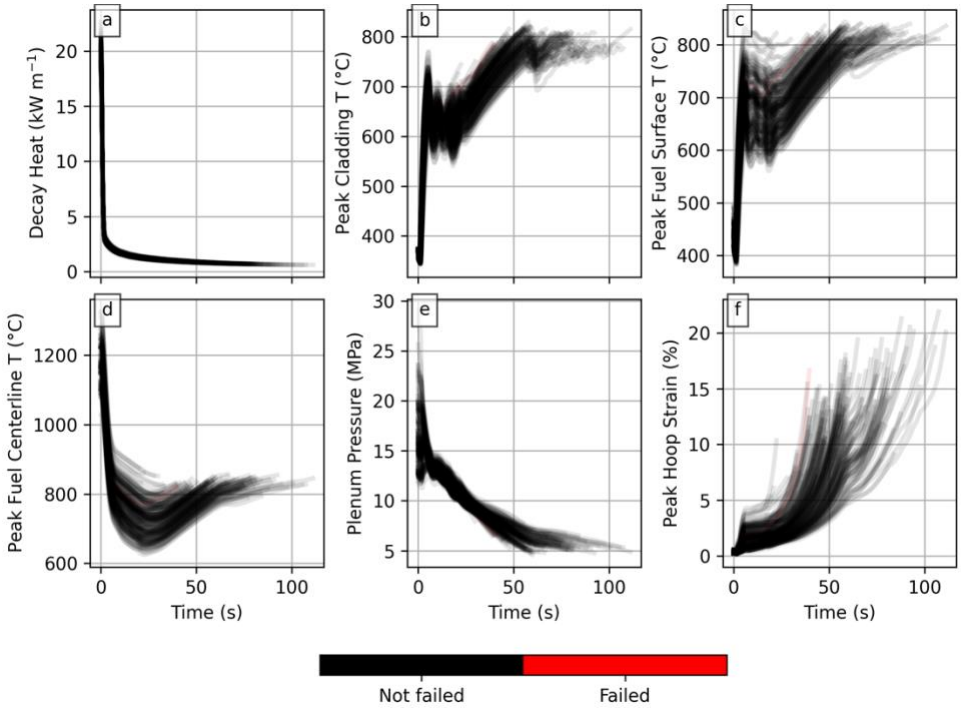

Figure 45. BISON predictions of fuel and cladding behavior of 203 high burnup, once burned rods. Lines are colored based on whether the rod exceeded the strain rate limit of 100 h^{-1}.

Figure 44 shows rods with higher temperatures and higher strains were more likely to fail. However, the BISON simulations in Figure 44 failed complete the transient simulation, and it is likely more rods might

have failed if the simulations had progressed to completion. Figure 45 shows the strain rate criterion only predicted a single failure, and again, more rods might have failed if the simulations had progressed to completion.

Using the BISON and TRACE results, it is now possible to assess core wide FFRD in high burnup rods. The strain rate criterion indicated negligible failures, and therefore, this evaluation will only consider results using the Chapman correlation. Furthermore, the Chapman correlation will provide a more conservative estimate on failure than the strain rate criteria and is widely used by the NRC in their fuel performance analysis. Generalizing the results of the subset analysis and applying these results to a full core application, results in 37% (~6,843 rods) of the once-burned high burnup rods are susceptible to FFRD with a margin of error of 6% (~1,110 rods) according to the Chapman correlation. Note that these core-wide values cannot predict the fraction of once-burned rod failures occurring beyond the first 100 seconds of the transient.

The distribution of the final pre-transient conditions of the once-burned rods are shown for failed and non-failed rods in Figure 46 to assess the relationship between steady state operating conditions and failure potential. Due to the relatively low number of rods, the distributions are not fully developed. However, the failed rods distributions' appear to be relatively normal distributions, while the non-failed rods all have bimodal distributions. Furthermore, plots c, d, e, and f show the two non-failed modes falling above and below the modes of the failed rods. This is an unexpected result and suggests the average operation conditions of once-burned rods are the most likely to result in failure.

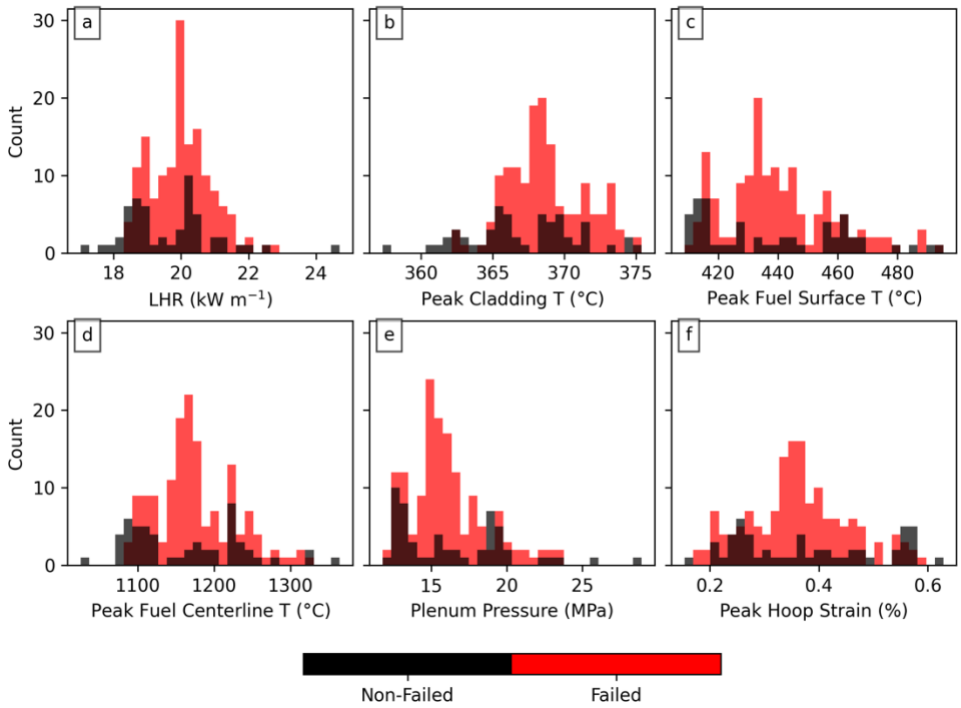

Figure 46. Distribution of pre-transient (a) LHR, (b) peak cladding temperature, (c) peak fuel surface temperature, (d) peak fuel centerline temperature, (e) plenum pressure, and (f) hoop strain, for both failed and non-failed once-burned rods according to the Chapman correlation.

Six parameters of interest are plotted for all 152 failed rods in Figure 47 in order to identify any correlations. The six parameters include the time of failure, the axial position of failure, the cladding surface temperature, heating rate, hoop strain, and burnup. Several correlations are clearly visible. First, plots a, h, o, v, ac, and aj are the six values plotted against themselves. The time results show all failures

occur after 17 seconds which correlates to the end of blowdown phase of the LOCA. The axial position plots show the majority of failures occur at a single position, 319 cm from the bottom of the cladding. A burnup analysis at the failure locations was performed and found the pellet average burnup at the failure location ranged from 62-67 GWd/tU, lower than the rod average burnups, see plot af. Strong correlations exist between time, temperature, heating rate, and strain. However, these all reflect the general trends of once-burned rods during the transient as seen in Figure 42 and do not provide any insight into the failure mechanisms.

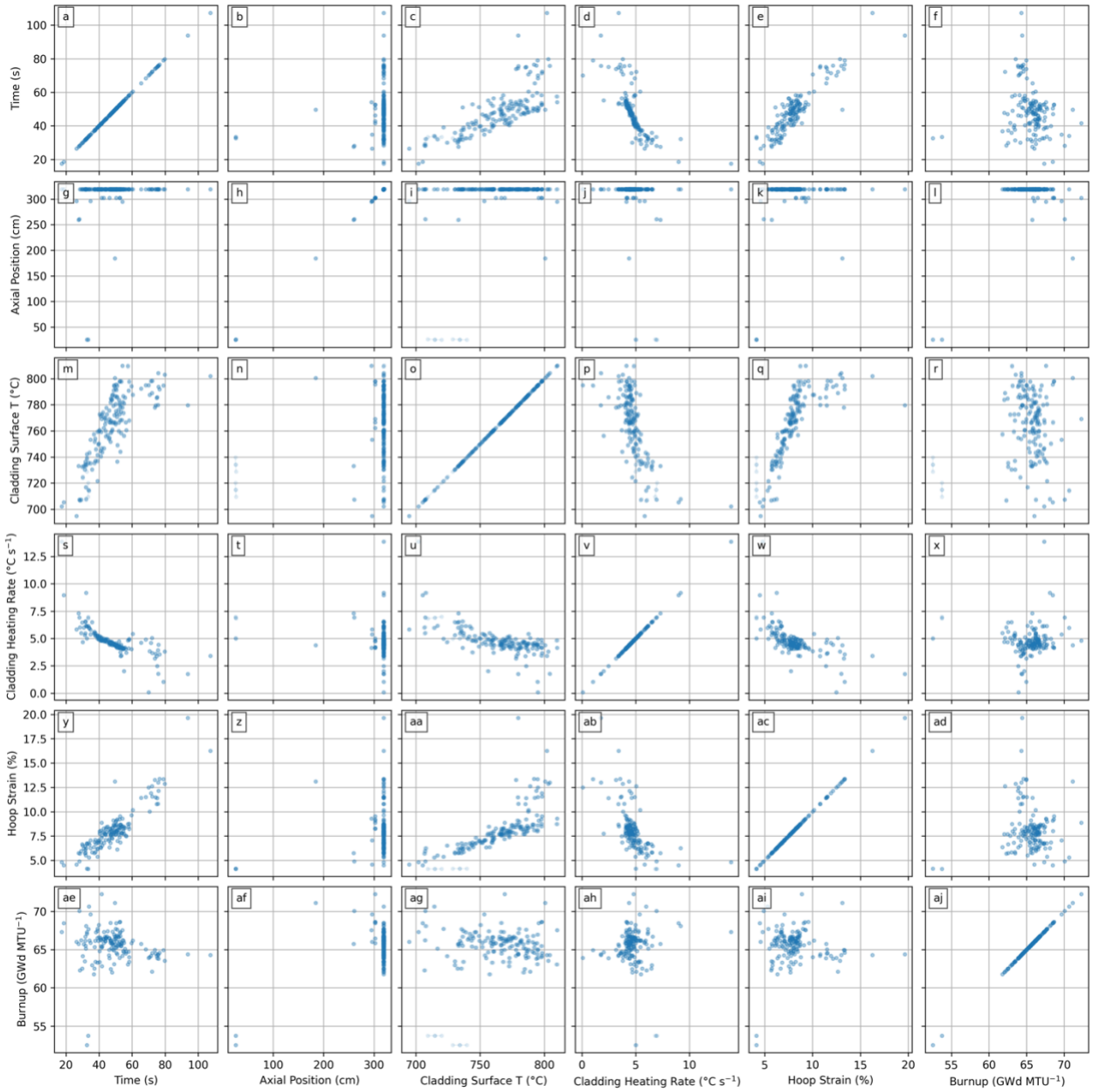

Figure 47. Comparisons of six BISON-predicted values at the point and time of first failure for 152 rods that failed according to the Chapman correlation. If multiple mesh elements failed simultaneously, then all failed elements are included. Seven conditions are compared: Time of first failure, axial position of failure, cladding surface temperature, cladding heating rate, cladding hoop strain, cladding hoop stress, and fuel burnup at the point of failure. Plots along the diagonal (a, i, q, y, ag, ao, aw) compare each condition to itself.

The most meaningful correlation in Figure 47, then, is the axial position of failure and corresponding pellet average (local) burnup. The TRACE results from Section 4 showed the PCT during SEH peaks generally occurred between 315 and 321 cm. To further investigate the relationship between PCT and failure, the axial temperature profiles of the 152 failed rods are shown in Figure 48 at the time of failure along with the position of the failure. As expected, the failures overwhelmingly occur at or near 319 cm and corresponds to the peak temperature.

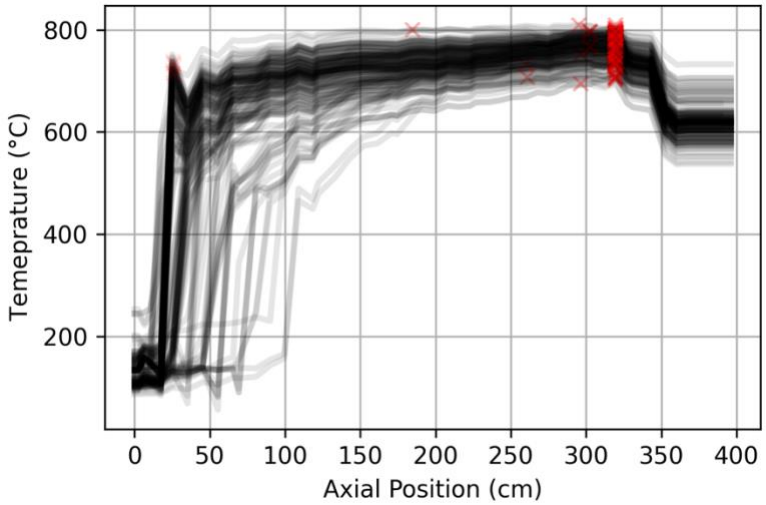

Figure 48. The cladding surface temperature at the time of failure for 152 rods that failed according to the Chapman correlation. For each rod, the full profile is shown in black and the point(s) of failure is marked with a red X.

Similar to Figure 48, Figure 49 shows the hoop strain along the axis of each failed rod at the time of failure with the point of failure marked with a red X. The failure position is usually 319 cm above the bottom of the cladding, and often corresponds to a sharp peak in the hoop strain. This shows there is a clear correlation between peak temperature, peak hoop strain, and failure.

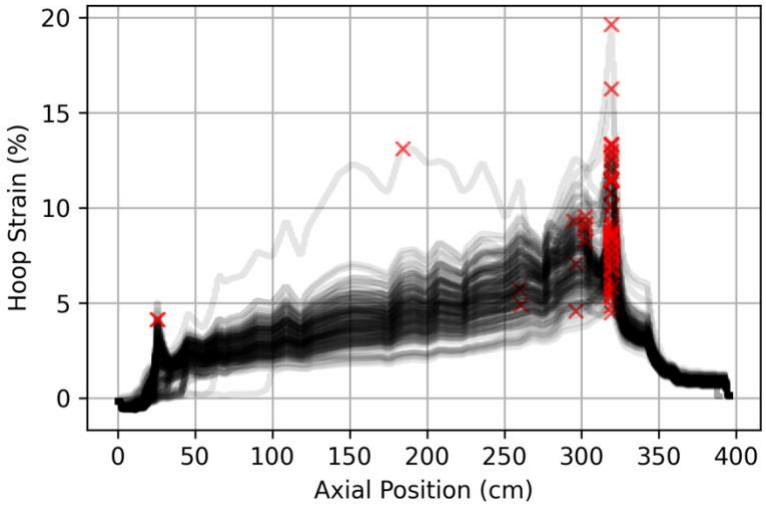

Figure 49. The cladding hoop strains at the time of failure for 152 rods that failed according to the Chapman correlation. For each rod, the full profile is shown in black and the point(s) of failure is marked with a red X.

The results above form the foundation for predicting the amount of fuel susceptible to dispersed into the reactor pressure vessels. The processes requires using correlations relating the fuel conditions to pulverization susceptibility. The procedure is as follows. First, deterime the axial location where failure occurred using the cladding failure thresholds previsouly discussed. Secondly, determine the length susceptible to FFRD per the hoop strain threshold reported in the NRC RIL [4]. However, this work assumes the mixing veins and grid spacers will restrict FFRD to between the assemblies structural components, and future work will investigate this assumptions applicability. Finally, the mass susceptible to pulverization can be estimated using correlations documented in the NRC RIL [4] or the Turnbull pulverization criateria [5]. The NRC RIL proposed two correlations for two different fragment sizes. The

two threholds consider fragment sizes for particles less than 1mm and less than 2mm, both thresholds are a function of burnup. The threshold equations take the form of equation 1 where a is 0.04 and 0.05 in the 1 mm and 2 mm correlations, respectively, BU is burnup (GWd/tU) and C is 75 GWd/tU and 80 GWd/tU in the 1 mm and 2 mm correlations, respectively.

$$f = \begin{cases} 0, BU \leq 55 \\ a(BU - 55),\ 55 < BU < C, \\ 1, BU > C \end{cases} \qquad \text{Eq. 1}$$

The Turnbull correlation is based on a threshold for local burnup and terminal temperature. One simiply evaluates the radial burnup profile and local fuel temperature when the terminal temperature is reached to estimate the mass susceptible to pulverization. On the otherhand, the NRC RIL thresholds calculated the mass suspetible to pulverization by assessing the local burnups determined in Figure 47ae. The Turnbull is more complicated, however, Figure 43 indicates the fuel temperatures flatten out and are comparible to the PCT at the axial location of interest. Figure 37 inidicates the PCTs range from 827-1000 ºC, and therefore, the analysis assumes all rods reach the highest relavent temperature (~917 ºC) to provide a conservative estimate of pulverization. The resulting predictions are provided in Table 10. Note the results are derived from the Chapman cladding failure criteria as the strain rate criteria indicated a single rod would fail. For each correlation, the average fuel susceptible to FFRD per failed rod is provided along with the total amount of fuel susceptible to FFRD from the 152 failed rods, projected fuel fuel susceptible to FFRD throughout the entire core, and the margin of error of the full-core amount (based on the ±6% failure margin of error calculated above).The NRC RIL for 2 mm particles predicts the most release in the range of 347–481 kg. The Turnbull correlation predicts the least release in the range of 103–142 kg.

The results do not include the potential impact of double ballooning, however, this phenomenon is a low probability given the thermal hydraulic conditions and cladding performance during the LOCA transient. During the heatup phase, the cladding has a near uniform temperature profile, and the instantaneous PCT is generally high in the core, see Figure 31. As the transient progresses, the instantaneous PCT moves axially upwards until the final PCT is eventually reached. Conversaly, the lower regions of the fuel rod will be quench prior to progressing to failure, which leads the axial regions adjacent (i.e., below) to the rupture location as potential double ballooning candidates. However, the rupture starts decreasing the rod internal pressure which would act to further reduce the driving force for subsequent rupture. It may certainly be possible for a double balloon event to occur, however, the possibility for rupture is highly unlikely.

Table 10. Summary of expected fuel dispersal based on three available correlations: The NRC RIL correlation for particles less than 1 mm in diameter, the NRC RIL for particles less than 2 mm in diameter, and the Turnbull correlation [REFS].

	NRC RIL 1 mm	NRC RIL 2 mm	Turnbull
Average fuel fuel susceptible to FFRD per failed rod (kg)	0.048	0.060	0.018
Total fuel fuel susceptible to FFRD simulated rods (kg)	7.35	9.18	2.72
Total fuel fuel susceptible to FFRD in full core (kg)	330.9	413.7	122.4
Margin of Error (kg)	±53.7	±67.1	±19.9

Results presented in Table 10 are intended to be overly conservative. However, there is margin with supporting justification that could be leveraed to remove the assumptions and conservatisms. One such assumption is the neglect for burst location and the potential for fuel below the rupture location to remain

in the fuel rod. The rupture locations were reported to occure at 319 cm between two assembly structural features located at ~310 cm and at ~335c m. Removing this assumption would assume approxiamtly two thirds of the material would be suspetible to dispersal, while the other third would remain in the fuel rod. The third consideration is the local burnup assumption. This work assumes the fuel in the rupture region has a similar local burnup, whereas this isn't the case. Figure 50 is an example of an axial burnup profile for a once burned fuel rod where the FFRD suseptability region is enclosed by the red box. As shown, the burnup profile in the rupture location is not uniform, and in fact, the rupture occurred near the peak local burnup. Therfore, the mass susceptible to FFRD is expected to be less as the fuel in this region has a lower burnup then the local burnup near the rupture cite.

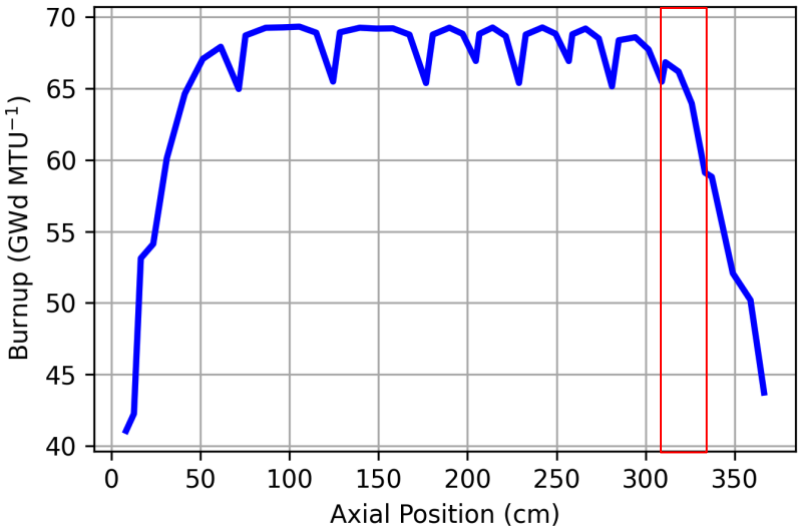

Figure 50 Example of an axial burnup profile for a once burnup rod in the center of the core.

5.3 DISCUSSION

Two failure criteria were used to assess cladding rupture in the BISON fuel performance simulations. The Chapman correlation predicted zero rod failures with a constant heating rate of 28 °C s^{-1}, but 152 rod failures with a heating rate of 1 °C s^{-1}. Therefore, the Chapman correlation is suggesting failure will not occur during the SEH phase of the LOCA and all failures are expected to occur during the DEH phase of the LOCA. The strain rate criterion predicted one rod burst. All predicted failures occurred in the once-burned rods. There are two important factors affecting the accuracy of these results. First, the heating rate was not constant. Figure 47 plot v shows that 151 of the 152 failures predicted by the Chapman correlation had heating rates greater than 1 °C s^{-1} (closer to 4-5 °C s^{-1}) at the time of predicted failure. At least some of these predicted failures would likely not have occurred if the heating rate were indicative of the instantaneous heating rate and not an assumed constant. The second factor to consider is the once-burned rod simulations did not finish. They all stalled before reaching their peak temperatures. Therefore, it is also likely additional once-burned rods would have failed if the simulations had reached completion.

Despite these shortcomings, the results were analyzed for patterns and conditions that were more likely to lead to failures. Two important correlations were found. First, the failure location was usually 319 cm above the bottom of the fuel rod. The location associated with both peak temperature and peak hoop strain. Second, 102 of the 152 bursts predicted by the Chapman correlation occurred at locations with local burnups ranging 62-65 GWd/tU. Applying the statistical methodology of standard error to these values results in a core wide cladding failure and FFRD susceptibility rate of 37±6%. The one rod that was predicted to fail according to the strain rate criterion had a burnup above 65 GWd/tU. This correlates to a FFRD susceptibility rate of 0–1%.

The fact that the two failure criteria disagree so drastically is problematic. It may be a function of the two shortcomings listed above (i.e., either the Chapman correlation over-predicts failures or the strain rate criterion would have predicted the failures later in the transient) or it may be one of the criteria is not appropriate for the operating conditions considered here.

A comparison of the failed rods to the steady state operating conditions showed unexpected behavior. The proportion of failed rods decreased as the rod temperature deviated from the mean temperature. More work is needed to better understand and quantify this behavior.

Three correlations were used to predict the amount of fuel susceptible to FFRD according to the Chapman correlation. Each correlation gave a different estimate, however the results ranged from 102.5 kg to 480.8 kg. These results were considered bounding. Furthermore, technical justifications were provided to remove the assumptions and utilize the avalible margin.

Future work should focus on incorporating a variable heating rate capability to the Chapman correlation allowing for the simulation to modify the heating rate in accordance with the simulation conditions. High cladding creep rates impacted BISON's ability to complete the transient simulation, and additional work should consider improving BISON's ability to handle high strain rates. This will ensure outlining failure are captured in the assessment. Uncertainties also need to be considered in the analysis and their impact on performance. The effects of grid spacers and transient fission gas on cladding strain, rupture, and FFRD susceptibility need to be considered and explicitly modeled. Finally, the relationship between operating conditions and failure will need to be better evaluated and understood in order to develop core management strategies designed to limit FFRD.

5.4 REFERENCES

1. D. A. Powers and R. O. Meyer. Cladding swelling and rupture models for LOCA analysis. Technical Report NUREG-0630, Nuclear Regulatory Commission, 1980.
2. F. J. Erbacher, H. J. Neitzel, H. Rosinger, H. Schmidt, and K. Wiehr. Burst criterion of Zircaloy fuel claddings in a loss-of-coolant accident. In Zirconium in the Nuclear Industry, Fifth Conference, ASTM STP 754, D.G. Franklin Ed., 271–283. American Society for Testing and Materials, 1982
3. V. Di Marcello, A. Schubert, J. van de Laar, and P. Van Uffelen. The TRANSURANUS mechanical model for large strain analysis. Nuclear Engineering and Design, 276:19–29, 2014.
4. RIL 2021-13, "Interpretation of Research on Fuel Fragmentation, Relocation, and Dispersal at High Burnup," December 2021
5. Yagnik, S. & Turnbull, J. & Hirai, M. & Staicu, D. & Walker, C.. (2015). An Assessment of the Fuel Pulverization Threshold During LOCA-Type Temperature Transients. Nuclear Science and Engineering. 179. 10.13182/NSE14-20.

6. SUMMARY AND FUTURE WORK

The work described herein built on previously developed methodologies to evaluate core FFRD susceptibility. This effort moved beyond the previous efforts by assessing steady-state operational, transient, and fuel performance parameters known to contribute to FFRD susceptibility. The results of the evaluation identify key parameters to consider when designing high burnup cores so utilities can design cores with the purpose of mitigating FFRD. Additionally, these results will help understand high burnup LOCA conditions to support the development of a consensus LOCA test plan. The intention is to further use this data to refine LOCA thresholds used for FFRD licensing analyses.

VERA in conjunction with the BISON fuel performance code was used to evaluate high-burnup core designs to characterize the operating conditions and fuel performance of high-burnup fuel rods during steady-state operation. The goal was to assess the susceptibility of high-burnup fuel rods to FFRD and identify mitigation strategies (i.e., core design optimizations). Nine operating conditions of interest were selected to characterize fuel rod temperature behaviors, burnup behaviors, and spatial relationships between them. A geometric sampling technique was developed and applied to down-select 753 fuel rods for fuel performance analysis in BISON, significantly reducing computational cost. The spatial distribution of the sampling technique and statistical comparisons between the two sets of rods helped ensure that the smaller set provided a representative sample of the larger set. Steady state fuel performance predictions for the selected rods were characterized in detail with respect to their behaviors over time, overall trends, and possible correlations between them. These operating conditions and fuel performance predictions set a baseline for how high-burnup fuel rods are expected to behave during steady state operation and provide initial conditions for the follow-on TH and transient analyses needed to assess the susceptibility to FFRD. Additionally, a preliminary study was then conducted to estimate the magnitudes of the effects that uncertainties in FGR predictions have on FFRD-relevant parameters such as FCT and RIP. The analysis indicated several FFRD-relevant operating conditions and fuel performance behaviors were observed to correlate to fuel rod and assembly locations, indicating that core design and shuffling patterns may influence the character and/or magnitude of FFRD susceptibility.

The TRACE model was based on the BEMUSE OECD International Benchmark conducted in the late 2000s to simulate a realistic large break LOCA (LBLOCA) event in PWRs. This is important as the BEMUSE benchmark is the same reactor design as the reactor used for the analysis. Additionally, TRACE was benchmarked to the BEMUSE results and was determined to provide an overly conservative estimate on the peak PCT in the core. This model characteristic was then applied to the high burnup core design in question. Additional down selection of the 753 to 281 fuel rods was performed as many of the 753 fuel rods were in previous cycles but not the cycle being analyzed. TRACE results were analyzed for the SEH (blowdown) and DEH (post blowdown) LOCA phases. Key parameters considered in the analysis were PCT as a function of rod average burnup, local pellet burnup, LHR, local LHR, and axial location on the fuel rod. The results definitively show the PCT for both conditions routinely occur at the top of the fuel rods where the local burnup was less than the rod average burnup. Burnup was observed to have a negligible impact on the PCT, whereas the local LHR (and average LHR) strongly correlate to PCT. These results suggest two opportunities for minimizing FFRD. First, reduce LHR late in life by optimizing the core design through assembly locations, incorporate enrichment zones within the fuel assembly, enrichment zones within the fuel (both axially and pellet radial enrichment zones), or push the peak LHR higher on the fuel rod to lower burnup regions.

BISON was then used to determine if, when, and where cladding rupture would occur and then was used to estimate FFRD susceptibility. The stress-based Chapman model and strain rate failure models were used in the BISON transient analysis to assess cladding rupture. Both failure criteria indicated all fuel rods would survive the SEH phase of LOCA. This is to be expected as the heating rate is rapid, and the

cladding rupture temperature increases with heating rate. Conversely, the Chapman correlation indicated multiple once-burned fuel rod failures would occur during the DEH LOCA phase, whereas the strain rate criteria predicted a single failure. Both correlations indicated cladding rupture would not occur in any of the twice-burned fuel rods. Note, this may change is the simulations ran to completion. The Chapman model was deemed conservative and used to complete the FFRD assessment. The results were further analyzed for patterns and conditions most likely to lead to failures. Two important correlations were found. First, the failure location was usually 319 cm above the bottom of the fuel rod. The location associated with both peak temperature and peak hoop strain. Second, 102 of the 152 bursts predicted by the Chapman correlation occurred at locations with local burnups ranging 62-65 GWd/tU. Applying the statistical methodology of standard error to these values results in a core wide cladding failure and FFRD susceptibility rate of 37±6%.

The average fuel released per failed rod is provided along with the total amount of fuel released by the 152 failed rods. Three different pulverization correlations were used, however, the methodology layed out in the NRC RIL was used as a guide for all cases. The projected fuel released throughout the entire core, and the margin of error of the full-core release amount (based on the ±6% failure margin of error calculated above).The NRC RIL for 2 mm particles predicts the most release in the range of 347–481 kg. The Turnbull correlation predicts the least release in the range of 103–142 kg.

The work comprised in the report is comprehensive. However, there are a few outstanding issues associated with quantifying uncertainties in the results. TRACE is a system code that is not intended to assess the transient thermal hydraulic behavior on a pin-by-pin level as was done in this report. Therefore, it is worth investigating the impact of subchannel thermal hydraulics on high burnup performance as higher PCTs or different rupture locations may significantly impact FFRD predictions. Additionally, the transient BISON analysis did not include a transient fission gas release (tFGR) model as one is not readily available. tFGR occurs during the LOCA transient as the fuel temperatures increase, primarily in the outer regions of the fuel. The release of fission gas during the transient may increase the RIP enough to have a significant impact on cladding rupture. Therefore, future work should consider assessing the impacts of tFGR timing, rate, and amount—and uncertainties in these parameters—on cladding rupture. Finally, it was assumed the grid spacers and mixing veins would prevent relocation beyond the axial location of interest. However, the grid spacer and mixing veins may reduce the burst temperature by minimizing the volume change during the LOCA. Future work needs to assess whether the grid spacers and mixing veins actually minimize relocation by keeping the local strain below the relocation strain threshold as well as assess the impact of the grid spacers and mixing veins on cladding rupture conditions.

7. ACKNOWLEDGMENTS

The effort to develop 24-month cycle design would not be possible without the collaboration of Southern Nuclear Company. Nuclear Energy Advanced Modeling and Simulation Program (NEAMS) of the US Department of Energy Office of Nuclear Energy supported the analysis herein. The authors would like to express appreciation to Aaron Graham of the ORNL for his review of this manuscript. Furthermore, Southern Nuclear Company contributions cannot be overstated, as they provided representative core designs, industry expertise, and overall vision for how NEAMS can support the industry through strategic modeling and simulation evaluations. Lastly, this research made use of the resources of the High-Performance Computing Center at Idaho National Laboratory, which is supported by the Office of Nuclear Energy of the U.S. Department of Energy and the Nuclear Science User Facilities under Contract No. DE-AC07-05ID14517.